ISAE-SUPAERO
&
POLITECNICO DI TORINO

Systematic assessment of acoustic sources localization algorithms

Supervisors:
Hélène Parisot-Dupuis
Francesco Avallone

Student:
Niccolo' Gariglio
309567

A.y. 2024-2025

Contents

Chapter 1

Introduction

Sound has always fascinated humankind. This is a study of why we can actually communicate between each others and also how animals do as well from a physical point of view: pressure fluctuations are produced and felt by humans and animals; these fluctuations can be called sound or noise; it will be explained better in details later.
Aeroacoustics is a discipline involved in fluid dynamics. It is about the sound generated by airflows, for example by turbulent vortices, and their propagationin a flow. Noise can be generated by turbulent flows at high Reynolds numbers: in this case high velocities can make initial terms being superior than viscous ones. However it is difficult to evaluate this mechanism because acoustics considers infinitesimal variations of variables involved compared to airflow mechanisms which caracterize turbulent flows.
Nowadays Aeroacoustics is very important: this field can contribute to the worldwide challenge of reducing noise pollution and can also reduce risks for structure safety. In addition it can make a travel or a route more comfortable for passengers: in civil aircraft customers experience represents the best advertisement for them. In military field it can be an advantage being more silent than the enemy: it is an example with submarines where sonar detects others' vehicles.
Taking the example of aviation, the work of researchers and engineers allows to significantly reduce the noise emitted by civil aircrafts since 1950 (see Figure 1.1. To continue in this direction, ACARE (Advisory Council for Aeronautics Reserch in Europe) advises to reduce for 2050 by 65% respect to sound levels in 2000. [7]

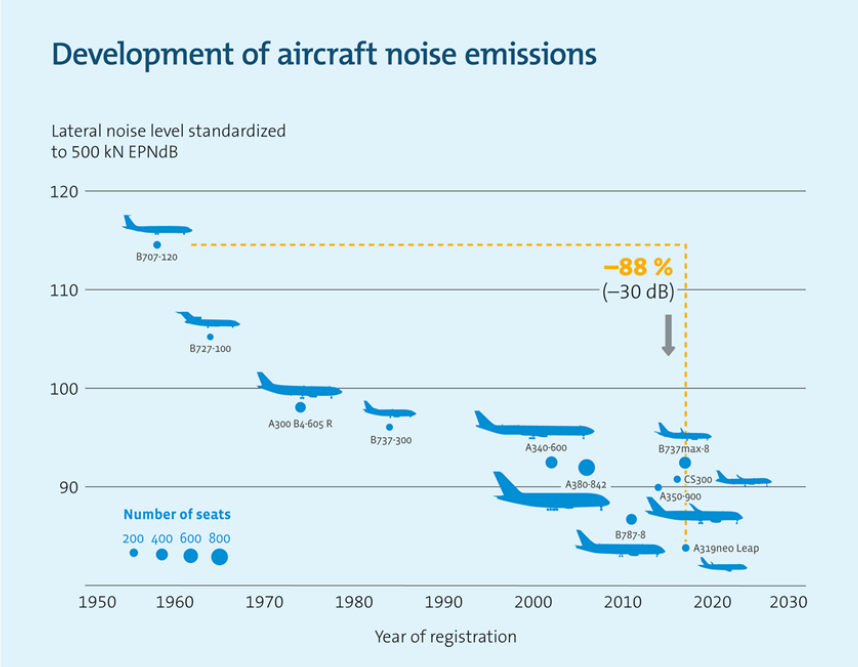

Figure 1.1: Noise emission reduction [1]

An interesting tool to better understand noise generation mechanisms is source localization by means of microphone phased array measurements. One of the most famous source localization method is the beamforming algorithm. In this thesis the main purpose is the systematic assessment of beamforming and other algorithms performances and the study of the influence of different parameters.

1.1 Acoustics and Aeroacoustics

In this chapter we are going to see some theory.
Acoustic waves are part of mechanical waves that require a medium of propagation, the propagation speed being related to the medium properties. Acoustics studies propagation of small perturbations, mainly pressure variations, isentropic, in a quiet medium.
Aeroacoustics studies the noise generated by airflows and sound waves propagation in a moving medium. The sound can be produced by the fluid turbulence itself andor by the interaction between the airflow and a surface, which can be rigid or vibrating, as an airfoil or a turbine blade. It is a part of instationary and compressible fluid dynamics.

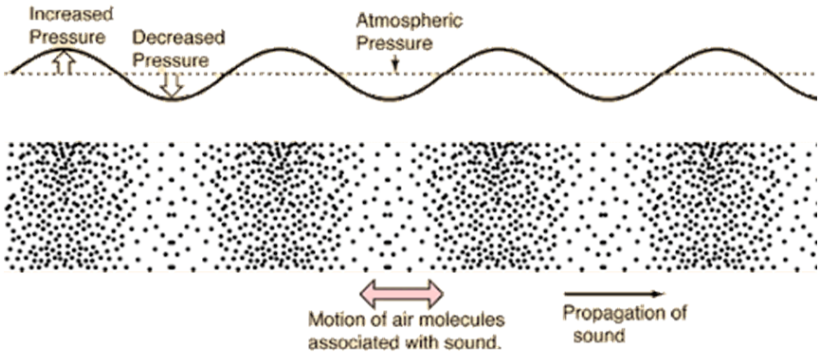

Figure 1.2: How sound waves propagate [2]

1.1.1 Acoustics

Acoustics studies propagation of small perturbations: they are pressure variations, isentropic, in a quiet mean. If these perturbations are within a frequency range and of a certain intensity they are felt by the eardrum as noise. Acoustics sources are mechanical vibrations.
Sound waves are associated to medium molecules oscillation, leading to a transportation of energy and not matter (see Figure 1.2). They can propagate in solids, fluids and gases and their propagation can be affected by obstacles, leading to reflection, refraction or diffraction.
Sound pressure waves can be descriped by their amplitude p' in Pa, frequency f in Hz and propagation speed c in ms. The frequency is related to the period T and the pulsation ω by the relation $f = \frac{1}{T} = \frac{\omega}{2 \cdot \pi}$. The frequency and the sound speed allow to derive two other characteristics of sound waves: the wavelength $\lambda = \frac{c}{f}$ and the wavenumber $k = \frac{\omega}{c}$. Human's ear can typically feel sound pressure waves in the frequency range 20-20000 Hz with a maximal sensitivity around 1-5 kHz. At 20°C the sound propagation speed is in air 340 m/s and approximately 1500 m/s in water.

Sound Pressure

Sound Pressure **p'** ($Pa = N/m^2$) is defined as the variance from a pressure reference value. A significant mean variation is represented by the *root mean square*, or *rms*, which is the positive square root of the mean square value defined for a periodic (T) signal as follows:

$$< p'^2 >= p'^2_{rms} = \frac{1}{T} \int_{t_o - T/2}^{t_0 + T/2} p'^2(t) dt \tag{1.1}$$

In case of aperiodicity it is possible to make T tending to infinity and evaluate the mean value.
Since sound pressure involves many scales and the human hearing is not linear it is more convenient to express the *Sound Pressure* in logarithmic scale and to get *Sound Pressure Level* in dB:

$$SPL = 10log_{10}\left(\frac{p'^2_{rms}}{p^2_{ref}}\right) = 20log_{10}\left(\frac{p'_{rms}}{p_{ref}}\right) \tag{1.2}$$

Reference pressure p_{ref} corresponds to the human threshold of audibility, which is 20 μPa in air, 1 μPa in water.

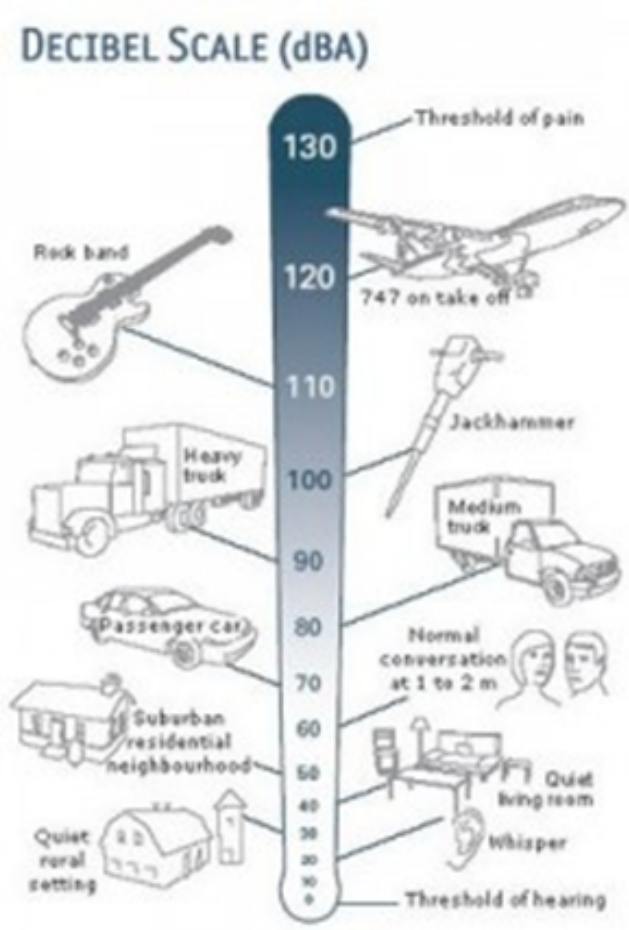

Figure 1.3: Sound Pressure Levels in real life [9].

Using this logarithmic scale, the threshold of audibility corresponds to 0 dB and the threshold of pain 130 dB (see Figure 1.3).

Linear acoustics

Linear acoustics considers medium pressure perturbations p'_{rms} small respect to mean medium pressure p_0:

$$\frac{p'_{rms}}{p_0} \ll 1 \tag{1.3}$$

This is the case for a lot of applications.
Using relationships for gas fluids we can see how also the other variables are small in air:

$$\begin{cases} p' = c_0^2 \cdot \rho' \\ \rho_0 = 1.225 kg/m^3 \\ \gamma = 1.4 \\ T_0 = 293.15 K \\ c = \sqrt{\gamma p_0/\rho_0} = 338.06 m/s \\ \frac{\rho'}{\rho_0} = \frac{p'}{\rho_0 \cdot c_0^2} = \frac{p'}{\gamma \cdot p_0} \leq 10^{-3} \end{cases} \tag{1.4}$$

With the assumption of small sound pressure amplitude respect to the medium mean pressure, acoustic variables satisfy linearized motion equations [2].

1.1.2 Aeroacoustic

Aeroacoustics studies noise propagation in a moving mean: sound is produced by the turbulence in the fluid current and by the interaction between the current and a surface, which can be rigid or vibrating, as an airfoil or a turbine blade.
They are part of fluid mechanics of a instationary and compressible current.
One difficulty can be the discrimination of acoustic fluctuations respect to aerodynamic one as the order of magnitude of aerodynamic fluctuations is bigger.

1.2 Motion Equations in fluid dynamics

Considering fluid (air or water) as a continuous medium a fluid particle can be seen as a point and its main characteristics are time and space functions (x,t). To describe them we consider mass, momentum and energy equations applied to a finite volume V. *Mass* equation says that nothing can be created or destroyed; a variation in *momentum* is equal to the applied forces and, like for mass, *energy* can not be created or destroyed.

1.2.1 Mass

Defining the material type we get the density ρ and so the mass $(\rho \cdot V)$. In a lagrangian system mass conservation is

$$d(\rho \cdot V) = \rho \cdot dV + V \cdot d\rho \tag{1.5}$$

If we are in a reference system which moves with same velocity $\vec{U}$ as the fluid equation (1.5) becomes

$$\frac{D\rho}{Dt} = \frac{\partial \rho}{\partial t} + \vec{U} \cdot \nabla \rho \tag{1.6}$$

with

$$\frac{1}{\rho}\frac{D\rho}{Dt} = \nabla \cdot \vec{U} \tag{1.7}$$

If we are in 3D coordinate (x_1, x_2, x_3) equation (1.7) can be written as

$$\frac{D\rho}{Dt} = \frac{\partial \rho}{\partial t} + u_i \cdot \frac{\partial \rho}{x_i} \tag{1.8}$$

with

$$u_i \cdot \frac{\partial \rho}{x_i} = u_1 \cdot \frac{\partial \rho}{x_1} + u_2 \cdot \frac{\partial \rho}{x_2} + u_3 \cdot \frac{\partial \rho}{x_3} \tag{1.9}$$

Replacing equation (1.8) in equation (1.7) mass law becomes

$$\frac{\partial \rho}{\partial t} + \nabla \cdot (\rho \vec{U}) = 0 \tag{1.10}$$

A mass source term in volume and time Q_m can be added to the second member of equation (1.10) to obtain the continuity equation or mass conservation equation in differential form:

$$\frac{\partial \rho}{\partial t} + \nabla \cdot (\rho \vec{U}) = Q_m \tag{1.11}$$

This equation is known as *Continuity Equation* or *Mass Conservation in differential form.*
Usually the term Q_m is equal to 0; it is considered for complex cases such as combustion.

1.2.2 Momentum

Momentum variations in volume $\rho\vec{U}$ are governed by the integral balance between the momentum flux $(\rho\vec{U}\vec{U})$, external forces in volume $(\rho\vec{f})$, surface forces represented by the tensor Π and momentum variation due to the insertion of a mass Q_m with a velocity equal to the one in the flow $(\vec{U})$ [2]; the integral formulation is

$$\frac{d}{dt}\int_\Omega \rho\vec{U}d\Omega = -\oint_\sigma \rho\vec{U}(\vec{U}\cdot\vec{n})d\sigma + \oint_\sigma \Pi\cdot\vec{n}d\sigma + \int_\Omega(\rho\vec{f} + Q_m\vec{U})d\Omega \tag{1.12}$$

where Ω is the Volume and σ the surface. We apply now Gauss Theorem to have all integrals in volume Ω.

$$\int_\Omega \frac{\partial}{\partial t}(\rho\vec{U})d\Omega = -\int_\Omega \nabla\cdot(\rho\vec{U}\vec{U})d\Omega + \int_\Omega \nabla\cdot\Pi d\Omega + \int_\Omega(\rho\vec{f} + Q_m\vec{U})d\Omega \tag{1.13}$$

Considering an arbitrary volume Ω we can not consider integrals and obtain:

$$\frac{\partial}{\partial t}(\rho\vec{U}) + \nabla\cdot(\rho\vec{U}\vec{U}) = \nabla\cdot\Pi + \rho\vec{f} + Q_m\vec{U} \tag{1.14}$$

This equation is known as *Momentum Equation in conservative differential form.*
In quasi-linear form the equation (1.14) can be written as

$$\rho\frac{\partial\vec{U}}{\partial t} + \rho\vec{U}\cdot\nabla\vec{U} = \nabla\cdot\Pi + \rho\vec{f} \tag{1.15}$$

1.2.3 Energy

E is the total energy in mass unit, it is the sum between internal energy (ϵ) and kinetic energy:

$$E = \varepsilon + \frac{U^2}{2} \tag{1.16}$$

Total energy variations (ρE) are due to the flux balance ($\rho E\vec{U}$), to surface sources such as work in time unit, surface forces ($\Pi \cdot \vec{U}$) and surface heat flux ($-q \cdot \vec{n}$), into volumic forces such as work in time unit, external forces ($\rho\vec{f} \cdot \vec{U}$) and into heat sources as Q_w and to energy associated to the insert of Q_m assuming the same energy E of the flow [2].
The differential conservative form of energy equation is

$$\frac{\partial}{\partial t}(\rho E) + \nabla \cdot (\rho E\vec{U}) = \nabla \cdot (\Pi \cdot \vec{U}) - \nabla\vec{q} + \rho\vec{f}\vec{U} + Q_m E + Q_w \tag{1.17}$$

Rewriting equation (1.17) in quasi-linear form we obtain

$$\rho\frac{\partial E}{\partial t} + \rho\vec{U} \cdot \nabla E = \nabla \cdot (\Pi \cdot \vec{U}) - \nabla\vec{q} + \rho\vec{f}\vec{U} + Q_w \tag{1.18}$$

1.3 Constitutive relationships

They are used to obtain later the **Navier-Stokes equations**. They are useful because they give other expressions of some terms in motion equations.

1.3.1 Newton law

It points its focus on the tensor Π rewriting it as a sum of an isotropic and an anisotropic part:

$$\Pi = -pI + \tau \Rightarrow \sigma_{ij} = -p\delta_{ij} + \tau_{ij} \tag{1.19}$$

Isotropic part $p\delta_{ij}$ corresponds to hydrodynamic pressure effect $p = -\frac{1}{3}(\sigma_{11} + \sigma_{22} + \sigma_{33}) = -\frac{1}{3}\sum_i \delta_{ii}$. $\delta_{ij} = 0$ if $i \neq j$ and to 1 if $i = j$.
The anisotropic part (τ_{ij}) is a deviation which corresponds in a simple fluid (τ_{ij} is symmetric) to the effect of viscosity.

$$\tau = 2\mu D + \lambda(\nabla \cdot \vec{U})I \tag{1.20}$$

$$\Downarrow$$

$$\tau_{ij} = \mu\left(\frac{\partial u_i}{\partial x_j} + \frac{\partial u_j}{\partial x_i}\right) + \lambda\delta_{ij}\frac{\partial u_k}{\partial x_k} \tag{1.21}$$

where D is the symmetric part.

1.3.2 Fourier Law

For heat flows we consider cases where thermal conductivity is isotropic and a linear dependancy from temperature gradient:

$$q = -k\nabla T \tag{1.22}$$

where k is the thermal conductivity.

1.3.3 Navier-Stokes Equations

Combining equation (1.22) and Newton Law into mass (equation (1.11)), momentum (equation (1.15)) and energy (equation (1.17)) equations we obtain **Navier-Stokes equations**:

$$\begin{cases} \frac{\partial \rho}{\partial t} + \nabla \cdot \left(\rho \vec{U}\right) = Q_m \\ \rho \left(\frac{\partial \vec{U}}{\partial t} + \vec{U} \cdot \nabla \vec{U}\right) = -\nabla p + \nabla \cdot \left[\mu(\nabla \vec{U} + \nabla \vec{U}^T) + \lambda(\nabla \cdot \vec{U})I\right] + \rho \vec{f} \\ \rho \left(\frac{\partial E}{\partial t} + \vec{U} \cdot \nabla E\right) = -\nabla \cdot (p\vec{U}) + \nabla \cdot \left\{\left[\mu(\nabla \vec{U} + \nabla \vec{U}^T) + \lambda(\nabla \cdot \vec{U})I\right] \cdot \vec{U}\right\} + \\ +\nabla \cdot (k \nabla T) + \rho \vec{f} \cdot \vec{U} + Q_w \end{cases} \tag{1.23}$$

Considering simpler cases in which viscosity and thermal conductivity can be neglected we get Euler's Equations.

1.4 Ideal gas

If there is only one type of gas or a homogeneous mixture and there are not any chemical reactions thermodynamic state of a gazeous fluid is defined completely by two state variables. It is possible to express any other state variable in function of the two indipendent chosen to get **State Equations**. For a *perfect gas* we have

$$\begin{cases} p = R\rho T \\ \epsilon = C_v T \end{cases} \tag{1.24}$$

where ε is the internal energy, C_v the specific heat at costant volume and $R = R/M$ is the ratio between Universal Constant of gases ($R = 8314$ J/(kMol K) and molar mass (M kg/kMol). Considering a perfect gas $\gamma = \frac{C_p}{C_v}$ and combining these two equations we get

$$p = (\gamma - 1)p\varepsilon \tag{1.25}$$

The two independent variables chosen are ρ (density) and S (entropy): $p = p(\rho, S)$.

$$\begin{cases} \left(\frac{\partial p}{\partial S}\right)_\rho = \frac{R\rho T}{C_v} = \frac{p}{C_v} \\ \left(\frac{\partial p}{\partial \rho}\right)_S = c^2 \end{cases} \tag{1.26}$$

where c is the sound speed; acoustic perturbations propagate at this velocity. c is a state variable because it is function of thermodynamic variables.

1.4.1 Differential form of state caloric equation

$$dp = c^2 d\rho + \frac{p}{C_v} dS \tag{1.27}$$

1.4.2 Entropy Transport Equation

Combining *internal energy equation* and *entropy definition* we get **Entropy Transport Equation**:

$$\begin{cases} \rho\frac{\partial\varepsilon}{\partial t} + \rho\vec{U}\cdot\nabla\varepsilon = -p\nabla\cdot q + \rho\Phi - \nabla\cdot q + Q_w \\ TdS = d\varepsilon + pd\left(\frac{1}{\rho}\right) \end{cases} \tag{1.28}$$

$$\Downarrow$$

$$\rho T\frac{DS}{DT} = \rho\Phi - \nabla\cdot q + Q_w \tag{1.29}$$

It can describe the entropy transport associated to a fluid particle; on the right there are entropy sources terms such as friction (Φ), heat diffusion (q) and heat (Q_w).

1.5 Euler's Equations

In case of acoustic propagation in a stationary flow there are the mean variables $(\cdot)_0$ and the acoustic perturbations $(\cdot)'$ we can write variables in the following way:

$$\begin{cases} U = U_0 + u' \\ p = p_0 + p' \\ \rho = \rho_0 + \rho' \\ c = c + c' \end{cases} \tag{1.30}$$

Under the assumption of linear acoustics, we have:

$$\begin{cases} |\frac{u'}{U_0}| << 1 \\ \frac{p'}{p_0} << 1 \\ \frac{\rho'}{\rho_0} << 1 \\ \frac{c'}{c} << 1 \end{cases} \tag{1.31}$$

and Q_m, Q_w and $\vec{f}$ are perturbations of the same order of the acoustic components.

Euler's Equations :

$$\begin{cases} \frac{\partial\rho}{\partial t} + \rho\nabla\cdot\vec{U} + \vec{U}\cdot\nabla\rho = Q_m \\ \rho\left(\frac{\partial\vec{U}}{\partial t} + \vec{U}\cdot\nabla\vec{U}\right) = -\nabla p + \rho\vec{f} \\ \rho T\left(\frac{\partial S}{\partial t} + \vec{U}\cdot\nabla S\right) = Q_w \end{cases} \tag{1.32}$$

Linearised Euler's Equations (LEE) :

$$\begin{cases} \frac{\partial\rho'}{\partial t} + \vec{U_0}\cdot\nabla\rho' + \vec{u'}\cdot\nabla\rho_0 + \rho_0\nabla\cdot\vec{u'} + \rho'\nabla\cdot\vec{U_0} = Q_m \\ \rho_0\left(\frac{\partial\vec{u'}}{\partial t} + \vec{U_0}\cdot\nabla\vec{u'} + \vec{u'}\cdot\nabla\vec{U_0}\right) + \rho'\vec{U_0}\cdot\nabla\vec{U_0} = -\nabla p' + \rho_o\vec{f} \\ \rho_0 T_0\left(\frac{\partial S'}{\partial t} + \vec{U_0}\cdot\nabla s' + \vec{u'}\cdot\nabla S_0\right) + (\rho_0 T' + \rho' T_0)\vec{U_0}\cdot\nabla S_0 = Q_w \end{cases} \tag{1.33}$$

From these equations we can see how Q_m, Q_w qnd $\vec{f}$, which are small to let to linearise, can be considered as acoustic source terms. S is the entropy of the flow.

1.6 Wave Equation

First of all we condiser an homogeneous stationary medium at rest: $\vec{U_0} = 0$ and p_0, ρ_0, c and S_0 are constant. LEE become:

$$\begin{cases} \frac{\partial \rho'}{\partial t} + \rho_0 \nabla \cdot \vec{u'} = Q_m \\ \rho_0 \frac{\partial \vec{u'}}{\partial t} = -\nabla p' + \rho_0 \vec{f} \\ \rho_0 T_0 \frac{\partial s'}{\partial t} = Q_w \end{cases} \tag{1.34}$$

Caloric equation (1.27) becomes

$$dp' = c^2 d\rho' + \frac{p_0}{C_v} ds' \tag{1.35}$$

Combining these equations (1.34) and (1.35) with the entropy equation (1.29) we obtain **wave equation** *for pressure perturbations in a homogeneous stationary medium at rest*:

$$\frac{1}{c_o^2} \frac{\partial^2 p'}{\partial t^2} - \nabla^2 p' = \frac{\partial}{\partial t} \left(Q_m + \frac{\gamma - 1}{c^2} Q_w \right) - \rho_0 \nabla \cdot \vec{f} \tag{1.36}$$

It describes acoustic wave production and propagation in free field generated by mass source Q_m, forces $\vec{f}$ and heat Q_w.
From this equation we can say that *sound is a small perturbation of pressure, density and velocity and propagates with wave motion.*

1.7 Acoustic Potential

In case of irrotational flow ($\vec{\omega'} = \nabla \times \vec{u'} = 0$) it is possible to define an *Acoustic Potential* φ':

$$\vec{u'} = \nabla \vec{\varphi} \tag{1.37}$$

In addition in isentropic condition and for irrotational forces such as $\nabla \times \vec{f} = 0$ we obtain *Bernoulli Equation*:

$$p' = -\rho_0 \frac{\partial \varphi'}{\partial t} \tag{1.38}$$

and using it in the equation (1.36) we rewrite it

$$\frac{1}{c^2} \frac{\partial^2 \varphi'}{\partial t^2} - \nabla^2 \varphi' = -\frac{Q_m}{\rho} \tag{1.39}$$

This equation can be useful to describe sound fields generated by analytical source models derived in the following and used in this Master's Thesis.

1.7.1 Planar Wave

In free field fluctuations are irrotational and isentropic. All variables are linearly correlated:

$$\begin{cases} p' = c^2 \rho' \\ p' = -\rho_0 \frac{\partial \varphi'}{\partial t} \\ T' = \frac{p'}{C_p \rho_0} \end{cases} \tag{1.40}$$

So pressure, density and temperature waves (and so acoustic potential) are solution of homogeneous sound wave equation:

$$\frac{1}{c^2} \frac{\partial^2 \varphi'}{\partial t^2} - \nabla^2 \varphi' = 0 \tag{1.41}$$

To define a planar wave we write the homogeneous sound wave equation in one-dimensional space dimension; equation (1.41) becomes

$$\frac{\partial^2 \varphi'}{\partial t^2} - c^2 \frac{\partial^2 \varphi'}{\partial X^2} = 0 \tag{1.42}$$

$$\Downarrow$$

$$\left(\frac{\partial}{\partial t} - c \frac{\partial}{\partial x} \right) \left(\frac{\partial}{\partial t} + c \frac{\partial}{\partial x} \right) \varphi' = 0 \tag{1.43}$$

The first part (with -) describes a progressive wave and the other one a regressive one: it can be one or a summation of those progressive and regressive waves.

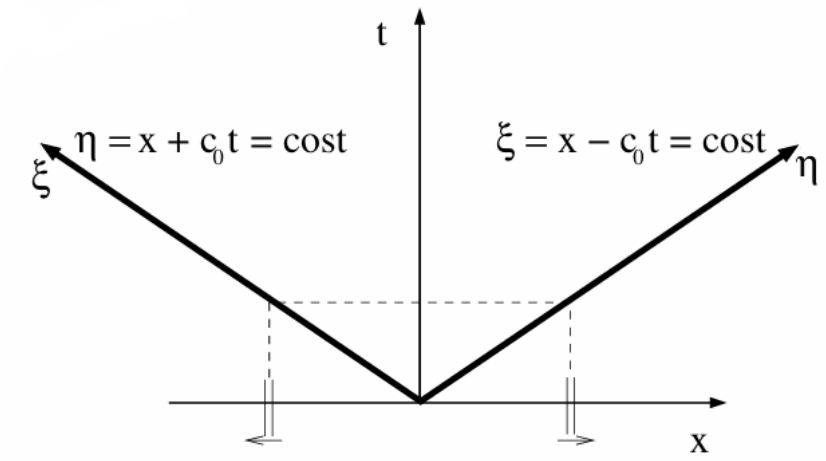

Figure 1.4: Planar wave scheme [3].

1.7.2 Spherical Wave

To derive spherical waves the sound wave equation need to be written in spherical coordinates where field variables are function of radius r and time t; equation (1.41) becomes

$$\frac{1}{c^2} \frac{\partial^2 \varphi'}{\partial t^2} - \frac{1}{r^2} \frac{\partial}{\partial r} \left(r^2 \frac{\partial \varphi'}{\partial r} \right) = 0 \tag{1.44}$$

In analogy with planar waves solution can be composed by a regressive and a progressive part:

$$\varphi'(r,t) = \frac{1}{r}\left[F(r-ct) + G(r+ct)\right] \tag{1.45}$$

Nevertheless the regressive part (G) in spherical contest means there is a signal coming from infinity, which is impossible (Causality principle is not respected, or Sommerfield condition is applied). For this reason solution reduces to

$$\varphi'(r,t) = \frac{1}{r}F(r-ct) \tag{1.46}$$

The term "$1/r$" represents a decay which is necessary to respect acoustic energy conservation: it is ditributed onto increasing surfaces and must be inferior with distance.

1.8 Acoustic Sources

As we have seen acoustic sources can be due to mass injection, momentum thanks to floating forces and energy thanks to entropy variations. In this part we will define analytical acoustic source models of different directivity: a monopole radiates in all directions, a dipole in two specific directions and a quadripole in four main directions (see Figure 1.5).

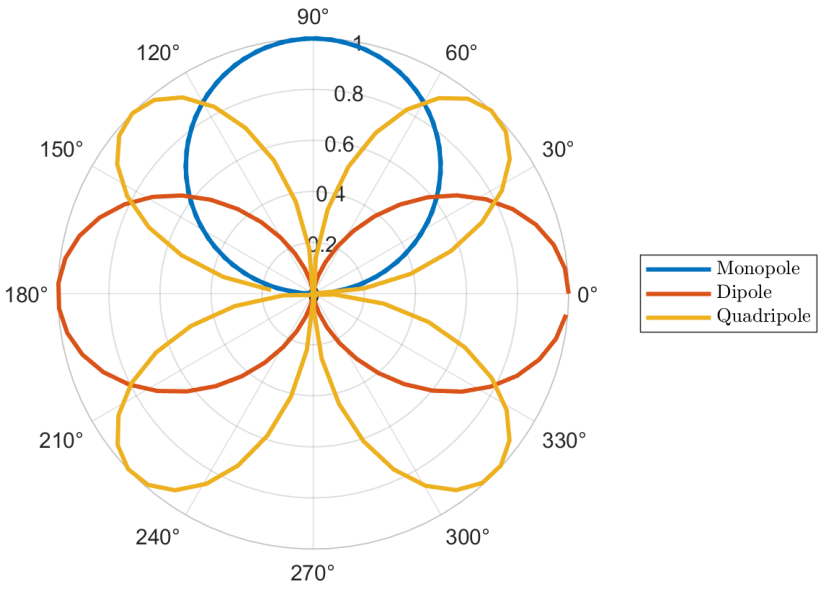

Figure 1.5: Typical sources' directivity.

In this Master's thesis only monopole and dipole will be treated.

1.8.1 Monopole

Monopole can be schemed as an infinitely small pulsating sphere of radius a and for this case it is possible to evaluate the acoustic potential respecting wall conditions ($u'_r(a,t) = u_0 e^{i\omega t}$) and Sommerfiled condition (to consider waves radiating only outward):

$$\varphi'(r,t) = \frac{A}{r} f\left(t - \frac{r}{c}\right) \tag{1.47}$$

where r is the radius, c the sound speed in the medium and A a constant.
Considering a frequency domain it is possible to rewrite the acoustic potential φ' and evaluate perturbations' pressure and velocity:

$$\hat{\varphi}(r) = \frac{A}{r} e^{-ikr} \tag{1.48}$$

where k is the wave number ($k = \omega/c$).
In the farfield when $kr >> 1$ spherical waves tend to planar waves.
Reducing a radius sphere to a point (radius tends to 0) corresponds to introduce a non-homogeneous term in wave equation (1.39):

$$\frac{1}{c^2}\frac{\partial^2 \varphi'}{\partial t^2} - \nabla^2 \varphi' = -q(t)\delta(r) \tag{1.49}$$

$$\Downarrow$$

$$\varphi'(r,t) = -\frac{q(t - r/c)}{4\pi r} \tag{1.50}$$

where q is the monopole mass flow rate (m^3/s) and δ the Dirac function equals to 1 at the monopole's location and 0 elsewhere.
A source can be considered as a point source when its volume is smaller than the wavelength, i.e. $ka << 1$.
The acoustic field radiated by a monopole is omnidirectional, which means that it radiates the same amount of energy in all directions.

1.8.2 Dipole

Dipole can be schemed as a sphere oscillating along one direction, leading to one axis of symmetry (see Figure 1.6). This source can be modelled as two monopoles very closed to each other radiating in phase opposition.

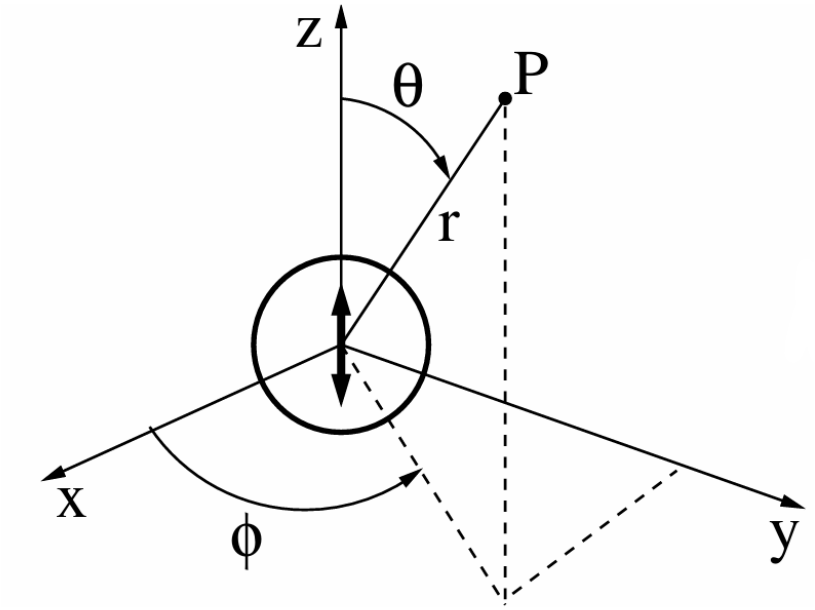

Figure 1.6: Oscillating sphere - dipole scheme [4].

By addiction of the acoustic field radiated by two monopoles. In the farfield the expression of the dipole acoustic potential is

$$\hat{\varphi}(r,\theta) = -\frac{A}{r^2} cos\theta (1+ikr)e^{-ikr} \tag{1.51}$$

In this case the acoustic field depends on theta with two main direction of propagation and one axis of symmetry.
To consider in theory a dipole we consider two monopoles at finite and very small distance: his acoustic field is a constructive or distructive combination of the monopoles in phase opposition. Acoustic field depends on θ.

1.9 Green's Function

Green's function **G(x, t; y, τ)** is the causal solution in the spatial point **x** at time instant **t** to an impulsive source (monopole) set in spatial point **y** and which emits at time instant τ to the non-homogeneous wave equation:

$$\frac{1}{c^2}\frac{\partial^2 G}{\partial t^2} - \frac{\partial^2 G}{\partial x_i^2} = q(t) = \delta(x-y)\delta(t-\tau) \tag{1.52}$$

We can say that Green's function can be seen as a *sound wave propagator*, which will be useful to build new or other ones.
Being the causal solution Green's function respects this principle: if $t < \tau$ G(x, t; y, τ)=0 and also $\frac{\partial G}{\partial t}(x,t;y,\tau) = 0$.
Other characteristics are the mutuality condition and asymmetry: for the first it is equal to invert source and receiver, but considering the reversed times; G(x, t; y, τ)=G(y, $-\tau$; x, -t). For the asymmetry the condition becomes $\frac{\partial G}{\partial t} = -\frac{\partial G}{\partial \tau}$.

In case of *free field* and having a monopole $q(t) = \delta(x-y)\delta(t-\tau)$ equation (1.52) has as solution *Free Field Green's function*:

$$G_0(x,t;y,\tau) = \frac{1}{4\pi|x-y|}\delta\left(t-\tau-\frac{|x-y|}{c}\right) \tag{1.53}$$

where $t - \frac{|x-y|}{c}$ is the delay-time.

Chapter 2

Source Localisation

Source localisation is a signal processing technique which leads to obtain sound source maps from farfield microphones array measurements. It is based on far-field microphone array measurements. As reported in [6] a source localisation algorithm performs a spatial filtering operation that makes it possible to map the distribution of the sources at a certain distance from the array and locate the strongest sources. Source localisation was initially used in other fields such as radio and seismic waves; with the improvement of technology there has been also a constant improvent, and so implementation, of source localisation: for exemple advancement in data acquisition and processing capabilities.

2.1 Delay-and-Sum (D&S) Beamforming

The first documented beamforming solution dates back at 1940's when it was used for military application to detect radio waves from submarines. In 1970's *Acoustic Beamforming* came out.
The D&S is an algorithm in time domain that relies on a source-receiver dependence. Wether the receivers are in the far-field or in the near-field with respect to the source, this algorithm seeks phase delays by virtually steering or focusing the array towards a particular direction (plane wave propagation) or a particular point in space (spherical wave propagation) [6].
In this Master's thesis the focus on a point in space will be used. For this reason a source grid of N points, or *Control Points*, will be used each located at $\vec{x_p}$, p = 1,..., N, in which a set of candidates (often monopoles) are virtually placed [6]; and a set of M-microphones will be used as well located at $\vec{x_m}$, m = 1,...,M : these can sample the sound field. It is convenient to have the origin in the phase center of array; in this way $\sum_{m=1}^{M} \vec{x_m} = 0$ [6]. Each time signal recorded by each microphone of the array is back propagated to each control point by taking into account the relative control point-receiver position in space and the propagation velocity of the acoustic wave in the medium considered: these two terms provide the time delay (or phase shift) to be taken into account when virtually focusing the array towards a certain control point. The delayed data are then summed yielding the beamformer output associated to that control point. If a source is on a control point, the delayed signals turn out to be cophased and the beamformer output is maximized [6]. On the contrary, if focusing on a control point different from a source, signals are not

cophased and so a lower output (beamformer) is obtained. You can see the whole explanation in the Figure 2.1.

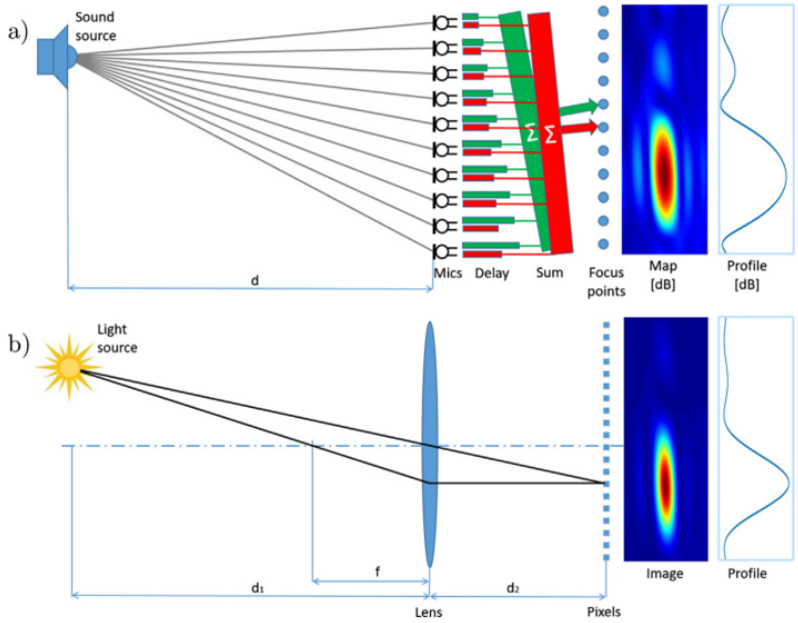

Figure 2.1: Sound detector model a) and optical camera model b) [6]

Here you can see the mathematical form for the beamformer *bf (p,t)* at p^{th} control point and at the t^{th} time instant:

$$bf(\vec{x_p}, t) = \frac{1}{M} \sum_{m=1}^{M} w_m \cdot A_m(\vec{x_p}, \vec{x_m}) \cdot p_m \left(t - \frac{|\vec{x_p} - \vec{x_m}|}{c} \right) \tag{2.1}$$

- p_m is the pressure signal at the m^{th} microphone
- w_m is a weighting factor
- $A_m(\vec{x_p}, \vec{x_m})$ is a scaling factor or a amplitude reduction

$\frac{|\vec{x_p} - \vec{x_m}|}{c}$ can be seen as a time delay $\Delta_m(\boldsymbol{k})$.

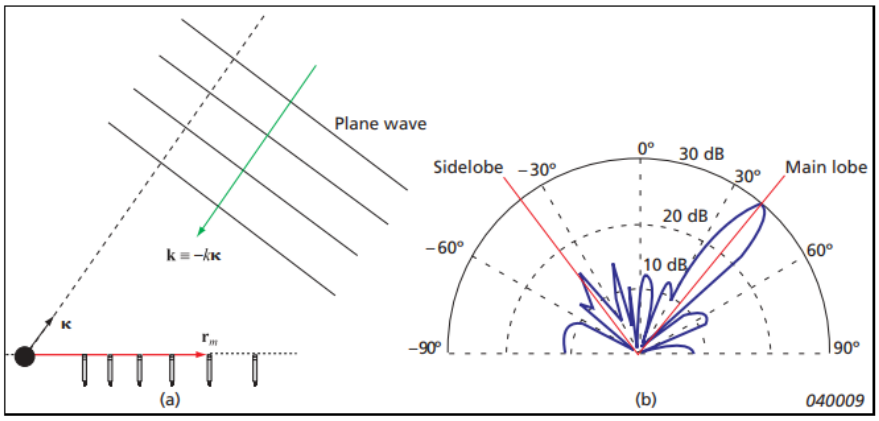

Figure 2.2: Figure at a set frequency. a) A microphone array, a far-field focus direction and a plane wave incident from the focus direction; b) A typical directional sensitivity diagram [11]

Figure 2.2 shows an example of a microphone array response to a farfield incident plane wave, the main lobe is in the direction of the plane wave and lower sidelobes visibles in other directions are related to the microphone distribution.
It is important that time delays are in such a way that signals associated with a plane wave, incident from the direction $\mathbf{k}$ will be aligned in time before they are summed [11]. This can be obtained imposing

$$\Delta_m = \frac{\boldsymbol{k} \cdot r_m}{c} \tag{2.2}$$

If a signal comes from other far-field directions it will not be aligned for the summation and not be added coherently. Using (2.2) we have a directional sensitivity.
To accelerate the calculation it can be useful to write (2.1) in the frequency domain:

$$B(\boldsymbol{k}, \omega) = \sum_{m=1}^{M} A_m w_m \cdot P_m(\omega) e^{j\mathbf{k} \cdot r_m} \tag{2.3}$$

We can say that we have tuned the beamformer on the far-field direction $\mathbf{k}$.
If we get signals arriving only from this specific direction we would be able to get a perfect localisation of sound sources; this is ideal. For this reason a new parameter is used: $\boldsymbol{k}_0$. This will be useful to investigate how much leakage we get from plane waves incident from other directions [11]. This will be more clear seeing Figure 2.3.

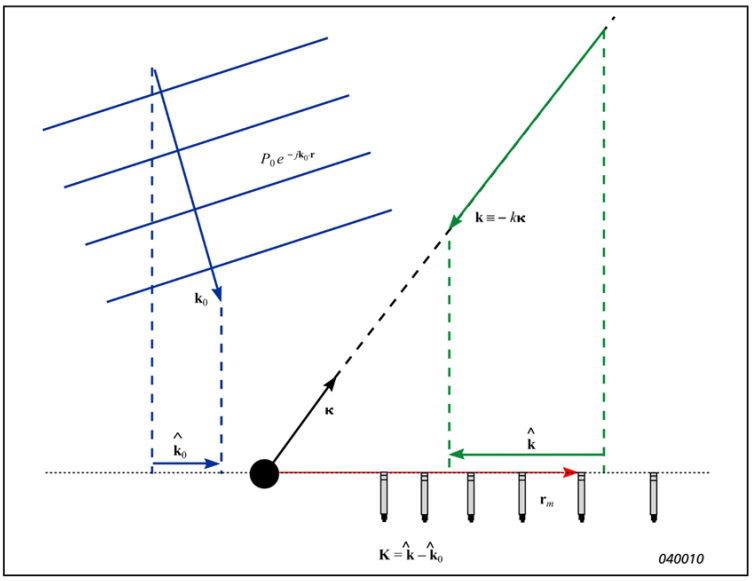

Figure 2.3: k0 and k [11]

Introducing k_0 in the beamforming formulation in the frequency domain (equation (2.3)) P_m becomes:

$$P_m(\omega) = P_0 e^{-j\mathbf{k}_0 \cdot r_m} \tag{2.4}$$

and consequently (2.3) changes:

$$B(\boldsymbol{k}, \omega) = P_0 \sum_{m=1}^{M} A_m w_m e^{j(\mathbf{k}-\mathbf{k}_0)\cdot r_m} = P_0 W(\mathbf{k} - \mathbf{k}_0) \tag{2.5}$$

with the function W:

$$W(\mathbf{K}) = \sum_{m=1}^{M} w_m e^{j\mathbf{K}\cdot r_m} \tag{2.6}$$

This is the array pattern associated to the microphone distribution and leading to sidelobe: they create in source maps the Ghost images.

Equation (2.5) can be reformulated in a vector-matrix notation:

$$BF(\boldsymbol{k}, \omega) = g^H W p \tag{2.7}$$

- **g** is the steering vector. It is common to include A_m within it
- the exponent H represents the complex conjugate transpose
- **p** is a vector: its elements are the complex pressures $P_m(\omega)$ measured at each microphone location
- **W** is a diagonal matrix: its elements are the weighting factors

We can now express the Fast Fourier trasformation (FFT) of the received signals by a microphone in x_m in the steering vector ($\mathbf{g}$) coordinates and of the strength of the source, $\mathbf{q}$, located in x_p: in a vectorial form it becomes $\mathbf{p} = q\mathbf{g}$ [10]. There are many hypothesis in literature about writing the vector $\mathbf{g}$: here sources are supposed as monopoles and uncorrelated between each other in a no-dissipation propagation medium. So in this case vector $\mathbf{g}$ is rewritten using the free-field Green's function for every microphone and control point [10]:

$$g\left(\|\vec{x_p} - \vec{x_m}\|, \omega\right) = \frac{e^{-jk\|\vec{x_p} - \vec{x_m}\|}}{4\pi\|\vec{x_p} - \vec{x_m}\|} \tag{2.8}$$

So if we want to find the source strength q we need to minimize $\mathbf{p} = q\mathbf{g}$: using Ordinary Least Squares (OLS) we get a formula for q.

$$q = \frac{g^H p}{\|g\|^2} \tag{2.9}$$

Then we get the autopower for a source placed in x_p using beamforming algorithm:

$$bf(x_s, \omega) = qq^H = \frac{g^H C g}{\|g\|^4} \tag{2.10}$$

$\mathbf{C}$ is the Cross-Spectral Matrix (CSM) of the pressures caught by microphones (matrix below). It has on the main diagonal the autospectra of the microphones; on the superior triangle all the cross-spectra of the microphone and in the lower one the complex conjugate cross-spectra.
Cross-spectra are related to the degree of linear correlation between two signals, so the result will be 0 when there is no correlation.

$$\text{CSM} = \begin{vmatrix} S_{11} & S_{12} & ... & S_{1M} \\ S_{12}^* & S_{22} & ... & S_{2M} \\ ... & & & \\ S_{1M}^* & S_{2M}^* & ... & S_{MM} \end{vmatrix}$$

2.2 Test design criteria

To design a beamforming test we need to choose the microphone array and its location according to the characteristics of the source we want to study. The main beamforming performance parameters are discussed in this section.
Typical structures are always recognized even if sensitivity and directivity differ from any array pattern: sidelobes and a manilobe are always present, maybe the first ones in different intensity or position. Even if they are not fully desired, they can provide useful information such as the ability to filter out unwanted signals propagating from other directions [6]. The main performance parameters influenced by array design are

- Resolution
- Maximum Sidelobe Levels (MSL) and Mainlobe-to-Sidelobe Ratio (MSR)
- Spatial aliasing

- Point Spread Function (PSF)
- Array design

2.2.1 Resolution

It is the ability to solve and separate sources close to each other [6].
To illustrate that let's consider two planes waves of wavenumbers k_1 and k_2 incident on a microphone array of an array pattern W. Assuming $A_m P_0 = 1$, the beamformer output is [11]:

$$B(\boldsymbol{k}, \omega) = W(\mathbf{k} - \mathbf{k}_1) + W(\mathbf{k} - \mathbf{k}_2) \tag{2.11}$$

In array signal processing the Rayleigh criterion is commonly used: two incoherent sources (from different directions) can be exactly resolved when the peak of the aperture smoothing function due to one source falls on the first zero of the aperture smoothing function due to the other [6]: so when the peak of $W(\mathbf{k}-\mathbf{k}_2)$, corresponding to the plane wave with angle of incidence θ, falls on the first zero of $W(\mathbf{k} - \mathbf{k}_1)$. The reader can better see what explained above in the Figure 2.4 below.

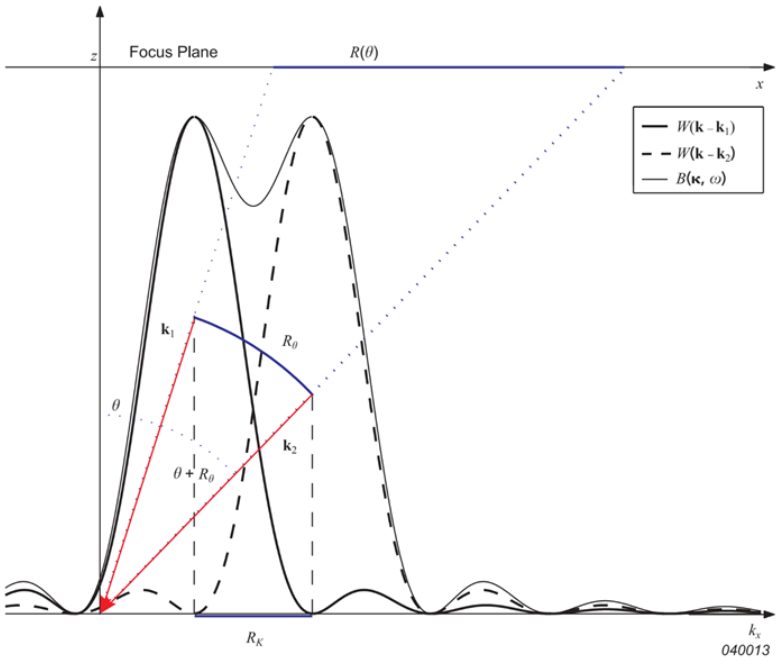

Figure 2.4: Beamformer output $B(\boldsymbol{k}, \omega)$ resulting from two plane waves number vectors $\mathbf{k}_1$ and $\mathbf{k}_2$ incident on a planar array [11]

We assume the required angular separation between $\mathbf{k}_1$ and $\mathbf{k}_2$ small at a finite distance (z), the minimum resolvable source separation in the radial direction $R(\theta)$ is

$$R(\theta) = \frac{z \cdot R_k}{k} \frac{1}{\cos^3 \theta} \tag{2.12}$$

where

- R_k is the main lobe width in the array pattern. It is the distance in the wavenumber plane between the main peak and the first minimum value of the array pattern.
- θ is the off-axis angle

According to Rayleigh criterion R_k is given by the first null, or minimum, K^0_{min} of the array pattern: $R_k = K^0_{min}$ [11]. It is difficult to find the exact value, but a good estimate can be done: we need to consider a limiting case where an infinite number of transducers uniformly distributed over a line segment of length D or a circular disc with radius D/2 is present. This means we are able to sample the sound field at all points within an area (aperture) instead of only at a few discrete positions [11]. In a continous case we use the *aperture smoothing function* as the integral expression for the array pattern:

$$W(\mathbf{K}) = \frac{1}{(2\pi)^d} \int_{|r|<D/2} w(\mathbf{r}) e^{j\mathbf{K}\cdot r\cdot d} d\mathbf{r} \tag{2.13}$$

- $d = 1$ for a line segment
- $d = 2$ for a circular aperture
- $w(\mathbf{r})$ is a continuous shading function

To see how equation (2.13) can be developped see [11] at pag 9.
In case of uniform shading equation (2.13) becomes for a linear aperture:

$$W(\mathbf{K}_x) = \frac{\sin(K_x D/2)}{K_x/2} \tag{2.14}$$

and for a circular aperture:

$$W(\mathbf{K}) = \frac{\pi D}{K} J_1(KD/2) \tag{2.15}$$

with $K = \sqrt{K_x^2 + K_y^2}$.
For both cases (line segment and circular aperture) the first zero is the same:

$$K^0_{min} = a\frac{2\pi}{D} \tag{2.16}$$

- $a = 1$ for a linear aperture
- $a = 1.22$ for a circular aperture

We can modify (2.12) taking advantage of $k = \frac{2\pi}{\lambda}$:

$$R(\theta) = \frac{a}{\cos^3\theta}\frac{z}{D}\lambda \tag{2.17}$$

If we are in the case of on-axis incidence (ideal) the result is

$$R(\theta) = a\left(\frac{z}{D}\right)\lambda \tag{2.18}$$

Resolution is proportional to wavelength. If the aperture size increases resolution improves; if the array-to-object distance increases it worsens.
Comparing the last two equations ((2.17) and (2.18)) we notice that the ratio $\frac{1}{\cos^3\theta}$

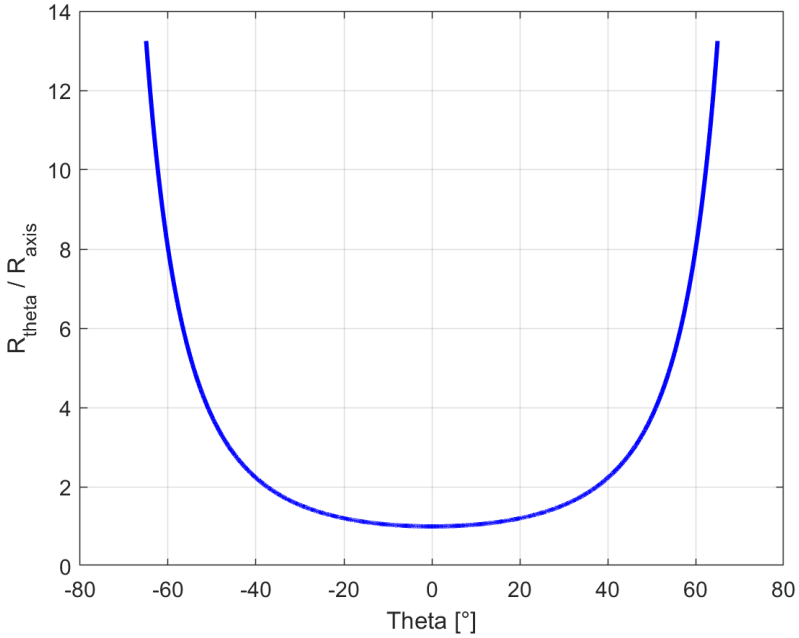

Figure 2.5: $R(\theta)/R_{axis}$ with respect to angle θ in [°]

Comparing Figure 2.5 with 2.4 we can say that if $|\theta|$ increases also the minimum distance between two sources to be distinguished: this means that the capability decreases and resolution worsens.

2.2.2 Maximum Sidelobe Levels

Sometimes array can get sources coming from directions which are different from the one it is steered into. The Maximum Sidelobe Level (MSL), can evaluate the ability of the array to reject these sources and not consider them as real ones. Sidelobes are indeed local maxima from non-focus directions and MSL measures the strength of the highest sidelobe [6]. If a array design is well phased, then it can have low MSL, relative to the main lobe.
The radial profile of the array pattern is defined as follows:

$$W_p(K) = 10 \cdot \log_{10}\left[\max_{|\mathbf{K}|=K} \frac{|W(\mathbf{K})|^2}{M^2}\right] \tag{2.19}$$

M is the number of microphones. MSL is defined as the maximum of equation (2.19):

$$MSL(K) = \max_{K^0_{min}<K'\leq K} W_p(K') = 10 \cdot \log_{10}\left[\max_{K^0_{min}<|\mathbf{K}|\leq K} \frac{|W(\mathbf{K})|^2}{M^2}\right] \tag{2.20}$$

It is possible to look at Figures 2.6 and 2.7 to see how MSL can be evaluated for a discrete array.

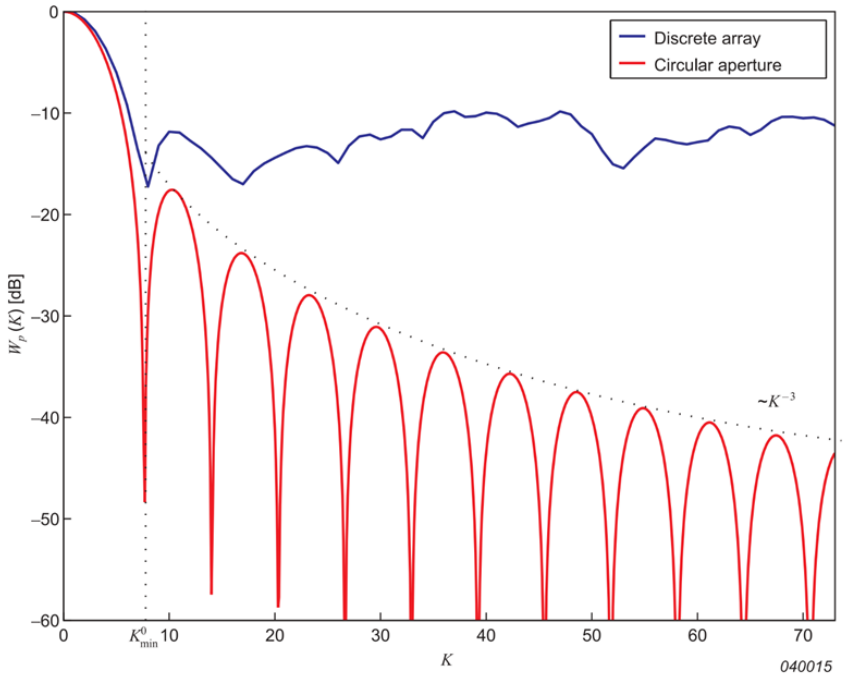

Figure 2.6: Comparison of the aperture smoothing function [11]

The aperture smoothing function of the uniformly shaded circular aperture represents theoretically the best sidelobe suppression attainable [11]. Due to the finite number of the discrete array, the sidelobe levels are much higher [11].

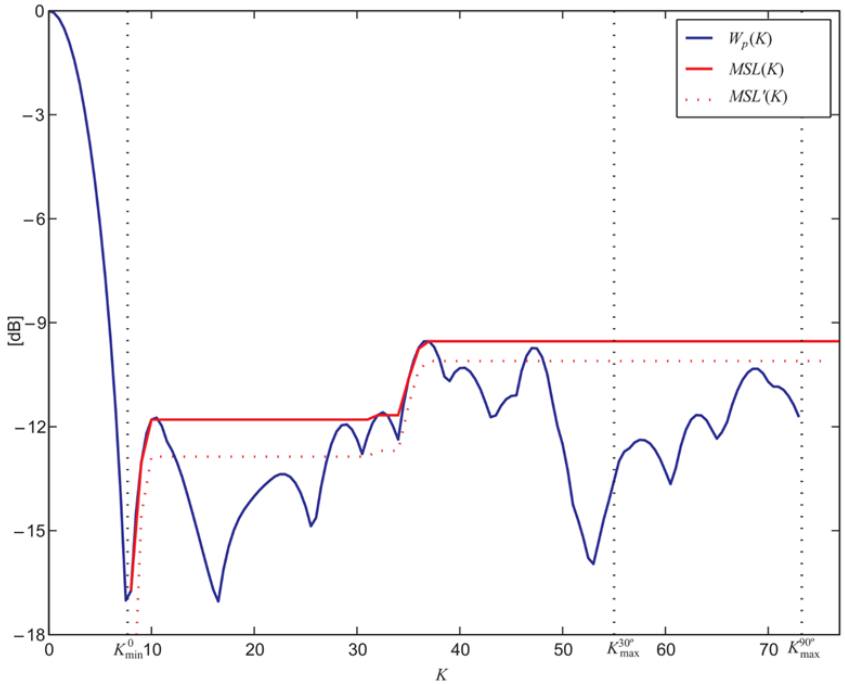

Figure 2.7: Comparison of the aperture smoothing function and MSL in dB [11]

For a fixed frequency ω a section $|\mathbf{K}| \leq 2K = \frac{2\omega}{c}$ of the array pattern will be visible.

The lower the MSL the more accurate is a beamformer to provide accurate source maps with a low degree of false images.

2.2.3 Spatial Aliasing

If we need to sample a time domain signal we need to take count of the Nyquist frequency: $f_N = f_s/2 = \frac{1}{2T_s}$. This is the highest frequency that can be reconstructed unambiguously; $f_s = 1/T_s$ is the constant sampling rate [11]. The concept is similar on a spatially domain signal: if the sampling interval is **d** the spatial Nyquist angular frequency, or Nyquist wave number, is $K_N = \pi/d$ with a period length equal to *2d*, [11]. This means that plane waves at $\lambda < \lambda_{min} = 2d$ cannot be reconstructed well from the spatial samplings. This latter condition implies that the highest frequency f_{max} of a signal possible to reconstruct is

$$f_{max} = \frac{c}{\lambda_{min}} = \frac{c}{2d} \tag{2.21}$$

We can now understand that spatial aliasing can happen when the aperture of the array is not adequately sampled in space by the sensors. A spatial undersampling of the array aperture results in the inability to distinguish between multiple directions of arrivals. In an acoustic map, this effect yields ghost sources of levels similar as true sources [6].
This phenomenon is typical in case the array is regular, so with a constant space between microphones.

2.2.4 Array Design

It is very important and can have huge impacts on results and on tests themselves. The array geometry affects the performance of a beamformer array because it defines the beamformer response trough the array pattern [11]. From this latter one we can get the MSL, and so the ability of the pattern to suppress ghost images as function of frequency. This can be helpful: we can build an array at a given frequency.
Designs can be regular or irregular (see Figure 2.8).

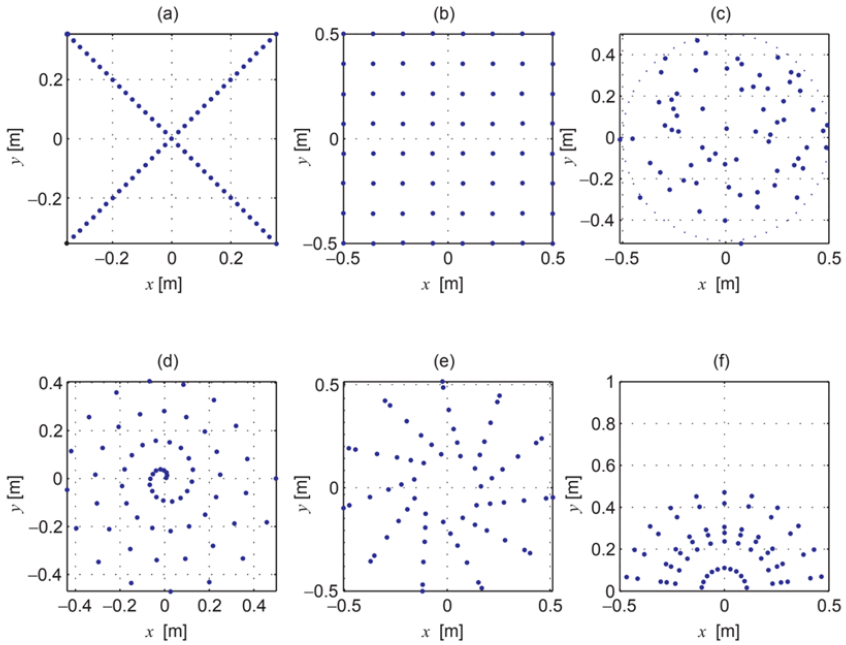

Figure 2.8: Different types of array [11]

a) Cross-array (regular)

b) Grid array (regular)

c) Optimised random array (irregular)

d) Archimedean spiral array (irregular)

e) optimised wheel array (irregular)

f) optimised half-wheel array (irregular)

Here below we can see a comparison of MSLs for the 1 m-arrays depicted in figure 2.9.

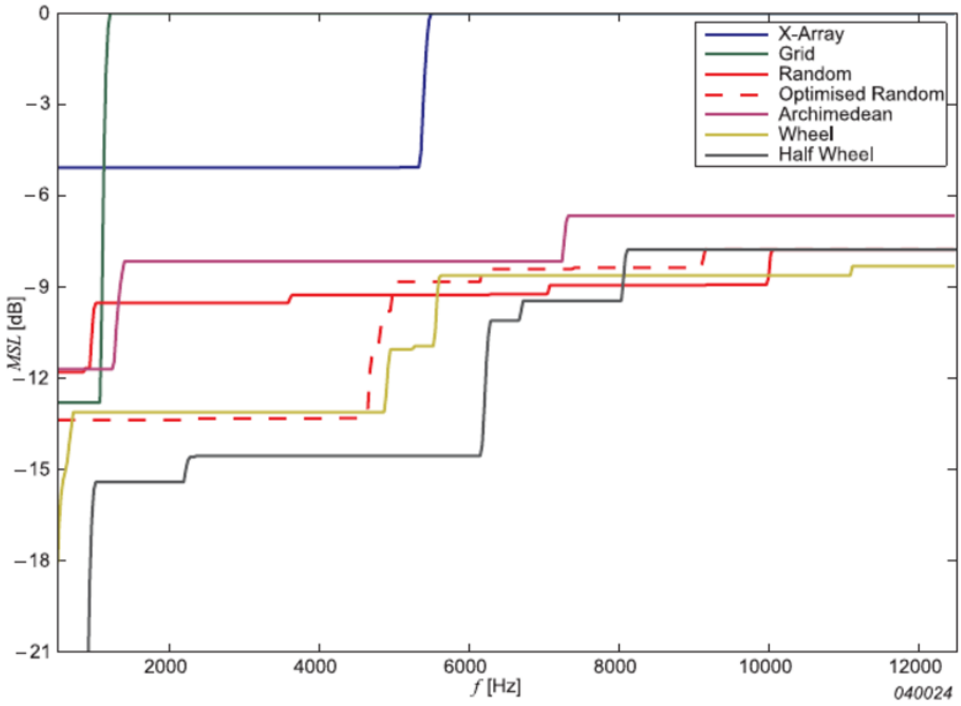

Figure 2.9: MSL of the different arrays [11]

Regular arrays

The simplest regular arrays are the so-called **ULA (Uniform Linear Arrays)** [11]: a one-dimensional linear array with the same distance between microphones (d). Usually we handle planar arrays, but ULA can be helpful to demonstrate some important feautures.
M microphones are spaced and located along the array with spacing d at $x_m = (m - M_{1/2})d$, m=0,...,M-1 [11]. In this way of writing the 0-coordinate will be at the center of the array. In case of uniform shading equation (2.14) becomes:

$$W(K) = \frac{\sin(MKd/2)}{\sin(Kd/2)} \tag{2.22}$$

Equation (2.22) is a periodic function in K and has a maximum for K=0 (the *main lobe*); in addition it gives many other maxima as the main lobe at $K = p(2\pi/d)$, $p = \pm 1, \pm 2, ...$: they are called *grating lobes* [11].

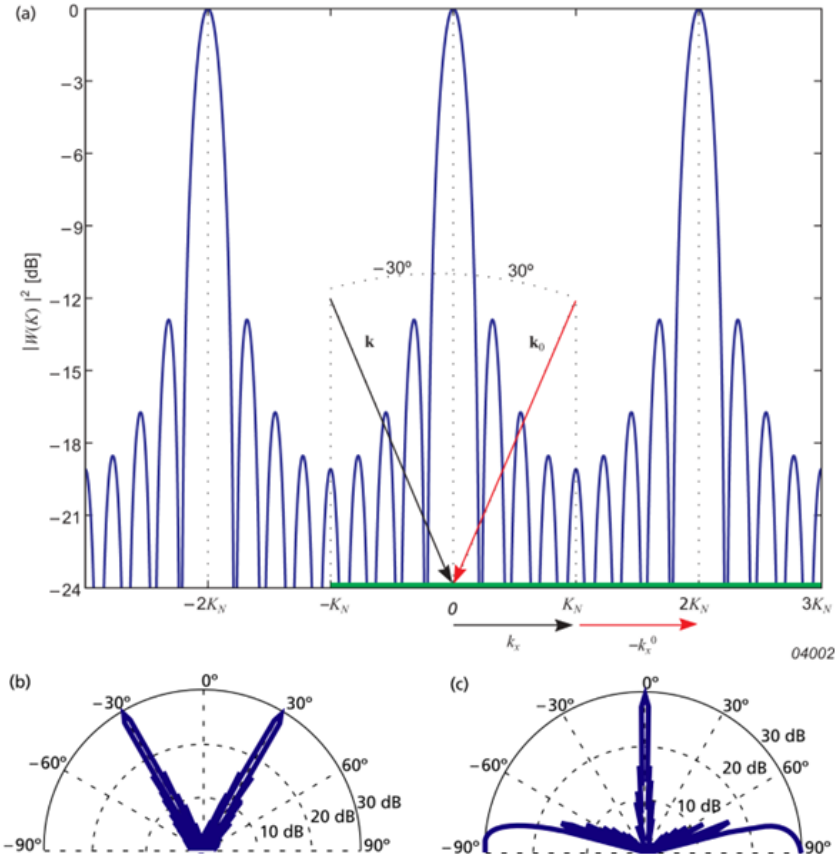

Figure 2.10: Sidelobes structure in a regular array with grid spacing d [11]

As we can see in figure 2.10 there is a mainlobe at $K = 0$ and many grating lobes at multiple of K. $\mathbf{k}_0$ is the wave number vector at incidence angle 30° and in the direction $-30°$ there is the focus direction wave number $\mathbf{k}$ [11]. However $|\mathbf{k}| = |\mathbf{k}_0| = k$ and the frequency is such that $k = 2K_N$. The resulting Nyquist wave number is K_N and so the mainlobe and the grating lobe at $2K_N$ contribute when beamforming is applied at the visible region (the green line), which is in $-K_N < k_x < 3K_N$ [11].
k_x is the projection of $\mathbf{k}$ onto the x-axis, k_x^0 the projection of $\mathbf{k}_0$ and is equal to the Nyquist wave number K_N.
The graph in b) represents a ghost source seen at $\theta = -30°$ and a real source in $\theta = 30°$.
c) represents a directional source map as b) but in on-axis incidence situation at the same frequency [11].
There are several different types of windows used to reduce spectral leakage when performing a Fourier Transform on time data and converting it into the frequency domain [15]. This will be discussed later.

A **Grid Array** is a very simple solution: it is two-dimensional with microphone spacing d. It is possible to see an example in figure 2.8 b). In this example it is 8 x 8 grid array with $d = 1/7m$; the highest frequency is $f_{max} = 1.2$ kHz (figure 2.9) [11]. For this type of array it is common to have such a sharp cut-off at f_{max}; if beamforming is applied at $f > f_{max}$ grating lobes can show up as false sources, resulting as *ghost sources* in the source map [11].

The grid spacing d is approximately calculated as

$$d \simeq \frac{D}{\sqrt{M}-1} = \frac{1m}{\sqrt{64}-1} \tag{2.23}$$

where D is the aperture size (1 m) and M is the number of transducers or microphones: 8 x 8, so 64.

The **Cross Array** can be seen in figure 2.8 a). It is used only in high frequencies. It is basically a combination of two linear arrays. In this case the grid spacing d is calculated in another way:

$$d \simeq \frac{2D}{M-1} \tag{2.24}$$

so the maximum frequency is higher than the grid array (see figure 2.9), between 5 and 6 kHz.
The cross array pattern shows high sidelobes along the directions of the linear arrays and a good suppression of sidelobes in all the others. This latter problem can be however circumnavigated considering a single linear array once separately and then combining them by the means:

$$B_{X-array}(\mathbf{r},\omega) = \sqrt{B_1(\mathbf{r},\omega)\cdot B_2(\mathbf{r},\omega)} \tag{2.25}$$

This results in a much improved sidelobe structure, but problem with ghost sources remains. In addition doing this resolution is degraded.

Irregular Arrays

Irregular arrays can provide a solution against *spatial aliasing*, which affects regular arrays: it can be avoided when the array geometry is totally non-redundant, that is no difference vector between any two transducer positions is repeated [11]. This means having an irregular or random geometry resulting in not having a sharp cut-off frequency but a gradual encrease of Maximum Sidelobe Levels (see figure 2.9).
This solution generally outperforms the regular one, but it is difficult to predict what is the best design to make. Another difficulty is to realise the transducer support structure due to the complicated geometry and consequently operation in a practical measurement can be complicated [11].
To achieve high resolution at high distance it is mandatory to have large dimensions of the arrays: an array with several meters is often required.
Here the optimised array will be treated.

Optimised Arrays offer the possibility to control irregular arrays' performances by numerically optimise the geometry: this can be done by adjusting microphone coordinates for a given frequency range so that maximum sidelobes are minimised over that range. Naturally we need to impose that transucers do not overlap [11].
To see how efficient this solution can be we can take a look at Figure 2.9: the optimised random array can actually decrease Maximum Sidelobe Levels for several dB below f_{max}.
A valuable example of optimised arrays is the Bruel & Kjaer Wheel Array, where the spokes are kept at the same angle away from the radial direction, similar to e)

in Figure 2.8.

2.3 Deconvolution methods

Convenctional Beamforming (Delay & Sum) can give some problems due to the creation of ghost sources: deconvolution methods become important to *clean* a map obtained by beamforming. To do so deconvolution methods identify Point Spread Functions (PSFs), which are theoretical beam patterns obtained by applying Conventional Beamforming using synthetical microphone data of monopole point sources [16]. The aim is to replace these PSFs by single points or narrow beams and to reduce misinterpretation, to more accurately quantify position and strength of aeroacoustic sources [5]. A possible disadvantage is that these methods assume that source plots are built up by PSFs: the actual beam patterns can be different from the synthetically obtained PSF's. In addition time requested for computation is bigger.
One of the first deconvolution methods is DAMAS [5], but it has been slowly replaced by CLEAN-SC.

2.3.1 DAMAS

DAMAS is a deconvolution method which employs processed results (array output at grid points) over the survey regions and the associated array beamforming characteristics (relating the reciprocal influence of the different grid point locations) over the same regions where the array's outputs are measured. A linear system of N (number of grid points in region) equations and N unknowns is created. These equations are solved in a straight-forward iteration approach [5]. The end result is to detemine the true noise distribution to replace the one obtained by Conventional Beamforming.
It is noted that the iper-iteration execution time of the algorithm depends only on the total number of grid points employed in the analysis. To have more details about this method see [5].
In case of not-uniform directivity of the sources deconvolution methods do not work properly.

2.3.2 CLEAN-SC

This deconvolution method has been developped later after DAMAS. It bases on fact that sidelobes are **S**patially **C**oherent with real sources (CLEAN-**SC**). It is an effective tool to remove dominant sources from source plots and unmasking secondary sources [16].
The advantage is that it does not use any PSFs (this is also a reason why not everyone agrees on defining CLEAN-SC as a deconvolution method). Beam patterns of individual noise sources are determined by analyzing the measured spatial coherence [16].
At each iteration if there is a part of the SPL-plot which is spatially coherent with the peak source it is removed. As result we get a map which has significant improvements in spatial resolution.

A disadvantage of this method is that it requires more time than a normal beamforming method: esteems are about the double.
Below on Figures 2.11, 2.12 and 2.13 an example is shown in the case of 3 sources uncorrelated (D) for different frequencies (200, 2000 and 20000 Hz) applying Beamforming and CLEAN-SC.

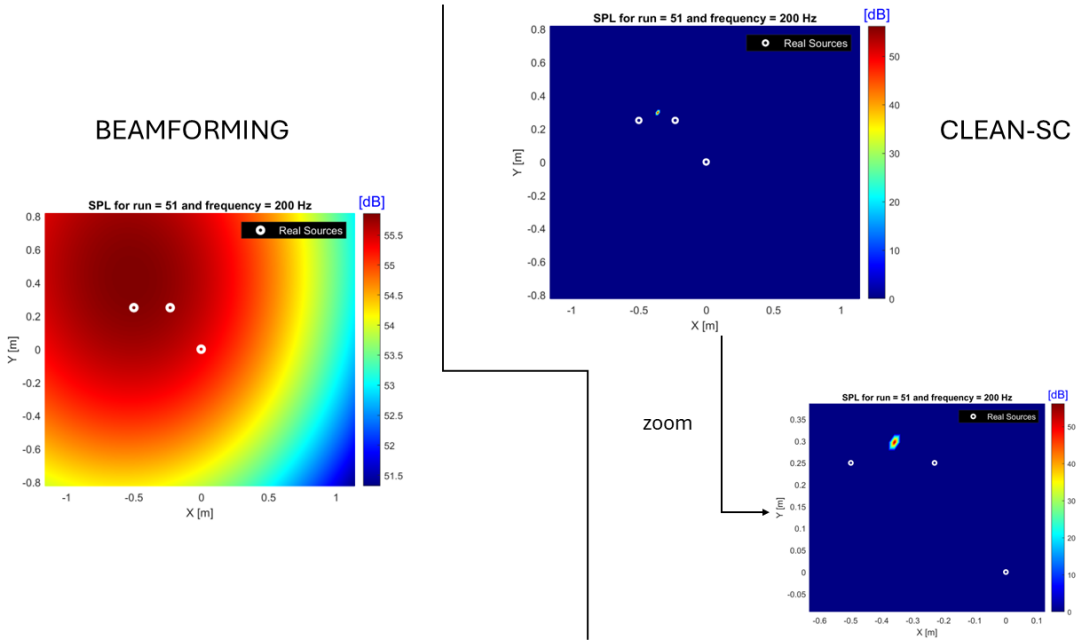

Figure 2.11: Difference between beamforming and CLEAN-SC for 3 uncorrelated sources (D) at 200 Hz

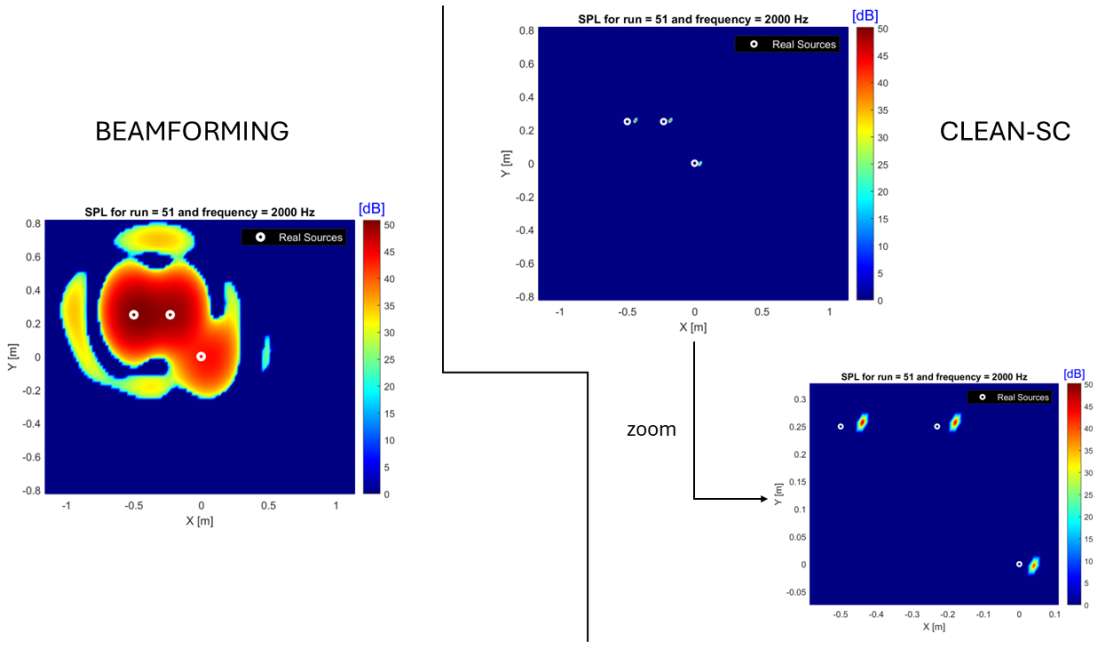

Figure 2.12: Difference between beamforming and CLEAN-SC for 3 uncorrelated sources (D) at 2000 Hz

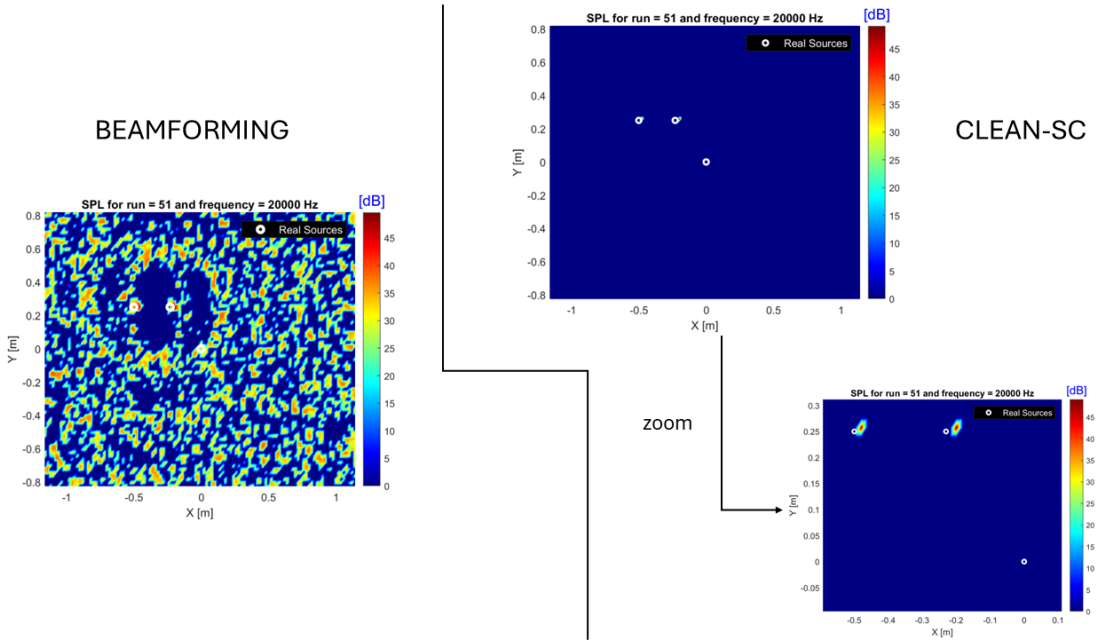

Figure 2.13: Difference between beamforming and CLEAN-SC for 3 uncorrelated sources (D) at 20000 Hz

2.4 Coherence - Anticoherence with a reference transducer

This is a way to clean more beamforming maps, but it is not a deconvolution method. A reference transducer can be used to correlate or anti-correlate microphone array signals with the reference before the beamforming process. These methods have been derived to facilitate the analysis and the understanding of acoustic map by establishing a relation between a noise or vibration source and the noise radiation identified on the acoustic map. The idea is to use a reference sensor representative of a source excitation and to display the acoustic map which is correlated (Coherence ref.) or uncorrelated (Anti-Coherence ref.) with the reference signal.
The average spectrum S_m of the microphone m is obtained by weighting the auto-spectrum of the microphone with a coherence or anti-coherence factor with the reference signal r and by adding a phase relationship with this reference.
The aim of this technique is to obtain cleaner maps than applying only beamforming by using a coherence reference with the microphones.

$$\begin{cases} S_m = coh_{rm} \cdot \sqrt{S_{mm}} \frac{\cdot S_{rm}}{|S_{rm}|} \text{ for Coherence reference} \\ S_m = (1 - coh_{rm}) \cdot \sqrt{S_{mm}} \cdot \frac{S_{rm}}{|S_{rm}|} \text{for Anti-coherence reference} \end{cases} \tag{2.26}$$

with coh_{rm}:

$$coh_{rm} = \frac{|S_{rm}|}{\sqrt{S_{rr}} \cdot \sqrt{S_{mm}}} \tag{2.27}$$

S_{mm} is the averaged auto-spectrum of microphone m and it is the diagonal element in the Cross Spectral Matrix (CSM); S_{rm} is cross-spectrum between *reference (r)* and microphone m and S_{rr} is the auto-spectrum of the reference sensor.

The acoustic imaging processing is then applied on the filtered averaged spectrum of each microphones of the array yielding to the acoustic map correlated or uncorrelated with the reference signal.
To solve properly this new condition on the problem we have applied classic formulas to solve and find a cross spectral matrix, but here we have added a 46^{th} row and column where we have stored the reference signal.

$$\text{CSM} = \begin{vmatrix} S_{1,1} & S_{1,2} & \dots & \dots & S_{1,45} & S_{1,46} \\ S^*_{1,2} & S_{2,2} & S_{2,1} & \dots & S_{2,45} & S_{2,46} \\ \dots & \dots & \dots & \dots & \dots & \dots \\ S^*_{1,45} & S^*_{2,45} & \dots & \dots & S_{45,45} & S_{45,46} \\ S^*_{1,46} & S^*_{2,46} & \dots & \dots & S^*_{45,46} & S_{46,46} \end{vmatrix}$$

Once the new matrix is composed and S_m are obtained on the diagonal we keep the 45x45 matrix and we apply beamforming on it: this will be the classic beamforming. In case of Coherence or Anti-coherence reference cross-spectral matrices will be rewritten applying equations (2.26): S_m, with m = 1,...,45, are the new elements.

$$CSM_{new} = \begin{vmatrix} S^*_1 S_1 & S^*_1 S_2 & \dots & \dots & S^*_1 S_{45} \\ S^*_2 S1 & S^*_2 S_2 & S^*_2 S_3 & \dots & S^*_2 S_{45} \\ \dots & \dots & \dots & \dots & \dots \\ S^*_{45} S_1 & S^*_{45} S_2 & \dots & \dots & S^*_{45} S_{45} \end{vmatrix}$$

Here an example is shown: 3 sources uncorrelated with a reference transducer on the source located at the center.

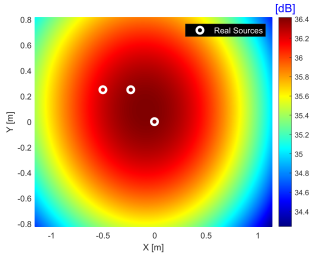

Figure 2.14: ref-Coherence

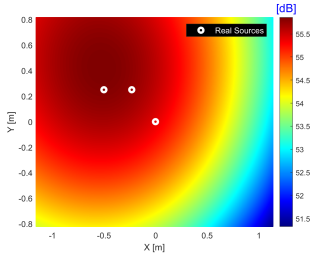

Figure 2.15: No ref-transducer

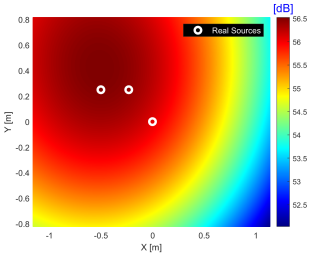

Figure 2.16: AntiCoherence

Figure 2.17: Comparison of conventional beamforming with coherence-anticoherence reference transducer at 200 Hz for 3 uncorrelated sources.

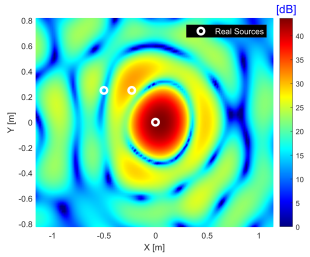

Figure 2.18: ref-Coherence

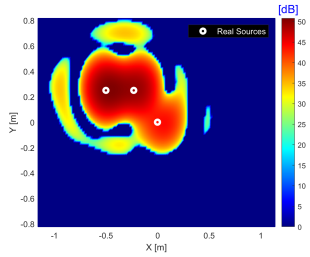

Figure 2.19: No ref-transducer

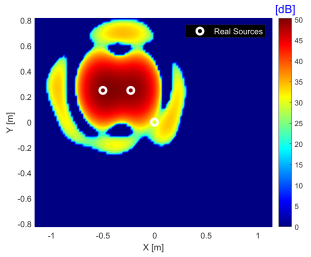

Figure 2.20: AntiCoherence

Figure 2.21: Comparison of conventional beamforming with coherence-anticoherence reference transducer at 2000 Hz for 3 uncorrelated sources.

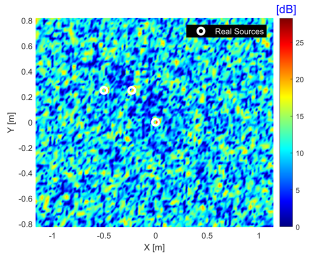

Figure 2.22: ref-Coherence

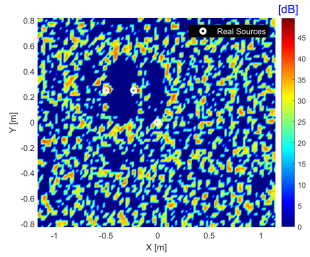

Figure 2.23: No ref-transducer

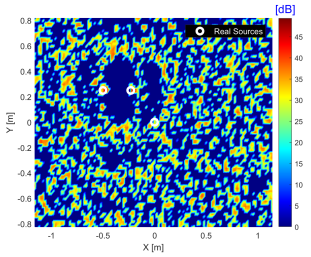

Figure 2.24: AntiCoherence

Figure 2.25: Comparison of conventioanl beamforming with coherence-anticoherence reference transducer at 20000 Hz for 3 uncorrelated sources.

Below in this Master Thesis systematic performance analysis will be applied to evaluate performance of different source localisation methods.

Chapter 3

Systematic analysis

3.1 Methodology

These methods have been developped to find potential sources' locations on source maps given by different source localisation methods: these maps are the outputs and they are matrixes which contain SPL (Sound Pressure Level) at each location on the source plane.

3.1.1 Local Maxima

This is the first method used to obtain potential sources from source maps and the simpler to understand at the beginning: Local Maxima detection algorithm finds the points on the matrix at highest SPL values.
The first step consists in a binarization of the SPL matrix: if the SPL value is greater than a certain value then this point, or pixel, is converted to 1; if not it remains 0. In this way we can create different regions where there is more chance to find an effective real sound source. Indeed using Beamforming it is easy to find many secondary lobes: this is why it is convenient to use a minimum level of SPL as criterium not to consider these secondary lobes as main ones.
M is the Matrix obtained by beamforming, M_b is the binary matrix and SPL_{max} is the maximum SPL in the M-matrix.

$$M_b = \begin{cases} 1 \text{ if } M(i,j) > SPL_{max} - m \cdot dyn \\ 0 \end{cases} \tag{3.1}$$

where dyn is the dynamic range, which is the difference between the maximum sound pressure level of the map and the maximum sidelobe level (MSL); m is a constant equal to 1.
Now the binary matrix is created, it is necessary to define these regions using the function *contourc* in Matlab: it finds all the regions where M_b is 1 and then it creates a list of points which sorround them.

$$Contours = contourc(x, y, M_b) \tag{3.2}$$

In *Contours* there will be a matrix built as follows:

$$\begin{vmatrix} Z_1 & x_{1,1} & x_{1,2} & ... & x_{1,N_1} & Z_2 & x_{2,1} & ... & x_{2,N_2} & Z_3 \\ N_1 & y_{1,1} & y_{1,2} & ... & y_{1,N_1} & N_2 & y_{2,1} & ... & y_{2,N_2} & N_3 \end{vmatrix}$$

Z_i says the height of the i-th contour line, N_i the number of points in the i-th contour line and ($x_{i,j}$, $y_{i,j}$) the coordinates of points for the i-th contour line.
It is important to remember that this function finds all the points neighbours of the regions: this means that the list of points in the Contours is made of ones which have M_b equal to 0 and are immediately out of a region of M_b equal to 1.
In Matlab there was a few problems with the comparison and creation of contours when the pixels closed to the edges were equal to 1: given the fact it is less probable to find any sources closed to the edges, a quick and efficient solution has been converting all the pixels closed to edges in 0 if they were 1. This could facilitate the coding process.
To handle this matrix of points at the best it has been added at the end this line of code:

$$Contours(2, end + 1) = round(max(y) \cdot 100); \tag{3.3}$$

in this way we have a fictitious limit; before of that we can take all the points, it behaves like a flag for the code.
Then from now to the end this process will be repeated $N_{times} = 30$. We divide the different regions by using as limits indexes those numbers which are greater than x or y. Then for each region we choose a random starting point: it will be compared with the 4 neighbours pixels and in case one of them is inside of the same region and has SPL greater than the starting point, the starting point will be changed and we go onto the new one. This process stops when we find the *Local Maximum* of that region.
Sometimes Matlab considers multiple regions equal to each other: so there is a condition on the code which does not consider multiple sources many times but only once.
We will have at least many *potential local maxima* as the number of regions. There is another condition to consider only those maxima which do not have any other pixels in their area with superior SPL; the radius to consider is 5 pixels. If the *potential local maxima* survive this last condition they are added to the *Local Maxima list*.
Here you have values of parameters used in the algorithm:

- $N_{itlm} = 400$: Number of iterations for each apply of this method
- $N_{times} = 30$: Number of repetitions of the whole processus
- $m = 1$: multiplicative factor of the dynamic range (dyn)
- $r_{lm} = 5$: minimum radius in which a local maximum can be considered as a source

It can be cleaner to the reader in the Figure 3.1.

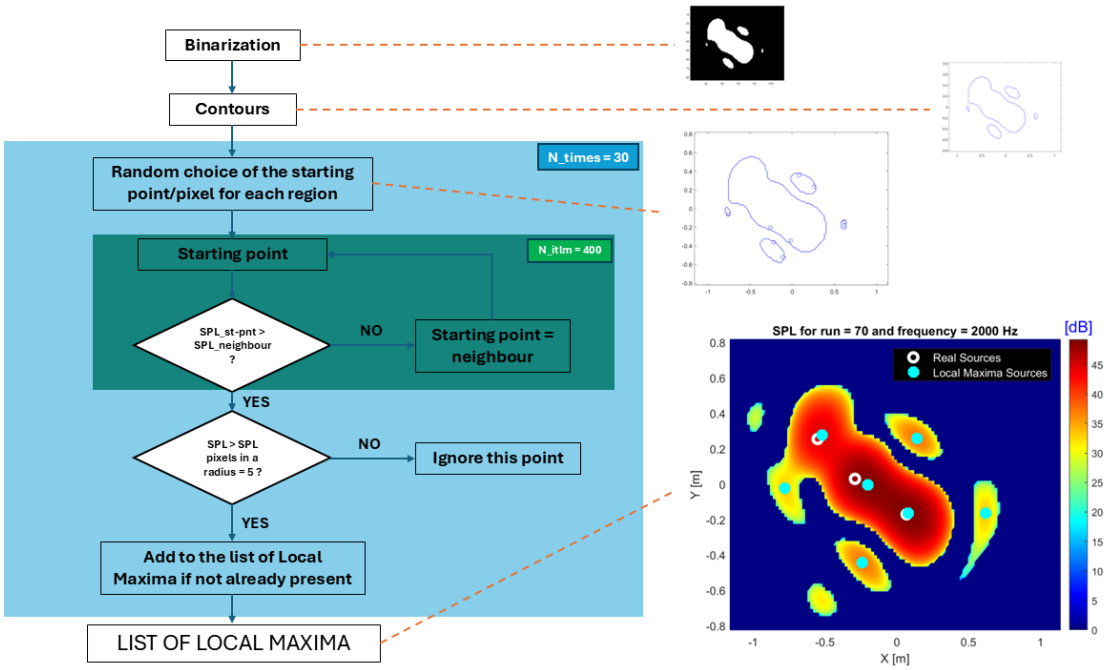

Figure 3.1: [Local Maxima] method applied to a conventional beamforming source map at 2000 Hz with 2 sources out of 3 in phase.

Optimisation: To see how the values have been chosen see [10]: it has been shown that N_{itlm} and N_{max} have a low impact on the number of potential sources identified by the algorithm. The respective values of 400 and 30 give the chance to find all the local maxima limiting the time of computation.
For the other parameters a sensitive analysis has been conducted by applying this method in different and multiple cases. The Figure 3.2 has been obtained from a conventional beamforming map in the case of three sources uncorrelated at f = 2000 Hz.

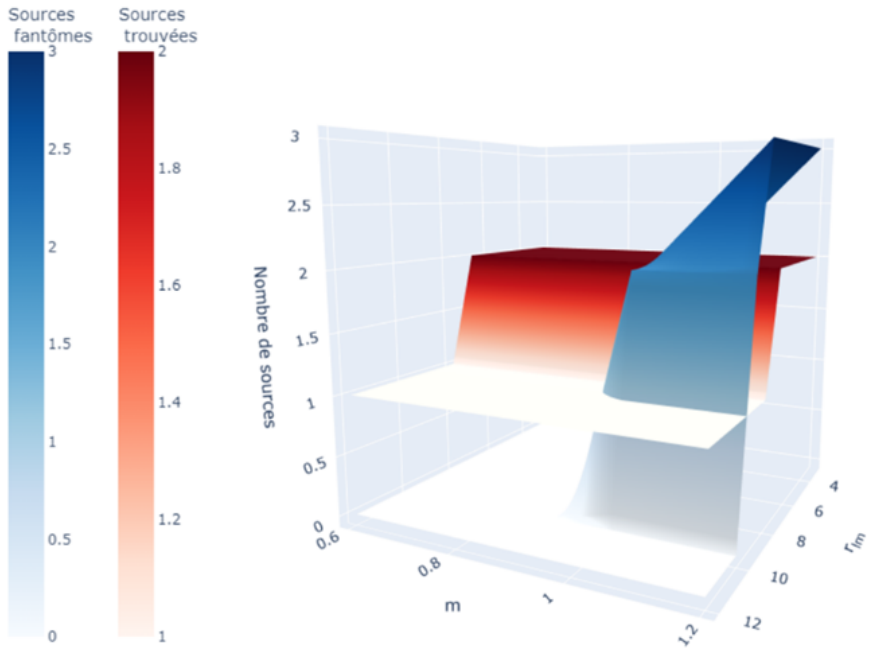

Figure 3.2: Potential sources identified in function of m and r_{lm} by Local Maxima [10].

We can observe how the number of ghost sources identified as potential sources increases if m increases; r_{lm} can give more potential sources identified if it decreases, but it gives also more ghost sources. The more m increases, less the method is selective; the more r_{lm} increases the more selective is the algorithm: each local maximum will be compared in a bigger area and so the number of sources will decrease. Via other cases the optimised number of these parameters are $m = 1$ and $r_{lm} = 5$.

3.1.2 Local Maxima with Big Axis

It is a variant of the classical Local Maxima Method. The difference is in the choice of the first starting point: instead of choosing randomly in a region, we build for each region the longest line linking two points within (this is the Big Axis) and we choose randomly a point belonging to this axis. The purpose is to be faster and to require less cost on computes: usually sources should be on this, or really close to, Big Axis. The process is described in Figure 3.3.

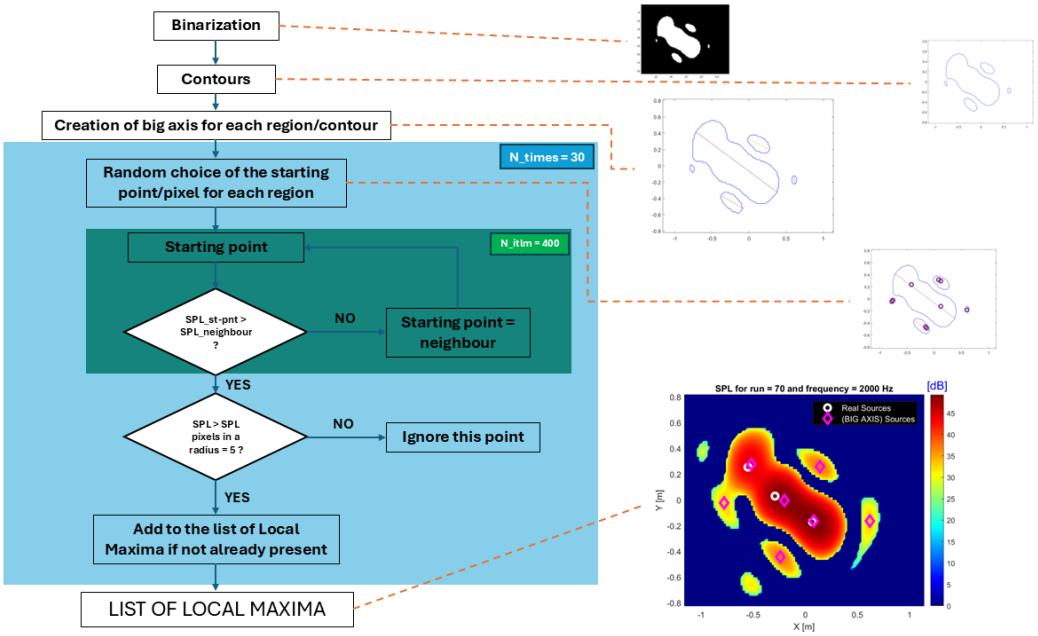

Figure 3.3: [Local Maxima method with BIG AXIS] applied to a conventional beamforming source map at 2000 Hz with 2 sources out of 3 in phase.

3.1.3 Metropolis-Hastings

This method to find potential noise sources on beamforming maps is based on the Metropolis-Hastings algorithm. It consists of the source map exploration through a random walk known as Markov Montecarlo chain: this statistical approach allows to avoid limitations of local maxima detection and to find additional sources [14].
It chooses a random starting point and compare it with random points within an area of radius r_{mh1}: if the SPL of the chosen neighbour is superior then it becomes the new starting point; if not a probability density $P = e^{\beta \cdot \Delta SPL}$ is calculated (β is a positive constant and ΔSPL the difference between the two points, in this case negative). Then a number n is chosen randomly between 0 and 1 (only at the first decimal level, so 0, 0.1, 0.2, ..., 1) and compared to the probability P. If $n < P$ the neighbour becomes the new starting point; if not the time spent on the starting pixel is added of 1. All the process is repeated N_{itmh} times: it should be high enough to have reliable results, but not too big not to require too computational time.
In the end we obtain a time source map, which is the time spent, in iterations, on each SPL source map point [14]. The process is described in Figure 3.4.

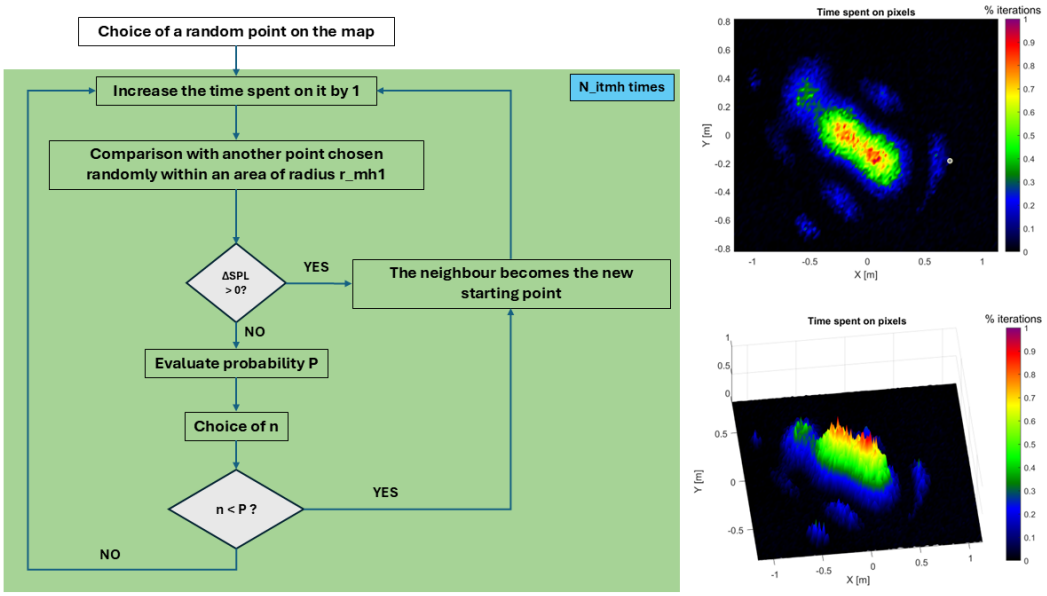

Figure 3.4: [Metropolis Hastings method] applied to a conventional beamforming source map at 2000 Hz with 2 sources out of 3 in phase.

After this process the algorithm select the local maxima on the time spent map: it starts from the upper left point, then it compares with the pixels around in a radius r_{mh2} and if the time spent on the neighbour is superior it moves on that new point and compare in another area of radius r_{mh2}; if this does not happen, the point is added to sources' list.
Then, once it has this list, it keeps only those maxima wich verify this condition:

$$\frac{t_{localmaximum}}{t_{max}} > t_{min} \tag{3.4}$$

with t_{max} the highest time spent on a point of the map and t_{min} the minimum time spent on one point to be considered as a potential source: this latter value is chosen by the programmer; here it is 0.6.

- $\beta = 0.2$
- $N_{itmh} = 1e05$
- $t_{min} = 0.6$
- $r_{mh2} = 5$
- $r_{mh1} = 11$ if freq $=$ 20000 Hz
- $r_{mh1} = 8$ if freq $=$ 2000 Hz or 200 Hz

These parameters have been optimised before; see [10] to read more.

Optimisation: as done previously with Local Maxima, and by consequence Local Maxima with Big Axis, we try to optimise this method based on the [10] job (see

Figure 3.5). Using a aleatory or random path in this method gives variable results: it is difficult to predict if we change some paramters the results obtained are due to this change or to the random path. For this reason studies have been repeated multiple times even if this affected the computation time.

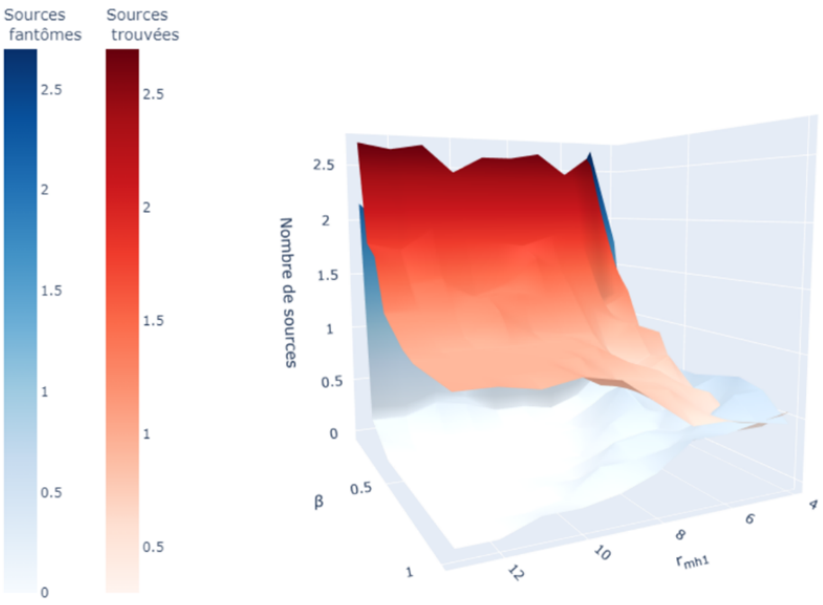

Figure 3.5: Potential source identified in function of of β and R_{mh1} by Metropolis-Hastings [10].

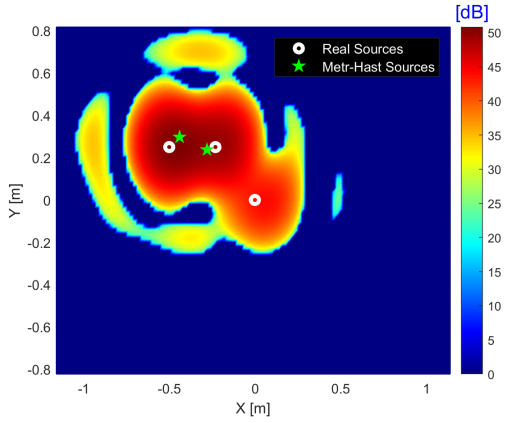

Figure 3.6: a)

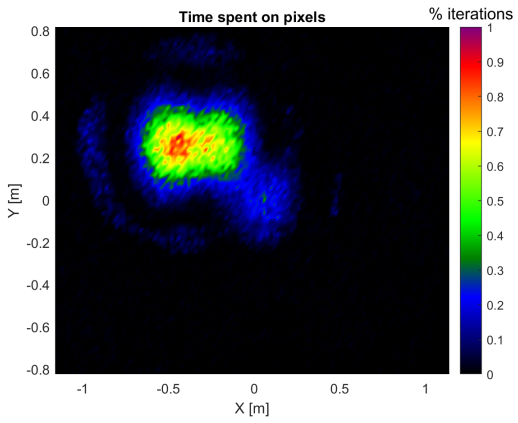

Figure 3.7: b)

Figure 3.8: Example of potential sources found by Metropolis-Hastings a) and the corresponding time-spent b) for 3 uncorrelated sources.

We can observe that if β decreases ghost and sources detected increase: the more β is low the more P is big ($P = e^{\beta \Delta SPL}$) and so the starting pixel has more chance to be moved. If β is too big, the random path will have the tendance to stay on the pixel where there is a strong sound level. The more r_{mh1} is small, the more the pixel with which will be compared will be neighbour: the random path will have

few chance to go out of an area at strong sound pressure level, even if this area corresponds to a *sidelobe* zone.
Via the repetition of 100 study cases values of $\beta = 0.2$ and $r_{mh1} = 11$ for $f = 20000Hz$ or $r_{mh1} = 8$ for $f = 200 - 2000Hz$ are optimised.
N_{itmh} will be big enough to let the random path pass on each pixel exhaustively, but not too much for having a massive computation time. The best compromised value is 1e5 (100000).
Time values on time-pixel map is normalised with the maximum value of the map (t_{max}). This is helpful to put a limit which select which pixels can be considered as sources and which can not. This limit is t_{min} and has been chosen equal to 0.6.
After all these parameters pixels which have normalised time-spent ≥ 0.6 are possible sources; selecting a comparison area of radius r_{mh2} let have only the biggest pixel as the possible sound source. Here it has been chosen empirically a value of 5 (pixels).
An example of potential sources found on the conventional beamforming source map and the corresponding time spent map is presented in Figure 3.8.

3.1.4 Fusion

This method is the combination of Metropolis-Hastings and Local Maxima or Local Maxima with big axis. It takes the potential source list of each and put them together in one. It can be useful because it takes the advantages from both: for exemple at low frequency Local Maxima in general is not really great, Metropolis-Hastings instead can evaluate well a good portion of the map. At high frequency it is at the opposite and in medium frequency sometimes there can be few problems but with a combination the only negative result is to have some ghosts: it usually finds all the sources. Examples of results are shown in Figures 3.9 and 3.10.

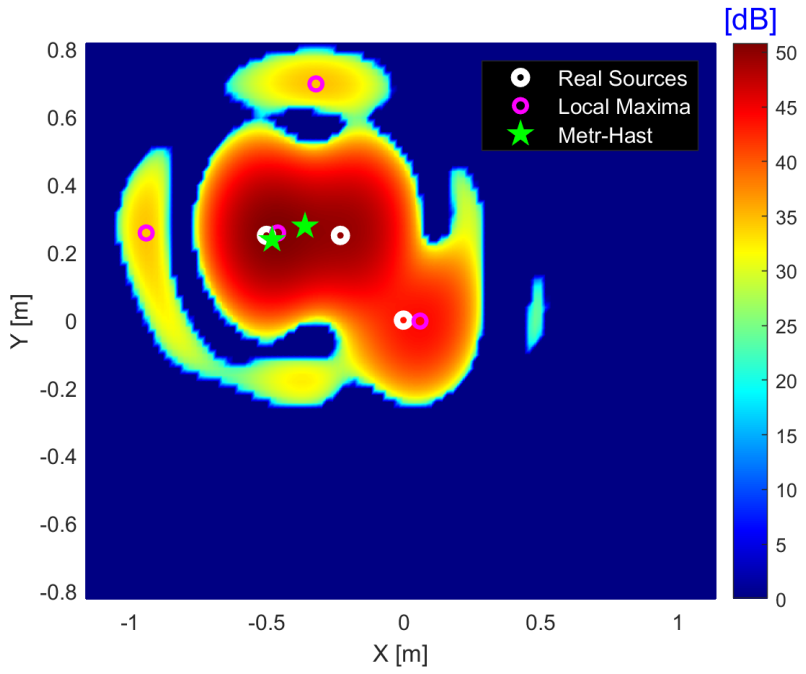

Figure 3.9: Fusion of local maxima and Metropolis-Hastings potential source lists for 3 uncorrelated sources at 2000 Hz.

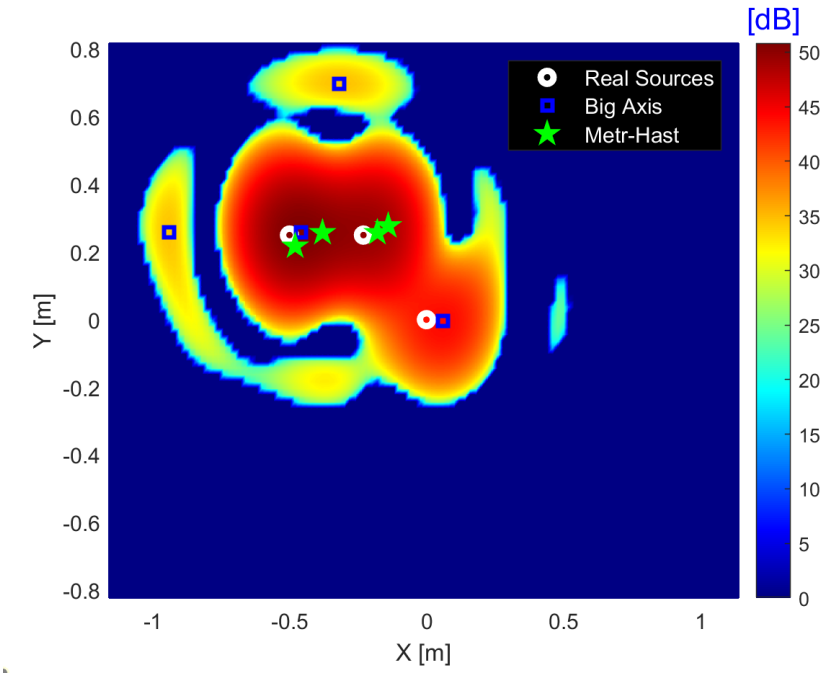

Figure 3.10: Fusion with local maxima with big axis and Metropolis-Hastings potential source lists for 3 uncorrelated sources at 2000 Hz.

From these examples we can see how Metropolis-Hasting does not always give the same results: this is due to the random choices through passages as the choice of the starting point, of the neighbour or "n".

Fusion with center of gravity

It can happen, especially at low frequency, to have multiple sources by Metropolis-Hastings in a small area, as you can see in the example Figure 3.11 below.

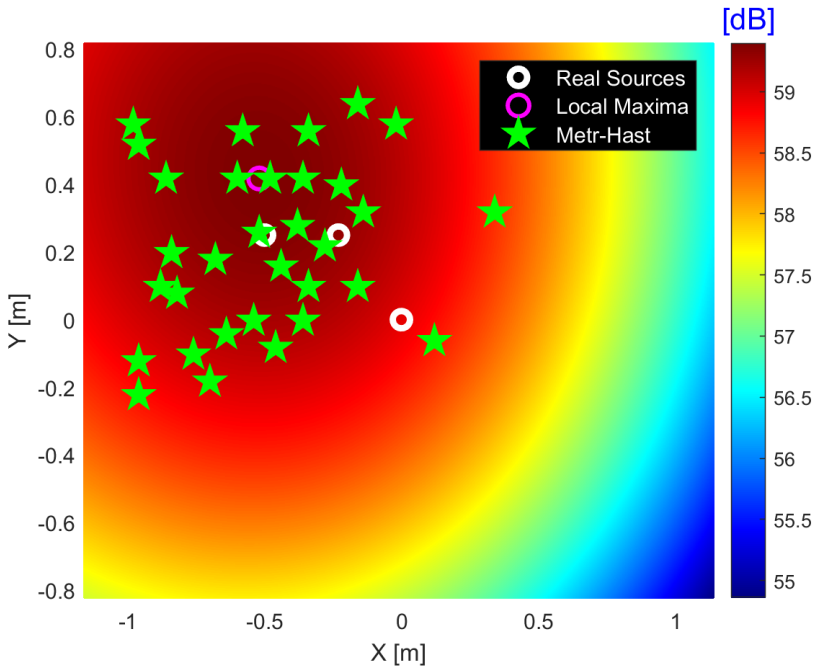

Figure 3.11: Fusion of local maxima and Metropolis-Hastings potential source lists for 3 uncorrelated sources at 200 Hz.

The method chooses a minimum distance that can be present between two sources: if their distance is smaller they belong at the same package. After it gets many packages it finds the center of gravity for each:

$$(x, y, SPL)_{C.G.} = \frac{\sum_{i=1}^{N}(x_i, y_i, SPL_i)}{N} \tag{3.5}$$

where N is the number of sources of each package.
Here d_{max} is 0.05 m at f = 20000 Hz, 0.15 m at f = 2000 Hz or 200 Hz. It has been defined via empirical way.
Considering an area where all the sources can fit, finding the center of gravity is a way to reduce the number of sources and have a cleaner map.

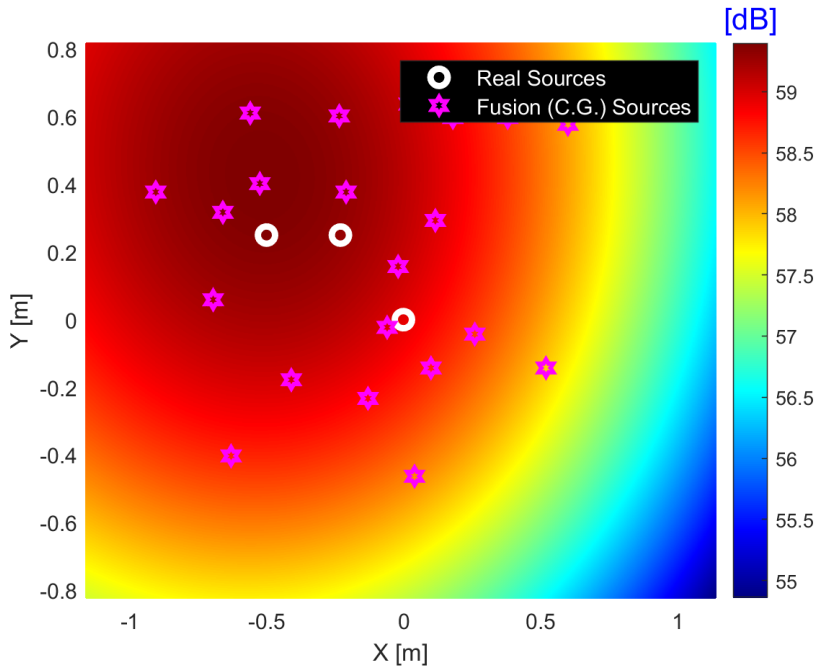

Figure 3.12: Fusion of local maxima and Metropolis-Hastings with center of gravity potential source lists for 3 uncorrelated sources at 200 Hz.

As you can see from the example Figure 3.12 it does reduce the number, but sometimes the centers of gravity do not correspond to the actual sources. In addition, some of the points used for the center of gravity may be closer to the real sources. In addition this method can be avoided by using a different value of r_{mh2}, more selective at low frequency, where resolution can be a problem. However this can directly influence time of compute.

3.2 Resolution

Resolution is defined as the area of the beamforming map where condition ($SPL_{max}-3$) dB is verified for a monopole source at the center of the source plane. As this value varies with frequency, the calculation was performed for frequencies = (200, 1000, 2000, 4000, 8000, 16000, 20000) Hz.

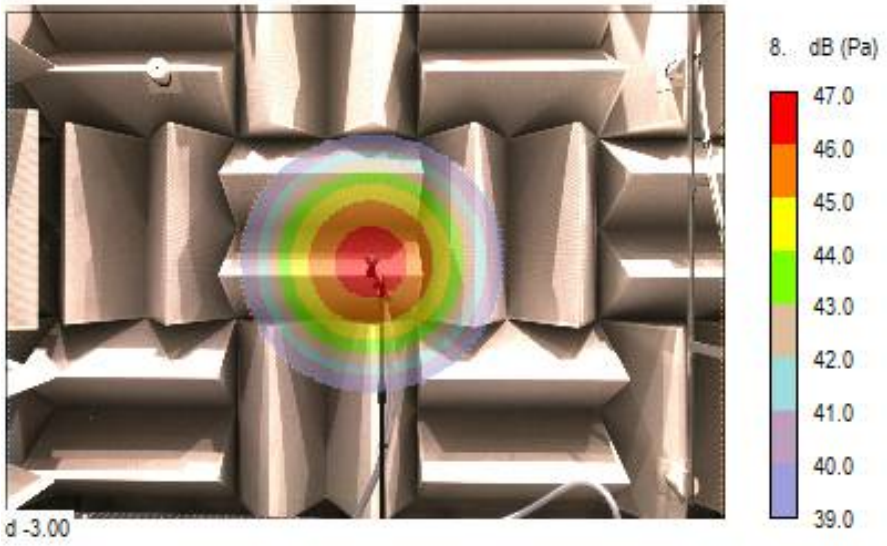

Figure 3.13: Resolution pointed out at frequency = 1000 Hz.

For each frequency we find the area of the map corresponding to $SPL_{max} - 3$ dB as in Figure 3.13 and the distance between the further points belonging to that area. At low frequency it can happen that this area can be bigger than the grid: so resolution in this case will be the minimum distance between the height or width of the grid.
In the table 3.1 values for different frequencies are shown. Those resolution values are dependent on the microphone array used and the distance between the source plane and the array.

Frequency [Hz]	**Resolution [m]**
200	1.6 (height Y-axis)
1000	0.5915
2000	0.3039
4000	0.1641
8000	0.1012
16000	0.0625
20000	0.0592

Table 3.1: Resolution in metres for different frequencies.

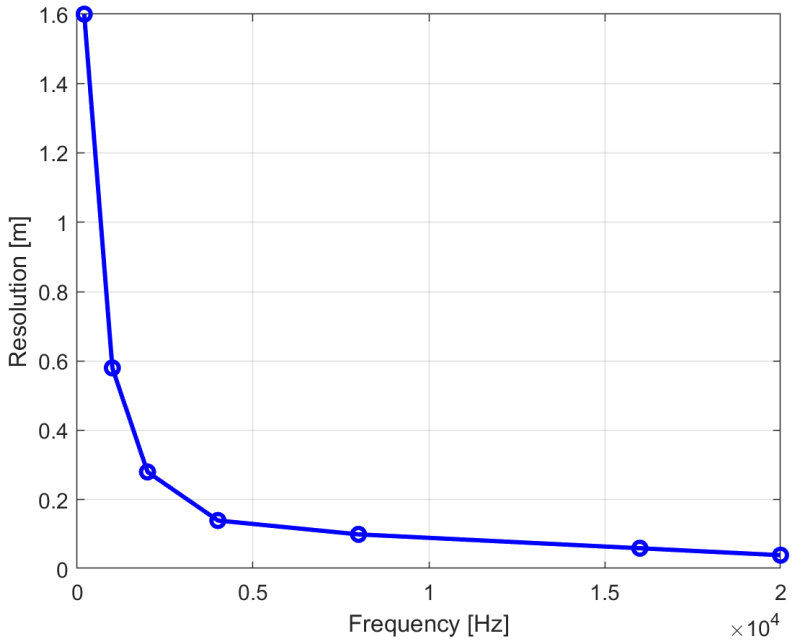

Figure 3.14: Resolution - frequency

In the Figure 3.14 we can see the dependecy of resolution and frequency: the more frequency increases, the smaller resolution becomes.
The corresponding d_{max} for each frequency is the half-resolution:

Frequency [Hz]	d_{max} **[m]**
200	0.8
1000	0.2958
2000	0.1520
4000	0.0821
8000	0.0506
16000	0.0313
20000	0.0296

Table 3.2: d_{max} for coupling for different frequencies.

To evaluate theoretically resolution values we can apply definitions given by [6] and [11]; for both resolution along the axis, so no angle between the two planes is given by:

$$R_{axis} = \frac{a}{cos^3(\vartheta = 0°)} \left(\frac{z}{D}\right) \lambda = a \left(\frac{z}{D}\right) \lambda \tag{3.6}$$

where a is a constant which is equal to 1 if the array is squared and 1.22 if the array is circular for [11] and 1.44 for [6]. z is the distance between the source and array planes, D the main dimension of the array, in this case being circular is the diameter; and λ is the wavelength. Resolution found by this method is the minimum distance for the beamformer to distinguish two different sources. By the equation (3.6) we can see how resolution depends on distance: more the distance is more resolution will be high.

In the Table 3.3 you can see wavelength and resolution values for each frequency: diameter for the array used in this study is 0.8 m and the distance from the source plane is kept at 3 m.

Frequency [Hz]	λ **[m]**	**resolution([6]) [m]**	**resolution([11])[m]**
200	1.7170	9.2718	7.8553
1000	0.3434	1.8544	1.5711
2000	0.1717	0.9272	0.7855
4000	0.0858	0.4636	0.3928
8000	0.0429	0.2318	0.1964
16000	0.0215	0.1159	0.0982
20000	0.0172	0.0927	0.0786

Table 3.3: Theoretical resolution for different frequencies.

Comparing tables 3.1 and 3.3 we can see how practical values are smaller than the theoretical ones: this could be good because using values in the first table we will be conservative.

3.3 Criteria

After finding the list of potential sources from source maps it is interesting to compare this list with the list of real sources which is available when analytical or known sources are used. Only potential sources which are closer to the real sources are coupled, but one real source can be coupled with only one potential source, others which remain uncoupled being considered as ghost sources. To do so it will be built a matrix D useful to evaluate some performance criteria:

$$\mathbf{D} = dist(Source_i, Source_j) \begin{cases} 1 \leq i \leq m(Source_i)_{1 \leq i \leq m} \ real\ sources \\ 1 \leq j \leq n(Source_j)_{1 \leq j \leq n} \ potential\ sources\ detected \end{cases} \tag{3.7}$$

Once obtained **D** we look for the minimum values within it: as soon as the first minimum is found values corresponding two indexes are pointed out (so we have which real source corresponds to which potential source detected), we have the first couple and we add 1 to all values on the same line and column of the protagonist pixel. In this way in a new research of a minimum we do not go on sources already coupled. This process will be repeated n_{times} equal to the minimum number between real sources and potential sources detected. To validate the couples obtained a condition on the distance will be introduced: if the distance between a real source and a source detected in a couple is $\leq$ than a certain d_{max} then the couple will be validated: d_{max} corresponds for each frequency to the half of the resolution.

Once a list of potential sources is obtained from a source localisation map, criteria indicating the performances of the source localisation algorithm can be calculated. This requires to know real sources, which is the case when analytical source fields are used or when reference sources are used in experiments.
The first criterium is for evaluating how many potential sources are detected as real

ones:

$$C_{nr} = \frac{N_{rps}}{N_{rs}} \tag{3.8}$$

- N_{rps} is the number of Potential Sources detected as Real
- N_{rs} is the number of real sources; it should be known in advance

Second criterium is for evaluating the number of ghost sources detected:

$$C_{nt} = \frac{N_t}{N_{rs}} \tag{3.9}$$

with N_t as the total number of sources detected. Making a difference between C_{nt} and C_{nr} we can get the actual evaluation of the number of ghost sources.
The following criteria are based on the coupling of real sources with the closest potential source to assess the accuracy source localisation maps.
Third criterium is for evaluating the average distance between real sources and potential sources: ADS, Average Distance Sources.

$$ADS = \frac{1}{N_{rps}} \sum_{k=1}^{N_{rps}} \|\mathbf{x}_k^{rps} - \mathbf{x}_k^{rs}\| \tag{3.10}$$

- x_k^{rps} is position of potential sources detected as real
- x_k^{rs} is the position of real sources

It is also possible to evaluate an dimensionless ADS by normalising with respect to the grid spacing in X and Y (supposing they are constant); this gives a distance in pixels.

$$ADS_{dim-less} = \frac{1}{N_{rps}} \cdot \sum_{k=1}^{N_{rps}} \sqrt{\left(\frac{x_k^{rps} - x_k^{rs}}{dist_x}\right)^2 + \left(\frac{y_k^{rps} - y_k^{rs}}{dist_y}\right)^2} \tag{3.11}$$

The last criterium is for the sound pressure level: ALO, Average Level Offset.

$$ALO = \frac{1}{N_{rps}} \cdot \sum_{k=1}^{N_rps} (SPL_k^{rps} - SPL_k^{rs}) \tag{3.12}$$

- SPL_k^{rps} is the Sound Pressure Level of the potential sources detected as real
- SPL_k^{rs} is the Sound Pressure Level of real sources

This last criterium gives the SPL difference between what the detection method has found and what is actually real; ideally it should be 0. Especially in low frequency this can be high. it will be seen more in detail later on this thesis.

Chapter 4

Anechoic Room Measurements

In this part we see the environment within which all the experimental data have been collected: the anechoic room from ISAE-SUPAERO has been used. This room allows echo-free measurements at medium or high frequency but passive wall treatment is less effective at low frequency and in practice no facility provides anechoicity below 50 Hz [8]. The ISAE-SUPAERO room is acoustically treated in the frequency range 80-16000 Hz and has dimensions of $5.02 \cdot 5.24 \cdot 5.34\ m^3$ $(L \cdot W \cdot H)$.

4.1 Arrays

Two types of microphone arrays have been used: a circular irregular array of 45 microphones (A_{45}) developped by Siemens and an optimised array (sun-flower distribution) of 120 microphones developped by MicrodB (A_{120}). The difference will be treated in part 5.3 in the array design. In the Figure 4.1 designs are shown.

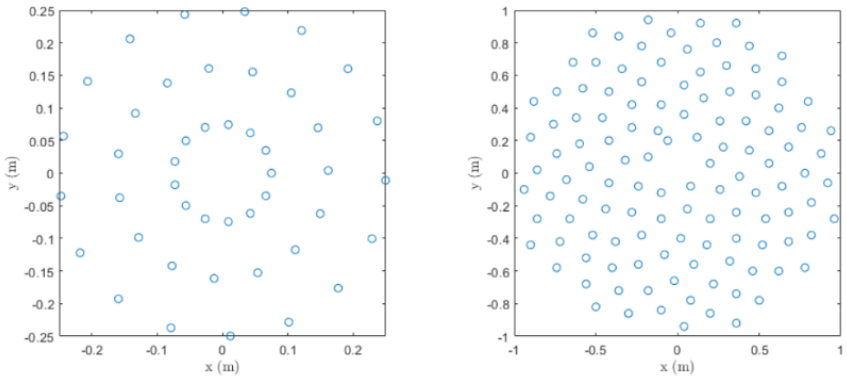

Figure 4.1: A_{45} on the left and A_{120} on the right [10].

Those arrays contain a camera with a wide angle lens on their centers which allows to take a picture of the source of interest and corrects automatically the picture for the wide angle distorsion. The microphones mounted on those arrays are 1/4 in. GRAS 40PH and acquisitions were performed at a sampling frequency of 51.2 kH z during 16.16 s [14]. These microphones are largely used in free-field measurements and acoustic localisation.
Each microphones distribution provides a different Main lobe to Sidelobe Ratio

(MSR), which is also called *dyn* or *dynamic range*: it is the difference between the maximum SPL and the Maximum Sidelobe Level (MSL)

$$dyn = MSR = SPL_{max} - MSL \tag{4.1}$$

MSR depends also on frequency. For the determination of this value at different frequencies for both arrays the monopolar source Q-MHF has been located at the center of the source plane. Distances between the source-plane and arrays were for A_{45} 1 m and 3 m for A_{120}. Values of MSR are in the table below.

Frequency [Hz]	A_{45}	A_{120}
200	20 (supplier)	16.7
2000	20(supplier)	16.7
20000	5	9

Table 4.1: Dynamic range (MSR) for different frequencies for both arrays.

In low frequencies cases sidelobes are out of aperture angles usually, for this reason suppliers' values are used.
In this Master thesis only array A_{120} will be used because it is more precise. Below the reader can see the A_{120} and sourceplane are usually located: at 3 metres without any tilt angle in most of the experiments.

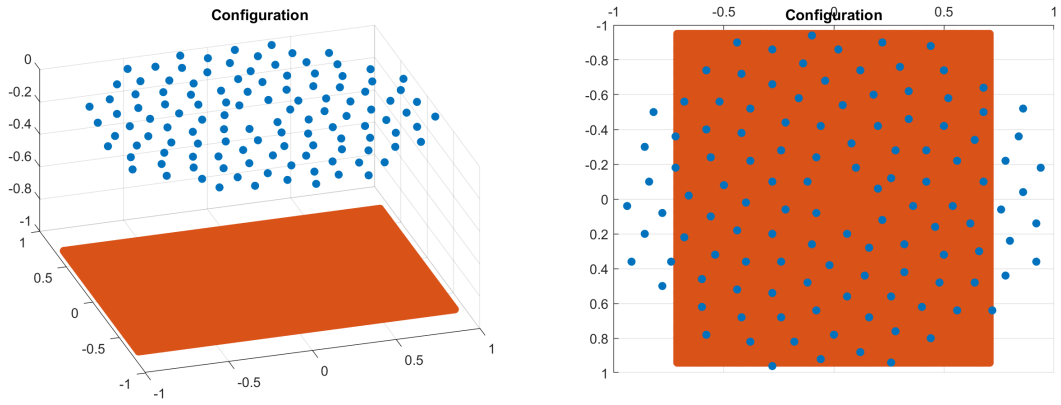

Figure 4.2: Array A_{120} and source plane.

4.2 Sources

Three sources have been used in this study, one monopolar LMS Q-MHF, which is usually used for noise and vibration, and two BMS coaxial neodynnium drivers type 4592ND. To allow source localisation post processing at different frequencies, a white noise on the frequency range 100-20000 Hz was used as a generation signal [14]. In addition the two identical sources allow to study different source correlation by sending them a white noise signal with different phase relationships. During this job the different types of sources have been written as S1 or S2 (see Figure 4.3).

Figure 4.3: S1 on the left and S2 on the right [10].

4.2.1 S1

S1 is considered as quasi-monopole *Mid High Frequency Source*; Q - MHF. This source is composed by a compressive room linked to a tube of radius 1.5 cm and 6 m in length, which end with a small cone with 1 cm diameter. Due to the small dimension of the cone it is possible to consider S1 as a monopole in the frequency range (150 - 10000) Hz [10]. Neverthless length of the tube makes a strong attenuation of the sound level at high frequency.

4.2.2 S2

S2 is *Coax Neo Compression Driver* type, at high frequency because it becomes directive. It has as well a compression room and it has a wide plate response (300 - 22000 Hz). This source has the advantage of producing high sound levels, which can help at higher frequencies, considering however how more directive it becomes.

4.3 Experimental Configurations

This thesis relies on different configurations used previously by Jomain (see [10] for more details) in his work. The different configurations to obtain beamforming (BF) maps are in the itemize below:

- Frequencies in Hz: 200, 2000 or 20000 (low, medium and high)
- Sources number: 1, 2 or 3
- Array configuration: A_{45} or A_{120}
- Sources position in the grid. See the table 4.2 below.
- Sources correlation: uncorrelated (D) or correlated in phase (P) or in phase-opposition (A).
- Sources relative sound pressure level (SPL): with or without attenuation of S2
- Distance between array and source planes

- Reverberation or diffraction effects: 1 plate inclined at 0° or 45° of 2 plates with those angles.
- Tilt angle between array and source planes

Study cases are a combination of the items above.
Table 4.2 gives the example of sources positions for the configurations with three sources (S1 and two sources S2).

Configuration Source	**S1**	**S2-1**	**S2-2**
1	(0;0)	(-0.5;0.25)	(-0.23;0.25)
2	(0;-0.22)	(0.07;-0.29)	(-0.28;-0.15)
3	(-0.55;0.255)	(0.07;-0.17)	(-0.29;0.03)
4	(0;0.21)	(0.18;-0.31)	(-0.18;-0.31)
5	(0.12;-0.265)	(0.265;0.11)	(-0.265;0.11)
6	(0.415;0.19)	(0.165;-0.3)	(-0.36;-0.07)
7	(-0.42;-0.015)	(0.35;0.25)	(0.09;-0.32)

Table 4.2: Different configurations of sources position.

More details on the sources configurations and positions can be found in Appendix A.

4.4 Sound Pressure Level

In [10] there are spectra for both types of source (S1 and S2) to evaluate the influence of the sound pressure level, which is the level at which sources emit the white noise signal. Each study case corresponds to a SPL in dB: a base SPL and SPL with a relative attenuation of sources S2 respect to the base level. This allows to study the ability of source localisation to identify S1 source at high frequency with the presence of S2 sources with different relative SPL.

Chapter 5

Experimental Results

In this chapter we take a look at all the different sources configurations we have had by the anechoic room and see the influence of different parameters. Using these test cases with known sources, the performances of different source localisation algorithms are assessed. The first and bigger part is dedicated to conventional beamforming, the second part to CLEAN-SC and the third one to the algorithm using the correlation with a reference sensor. The last part focus on the performance assessment of the 3 algorithms on an aeroacoustic test case.

5.1 Conventional beamforming

To have a clearer idea of the influence of different parameters only the fusion with big axis methodology will be used to assess the conventional beamforming performances: big axis has showed to be faster than without and, coupled with Metropolis-Hastings, can be useful and interesting.

5.1.1 Frequency effect

The caption of the measures has been done by using a white noise in frequence between 100 and 20000 Hz to have a constant PSD over frequency; only frequencies of 200, 2000 and 20000 Hz will be considered in all study cases.
However, to see how frequency influences source maps and detection sources capabilities we take a look at different frequencies: 200, 1000, 2000, 4000, 8000, 16000 and 20000 Hz; in this way we have all cases from low to high frequency domain. We have a monopole source (S1) in the center of the grid (0;0) which is in free field, the SPL is at base level and there is a distance source-array of 3 m. Results are in the following maps Figures 5.1 to 5.7.

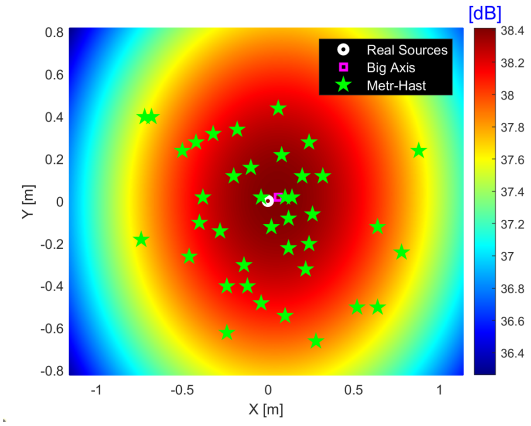

Figure 5.1: a) 200 Hz

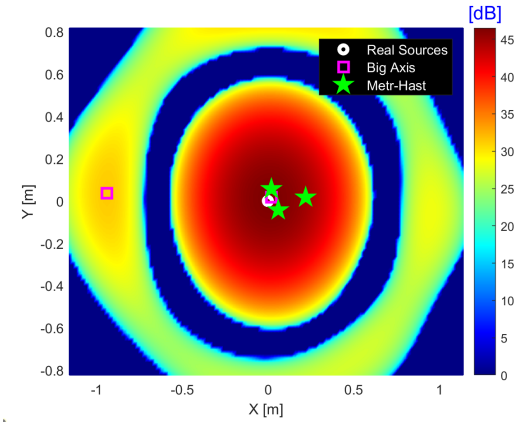

Figure 5.2: b) 1000 Hz

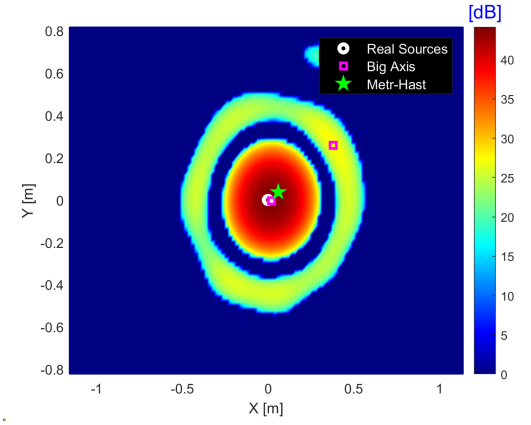

Figure 5.3: c) 2000 Hz

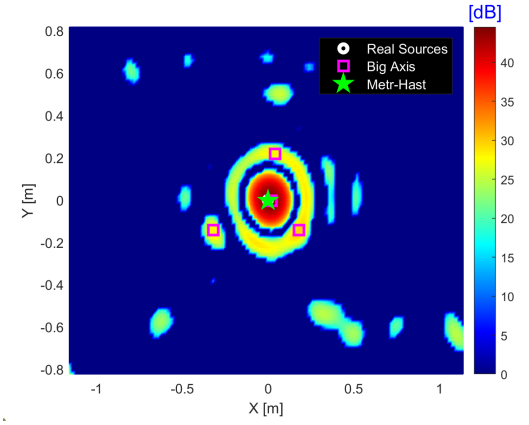

Figure 5.4: d) 4000 Hz

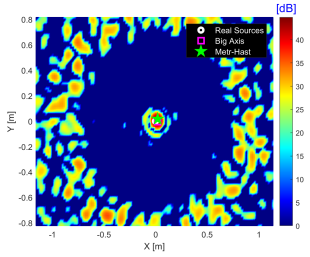

Figure 5.5: e) 8000 Hz

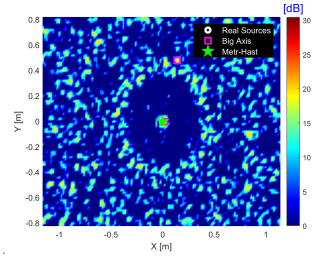

Figure 5.6: f) 16000 Hz

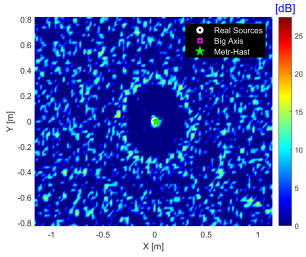

Figure 5.7: g) 20000 Hz

One of the first thing we can see is the reducing number of potential sources found by Metropolis-Hastings until it does not find any of them at high frequencies.
It is also noted that by increasing the frequency secondary lobes become smaller and more numerous. In addition resolution decreases with the frequency: this means that it will be simpler to recognize two different sources closed at high frequencies (see Figure 3.14).
In the Figures 5.8 and 5.9 we can see how resolution and frequency affected perfromances criteria:

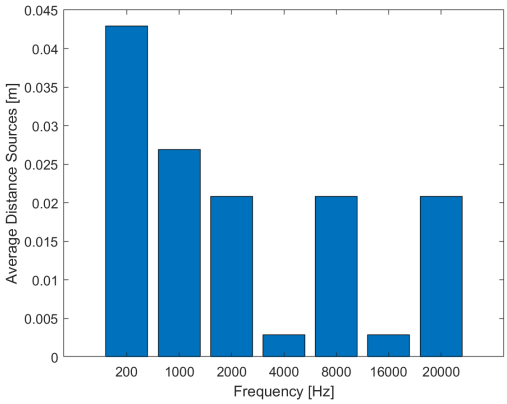

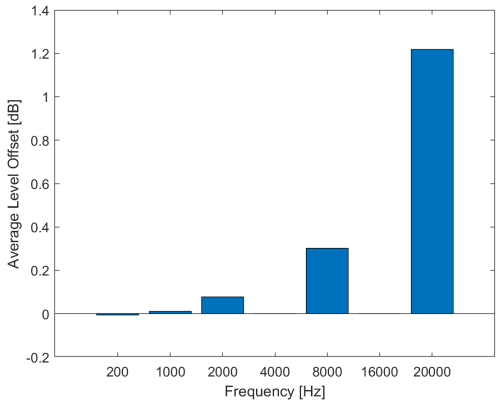

Figure 5.8: ADS for different frequencies. Figure 5.9: ALO for different frequencies.

First of all, as it is possible to see from images above, in every situation real source is found ($C_{nr} = 1$) [14]. At low frequency where there is a big region at similar SPL and there are several potential sources (spatial resolution is big [14]), ALO can be low and distance from the real source big; increasing the frequency the situation stabilises with an ADS around to 0.02 m, which is the grid space here. At 4 and 16 kHz systematic methodology finds exactly the source: distance is very low and same ALO. Apart of them situation at high frequencies stabilizes in distances from the source but ALO tends to increase: this is probably due to a general decrease of SPL on the maps and also that a source is more confined in a small region than at lower frequencies, so even if a detected source was close it would have a big difference is ALO.
Number of sidelobes increases with frequency, but systematic analysis has the capability to find only the real source with frequency increasing [14].

5.1.2 Array size

Here it is possible to see the difference between source maps obtained with an array of 45 microphones and one of 120 microphones for the source S1 at the center of the source plane at 2000 Hz (see Figures 5.10 and 5.11).

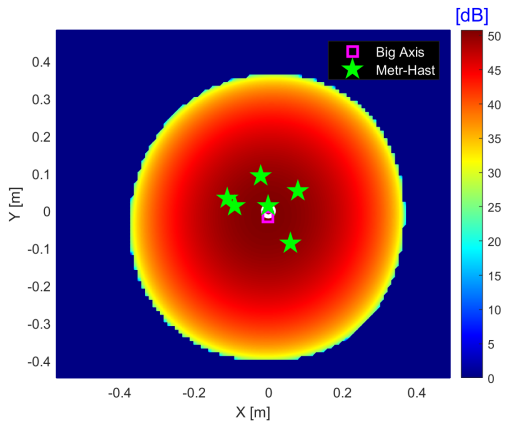

Figure 5.10: A_{45}

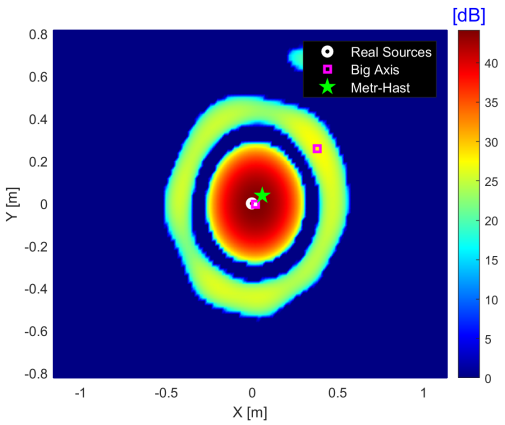

Figure 5.11: A_{120}

Both have the capability to find the correct source at the center [14]. A_{45} has a

worse resolution and it can affect in a different way the systematic analysis: in the same configuration and at the same frequency A_{45} finds more ghosts sources than A_{120}, which is more precise so. For this reason A_{120} is used in the following parts .

5.1.3 Sources' number

The number of sources in study cases varies between 1, 2 or 3: a Q-MHF monopolar source (S1) at the center and successively 1 or 2 additional uncorrelated CNCD sources (S2) [14].

1 source (S1)

With the monopole source S1 at the center, the systematic performance assessment method highlights the poor spatial resolution at 200 Hz with a lot of potential sources (high C_{nt}), whereas C_{nt} is close to 1 for higher frequencies. The real source S1 is found in all cases ($C_{nr} = 1$) with a good accuracy in terms of position.

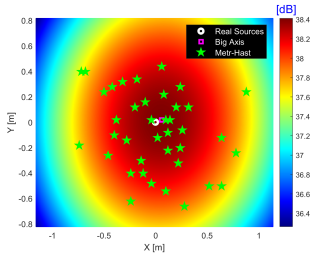

Figure 5.12: S1, 200Hz

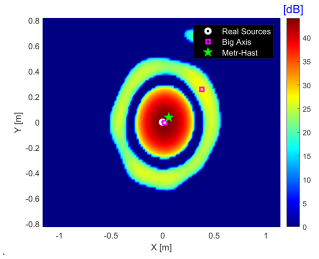

Figure 5.13: S1, 2000Hz

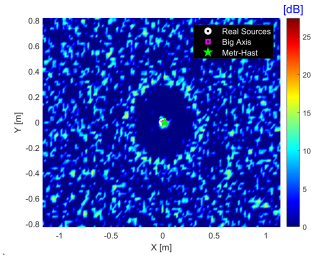

Figure 5.14: S1, 20000Hz

2 sources (S1S2)

In the case of two sources, it can happen sometimes that two sources and ghosts sources are found or just one of the two sources due to their proximity (they are not distinguished), especially at low frequencies due to the low spatial resolution. This is illustrated in the following for uncorrelated sources S1 and S2 at different frequencies and locations.

200 Hz:

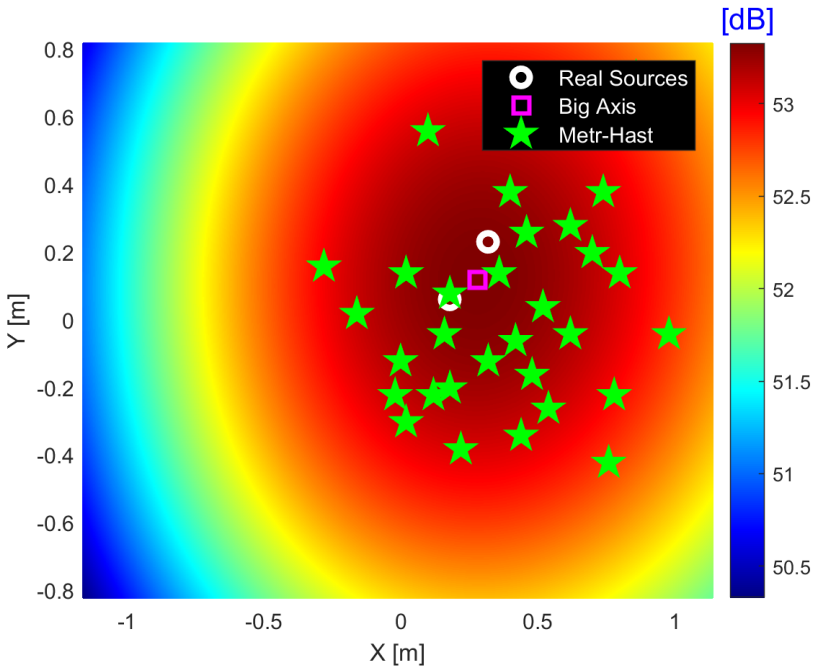

Figure 5.15: Two uncorrelated sources S1S2 at 200 Hz.

At low frequency Figure 5.15 results are similar to those obtained with the source S1 alone (Figure 5.12): many potential sources are found (high C_{nt}), so many ghost sources. This highlights the fact that low spatial resolution of conventional beamforming does not allow to obtain source maps able to distinguish to close sources.

2000 Hz:

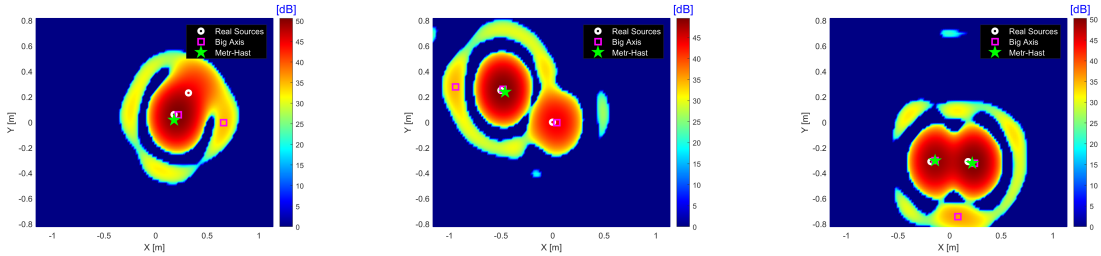

Figure 5.16: Two uncorrelated sources S1S2 at different locations at 2000 Hz.

As we can see detection method does not always find 2 real sources, as shown in the first figure: one of the 2 sources has low SPL compared to the other one and so it is not found. In case of two well distinguished sources, like in figure in the center, or 2 close sources at similar SPL like in figure on the right two sources are well detected.

20000 Hz:

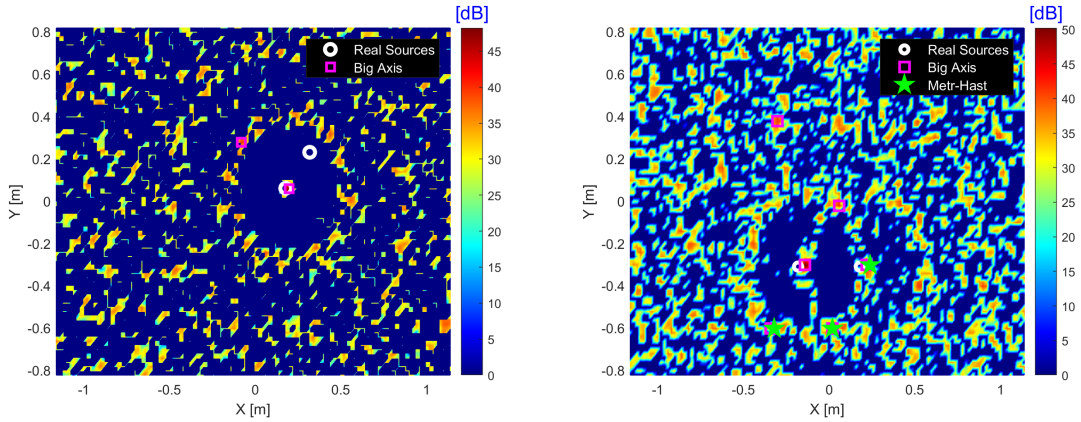

Figure 5.17: Two uncorrelated sources S1S2 at different locations at 20000 Hz.

At high frequency at least one of the two real sources are identified by the systematic performance analysis method ($C_{nr} = 0.5$ or 1). As the spatial resolution of the conventional beamforming is improved at high frequencies the case where one real source is not identified is associated with a lower SPL.

3 Sources

This part presents the analysis of the quality of conventional beamforming maps for three uncorrelated sources (S1 and two sources S2) at different frequencies and locations.

200 Hz: At low frequencies the low spatial resolution of conventional beamforming leads to perfromances similar in the case of one, two or three real sources (see Figure 5.18).

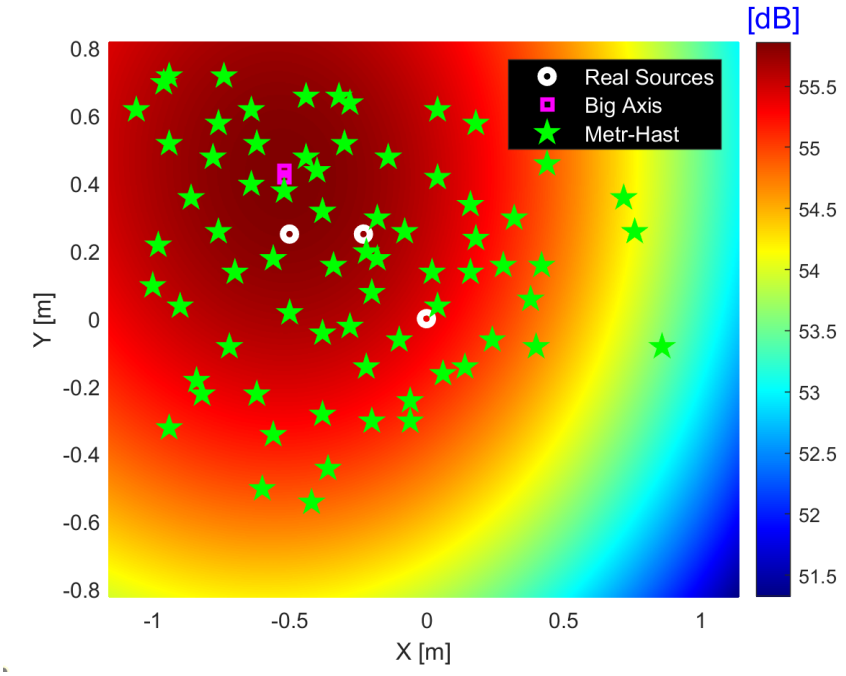

Figure 5.18: Three uncorrelated sources S1S2S2 at 200 Hz.

2000 Hz: Most of the times systematic analysis finds the three real sources ($C_{nr} = 1$), but can happen sometimes it finds just two of them ($C_{nr} = 0.66$). However it always finds at least two sources out of three.

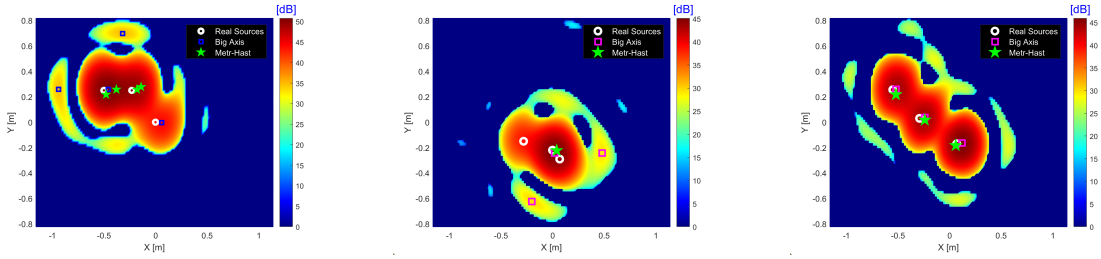

Figure 5.19: Three uncorrelated sources S1S2S2 at different locations at 2000 Hz.

Figure 5.19 on the left represents a case in which the conventional beamforming allows to obtain a map where the three real sources are clearly visible ($C_{nr} = 1$), but two ghosts sources are also present ($C_{nt} = 1.66$). Figure in the center instead shows a case where there are two real sources really closed which create an area at high SPL: this can hide the third source and consequently it is not detected. In the last Figure real sources are more distributed and well separated and detected by the conventional beamforming algorithm.

20000 Hz:
At high frequency most of the times the three real sources can be identified on the conventional beamforming maps but additional potential sources can be also visible due to increase of sidelobes with the frequency. Here two cases are shown (Figure 5.20).

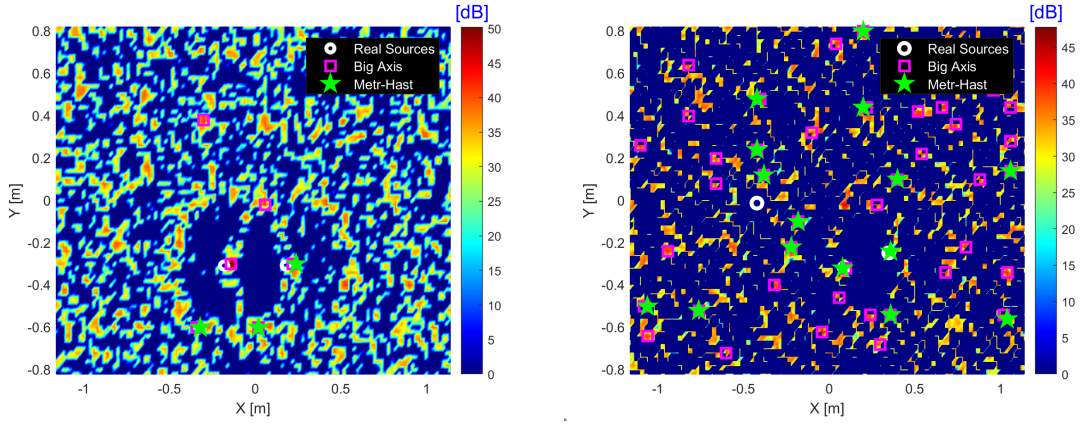

Figure 5.20: Three uncorrelated sources S1S2S2 at different locations at 20000 Hz.

Conclusions

From these examples the systematic analysis allows to see how the number of sources can affect the quality of conventional beamforming maps: in case of sources really closed one source can not be visible on the map, especially at low frequency where the spatial resolution is low. When one of the sources has a stronger SPL, this can make the others not clearly visible on the maps. Ideally if there is one source in the

map it is always found; more than one it becomes usual to find all sources and not anymore certain.

5.1.4 Distance between Sources

In this section it will be shown how distance between two real sources can affect the capability of clearly identify each real source on conventional beamforming maps. All cases studied in this part concern two uncorrelated sources at 2000 Hz, the variable being the relative distance between the two real sources (see Figure 5.21).

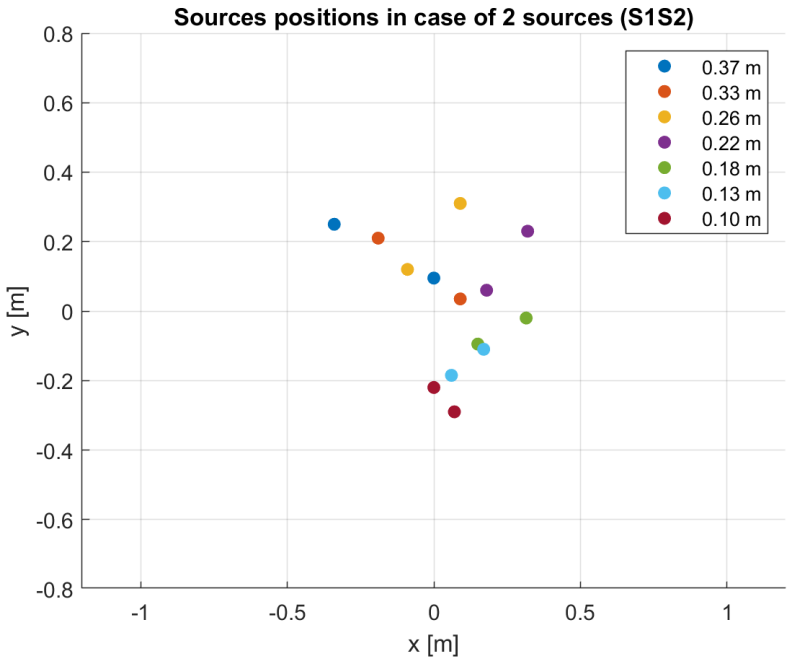

Figure 5.21: Sources Position.

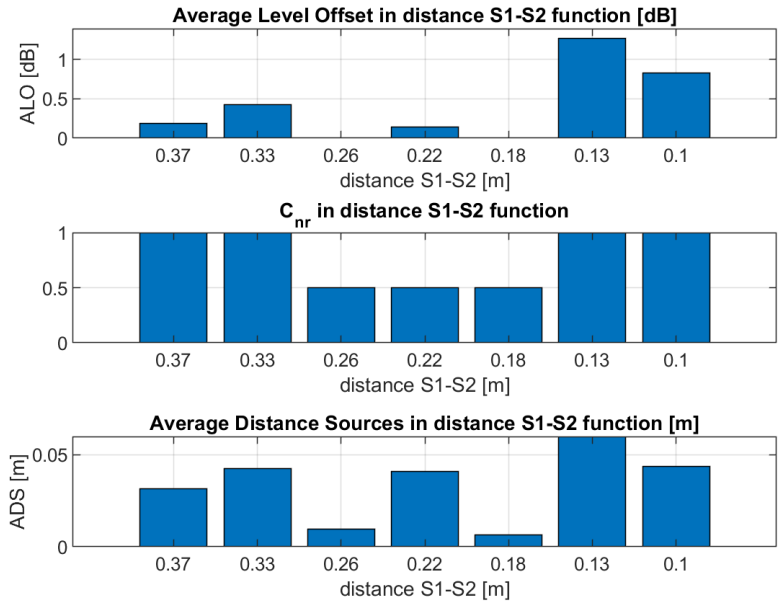

Figure 5.22: Sources distance influence on the performance criteria for unconventional beamforming.

Figure 5.22 presents the performance criteria for unconventional beamforming maps respect to the distance between two real sources. For distances 0.13 and 0.1 m in truth the beamforming maps show only one big source area of high SPL due to low spatial resolution, and thus the systematic analysis finds two sources closer to one than in between them (see figures 5.23 & 5.24)leading to $C_{nr} = 1$, but C_{nr} could be considered 0.5 in these two distances.

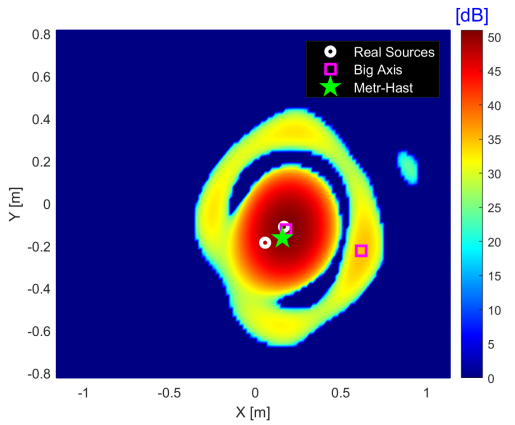

Figure 5.23: Two uncorrelated sources S1S2 at distance 0.13 m at 2000 Hz.

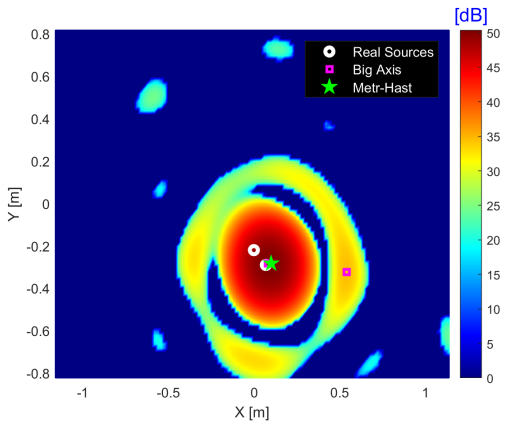

Figure 5.24: Two uncorrelated sources S1S2 at distance 0.1 m at 2000 Hz.

Looking at these cases and after these considerations we can say that the capability of the conventional beamforming algorithm to find two real sources decreases if the distance between them decreases as well: C_{nr} changes value from 1 to 0.5. When the two real sources are too close, one of the real sources can be identified two times by the systematic analysis, this leads to an increase of the inaccuracy of sources location and level (criteria ADS and ALO).

5.1.5 Correlation

Sources correlation is important to understand how they influence the quality of beamfoming source maps. One of the hyphotesis of beamforming is that there is no phase correlation between the sources to apply a *Delay-and-Sum* approach [14]. In this section we are going to see what happens if this hyphotesis is not respected. We will use two and three real sources configurations (S2S2 and S1S2S2) and cases where the two sources S2 are correlated in phase or in phase opposition. See the Table A.2 of appendix A to have more details on all the tested configurations.

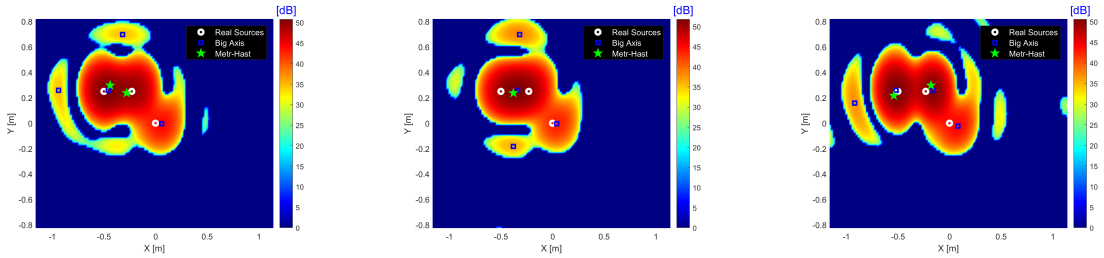

Figure 5.25: Three sources S1S2S2 at fixed location at 2000 Hz with the two sources S2: uncorrelated (left), in pahse (center) and in phase opposition (right).

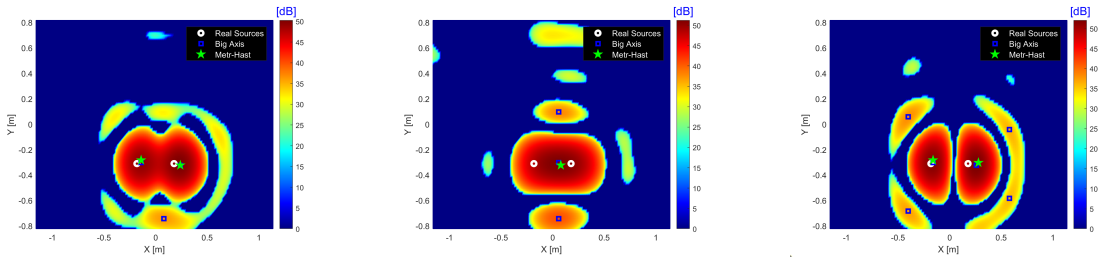

Figure 5.26: Two sources S2S2 at fixed location at 2000 Hz with the two sources S2: uncorrelated (left), in phase (center) and in phase opposition (right).

Figures 5.25 and 5.26 have been obtained at frequency 2000 Hz. Looking at the cases where two sources S2 are in Phase (**P**) the conventional beamforming does not distinguish anymore the sources: it finds something in the middle of two in both cases ($C_{nr} = 0.5$ or 0.66). In case of Phase-Opposition (**A**) situation is better: the real sources are well distinguished ($C_{nr} = 1$) and also some ghosts disappear for the three sources configuration; their number increases in 2 sources configuration however probably due to the symmetry.
In case of uncorrelation (**D**) conventional beamfoming finds properly real sources ($C_{nr} = 1$) plus a few ghosts sources.

At high frequency (20000 Hz) situation changes on the number of ghost sources we get (see Figures 5.27 and 5.28). Resolution has been changed from 0.0592 m to 0.0827 m to let to find any sources for configuration with two sources: with two sources. On contrary any sources would have been found making difficult a possible comparation.

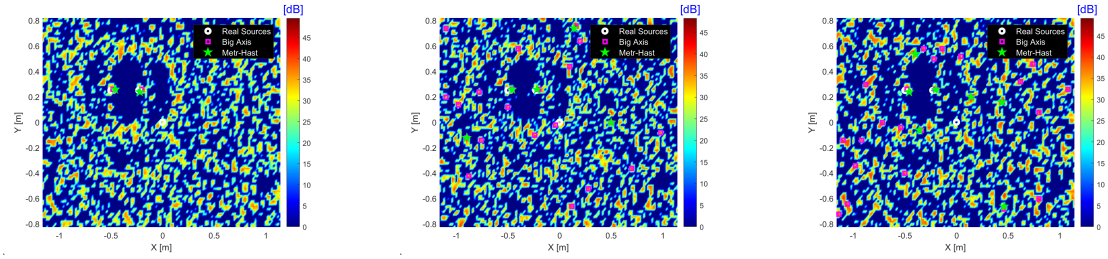

Figure 5.27: Three sources S1S2S2 at fixed location at 20000 Hz with the two sources S2: uncorrelated (left), in phase (center) and in phase opposition (right).

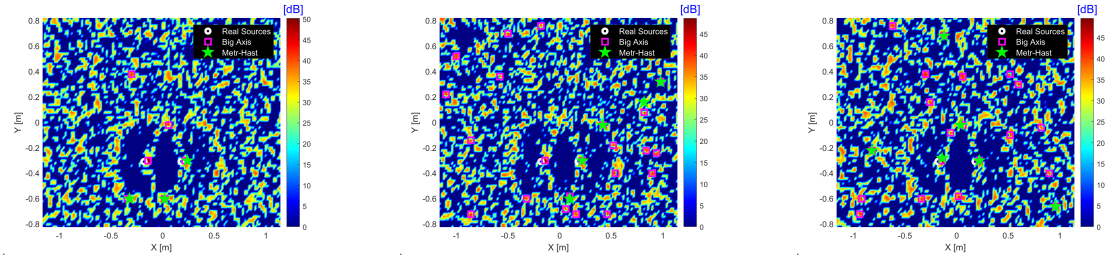

Figure 5.28: Two sources S2S2 at fixed location at 20000 Hz with the two sources S2: uncorrelated (left), in phase (center) and in phase opposition (right).

To better see the increasing number of ghost sources on conventional beamforming source maps, Table 5.1 below shows C_{nt} values for the configurations with 2 and 3 real sources and with 2 sources S2 uncorrelated, in phase and in phase opposition.

$\mathbf{n_{sources}}$	**Correlation**	$\mathbf{C_{nt}}$
3	D	1
3	P	7
3	A	10
2	D	3.5
2	P	13.5
2	A	11.5

Table 5.1: C_{nt} at 20000 Hz

There is something in common with the configuration at 3-sources: one source is never detected, it is the one always uncorrelated from the other two. This source is **S1** and, as written before, it works properly in frequency range 150-10000 Hz. So, at 20000 Hz, it will be never detected because its SPL at this frequency is lower than the ones of S2 sources. This result is common at other position-configurations. Figures 5.29 to 5.33 present a summary of all conventional beamforming performances criteria respect to the S2 sources correlation for the different frequencies.

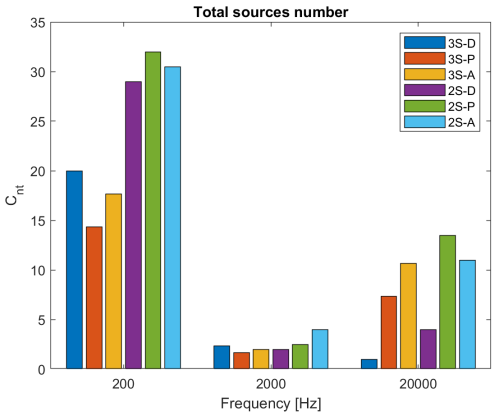

Figure 5.29: C_{nt}

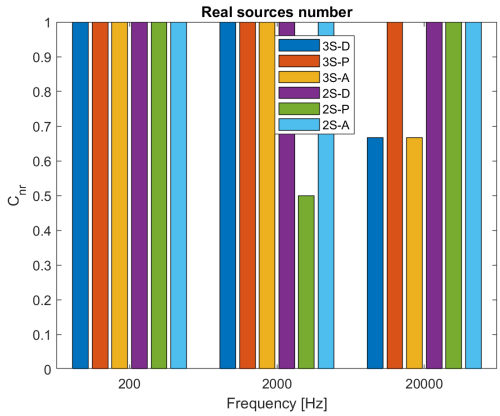

Figure 5.30: C_{nr}

We can see in figure 5.29 and table 5.1 at high frequency if there is correlation between sources S2, more ghost sources will be found.

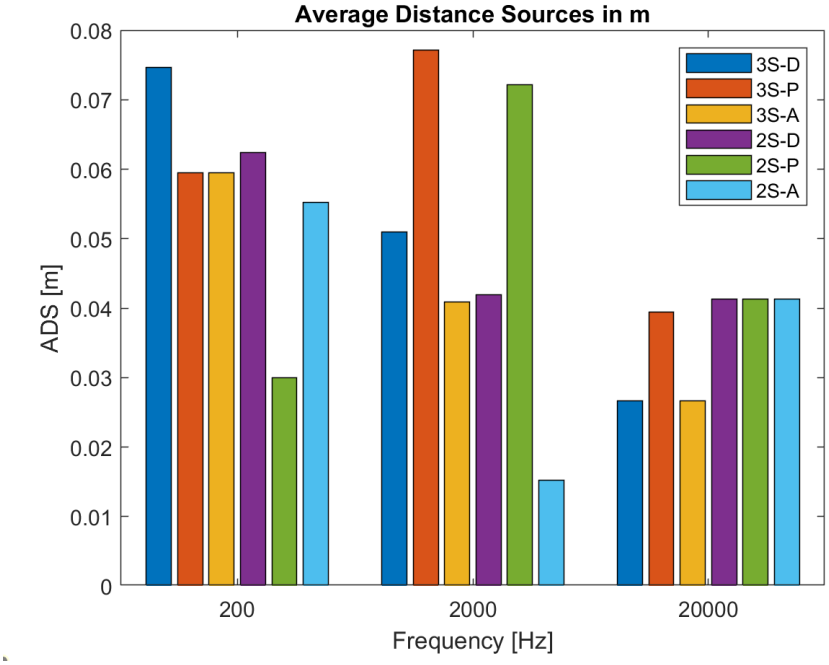

Figure 5.31: ADS in metres

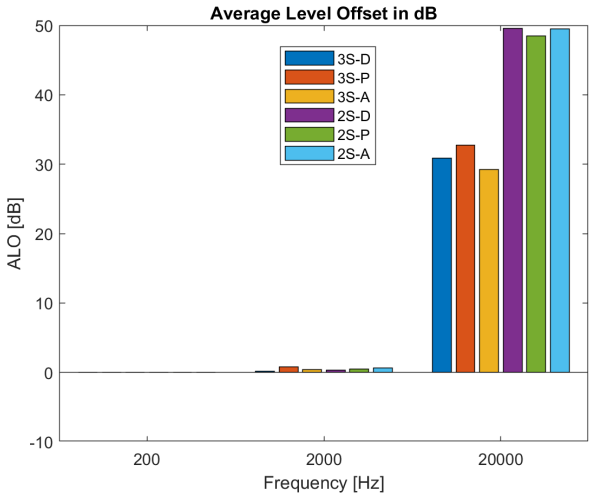

Figure 5.32: ALO in dB

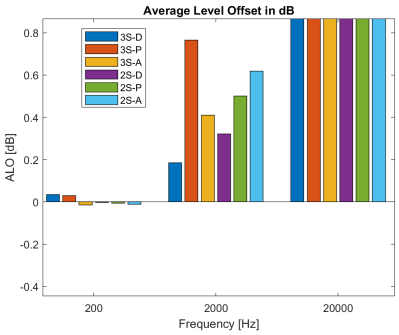

Figure 5.33: ALO - zoom

At low frequency distance between source (ADS) decreases with the correlation in sources, at mid frequency if the correlation is in Phase ADS is going to increase and at high frequency there is nothing we can say about.
At high frequency ALO remains constant with correlation; at mid frequency ALO increases if there is correlation: for Phase correlation a region at stronger SPL is created and systematic analysis goes to find potential sources at the center of it. Nevertheless this region has real sources at borders, so ADS and ALO increase.

5.1.6 Reverberation

It is sound interaction with surfaces and is responsible for the creation of echoes. It usually happens when there are sound-reflective walls as some plates. Here wood panels of 2.44*1.22 m were used and positioned behind the source plane [14]. In most of the study-cases there is not reverberation, but in one configuration with three uncorrelated sources S1S2S2 this situation has been analyzed: with no plate, with one plate at 45°, one at 0°, 2 plates at 0° and 45° and this later with 3 additional obstacles between the microphone array and the panels (see Figures 5.34 to 5.36). Comparison is attuated with respect to no-plate case, which is the equivalent case without reverberation.

2000 Hz

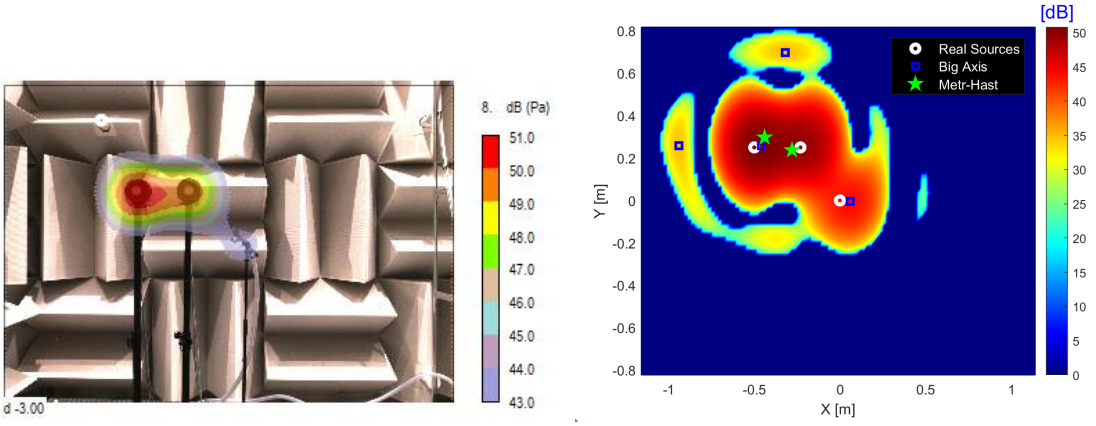

Figure 5.34: Three uncorrelated sources at 2000 Hz: no plate.

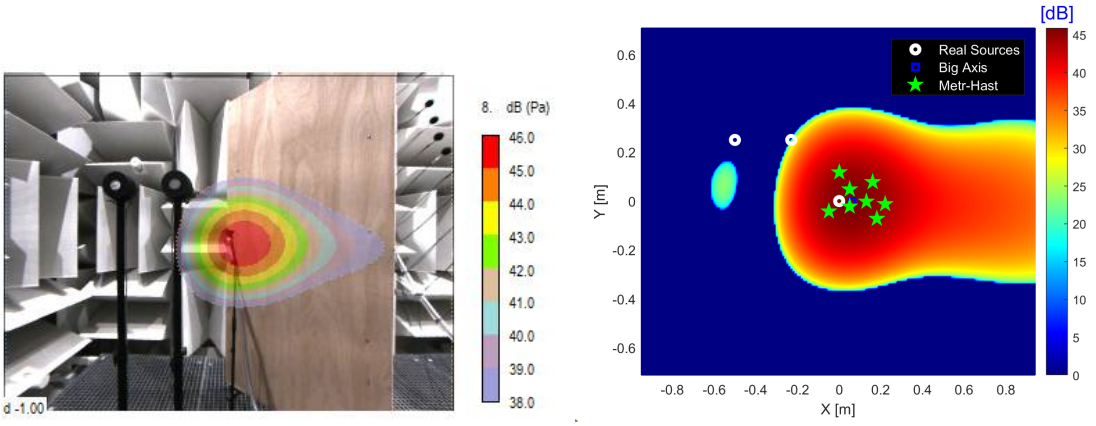

Figure 5.35: Three uncorrelated sources at 2000 Hz: 1 plate at 45°.

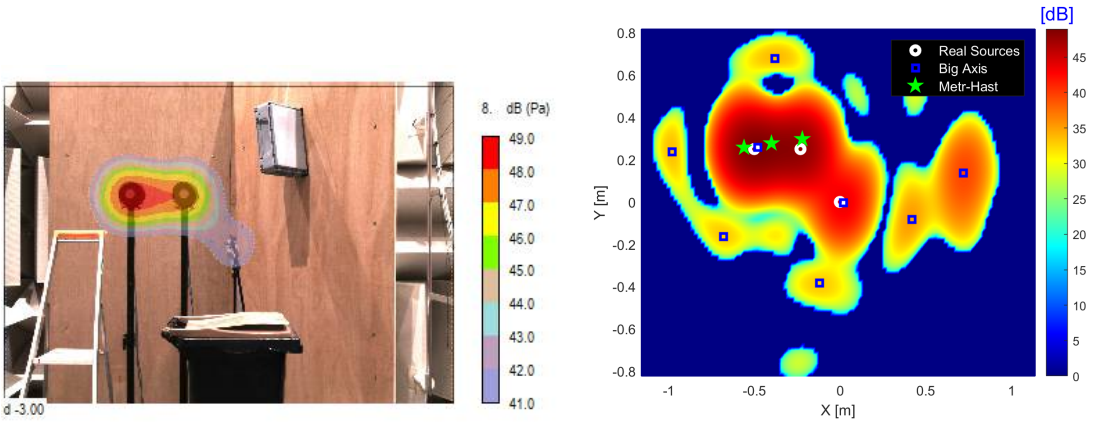

Figure 5.36: Three uncorrelated sources at 2000 Hz: 2 plates at 0° and 45° 3 obstacles.

The case with the plate at 0° is not presented because the source map is very similar to the one without plate apart a small area on the right. Inclining the plate at

45° (fig 5.35) only the real source S1 can be identified on the map and this source area is extended on the right towards the plate: beamforming solve the acoustic problem thinking there are acoustic sources which do not exist for real. The case with one plate at 0° and one at 45° is not presented here, but the map shows three real sources with ghost sources with relatively high SPL, especially on the right side where the plate is inclined at 45°. Obstacles (fig 5.36) are seen as acoustic sources which disturb sound propagation and they are identified as additional ghost sources.

20000 Hz

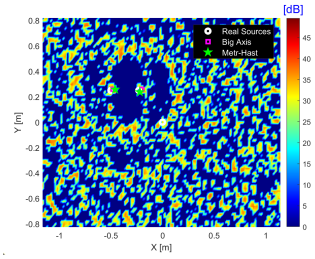

Figure 5.37: Three uncorrelated sources at 20000 Hz: no plate.

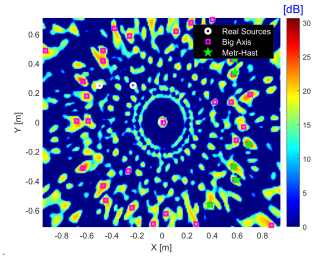

Figure 5.38: Three uncorrelated sources at 20000 Hz: 1 plate at 45°.

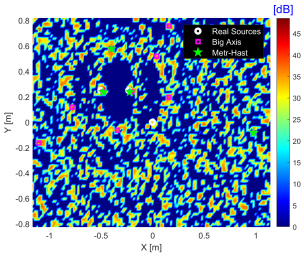

Figure 5.39: Three uncorrelated sources at 20000 Hz: 1 plate at 0°.

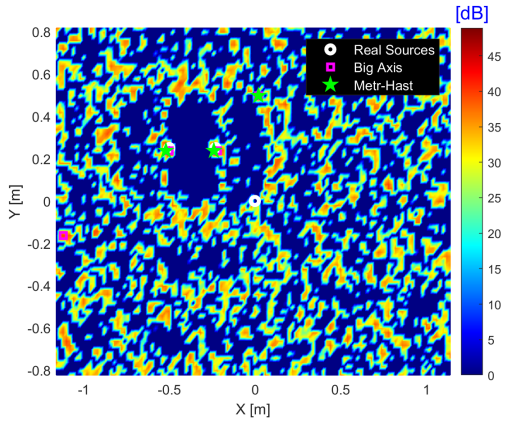

Figure 5.40: Three uncorrelated sources at 20000 Hz: 2 plates at 0° and 45° and 3 obstacles.

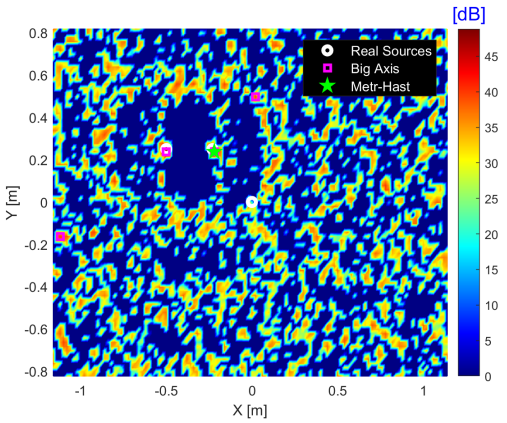

Figure 5.41: Three uncorrelated sources at 20000 Hz: 2 plates at 0° and 45°).

At higher frequency only the case where there is one plate at 45° presents a different map; the rest is similar. It looks like a plate at 45° can point toward one source which is the less powerful at that frequency: putting a wall at 45° corresponds to have a mirror or not having anything apart of another source symmetrical with signals; result is to have constructive interferency in the centre of the map. This phenomenon does not occur with plate at 0° because it points toward the two more powerful emphasizing them.
Figures 5.42 to 5.46 present a summary of all conventional beamforming criteria respect to the different propagation conditions (free field, plates withwithout obstacles) for the different frequencies.

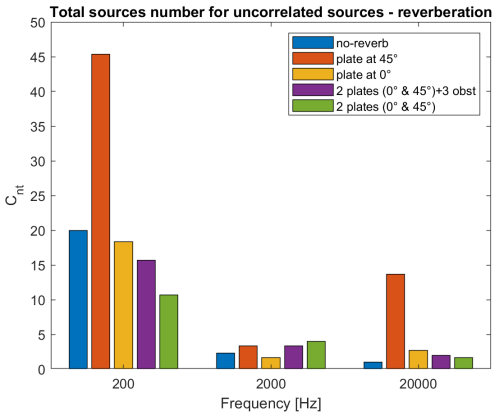

Figure 5.42: C_{nt}

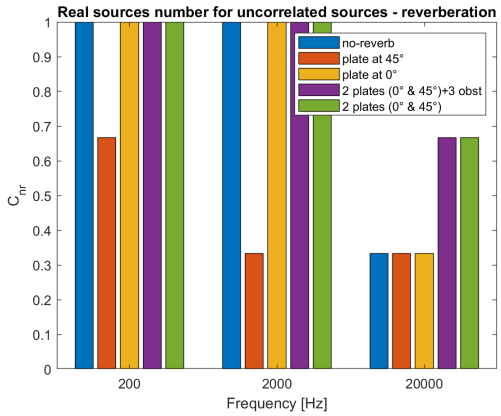

Figure 5.43: C_{nr}

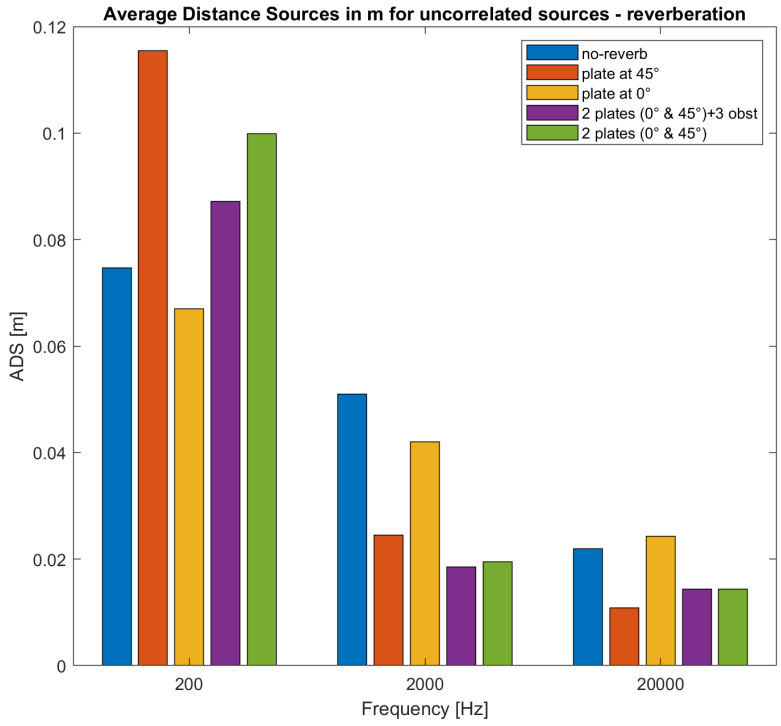

Figure 5.44: ADS in metres

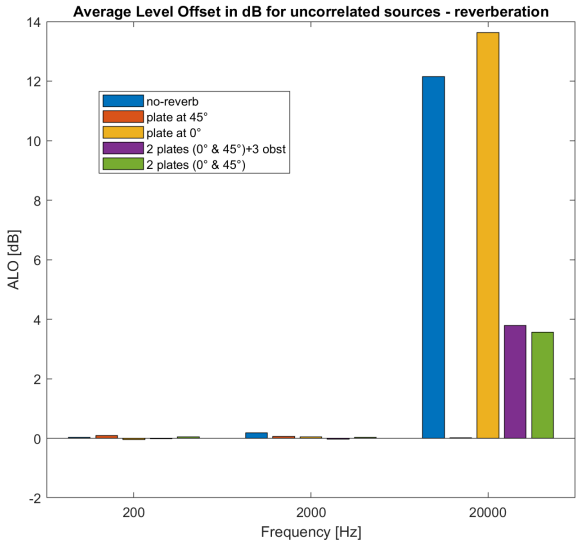

Figure 5.45: ALO in dB

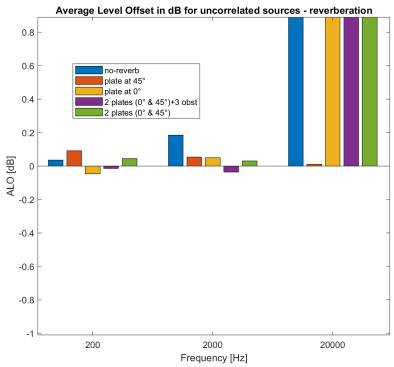

Figure 5.46: ALO - zoom

Conclusions

As conventional beamforming considers a free field propagation, image sources appear on the source map additionally to sidelobes when reflective panels are added and are identified as potential sources by the systematic analysis method [14].
Low frequency case with plate at 45° is the only one not to find all three sources and distance from sources found is even the biggest. This latter condition can be seen also in case of two plates where ADS increases from cases at no reverberation or plate at 0°.
For mid frequency, like in high frequency, with a plate at 45° it is possible to find only one source at the center of the map. Total number os sources found is more or less the same, but only for plate at 45° it finds one source. Looking at Figures 5.44 and 5.45 it is possible to observe how in case of reverberation systematic analysis can find closer sources to the real ones.
At high frequency, apart of plate at 45°, comparing figures 5.37 and 5.39 with figure 5.43 there is resolution problem: it is not big enough to detect a source. However with two plates and obstacles situation improves and we are able to find both two sources at closer distance and SPL (see figures 5.44 and 5.45).

5.1.7 Reverberation and Correlation

Here two parameters that do not correspond to conventional beamforming assumptions are studied together: correlation and reverberation. For this part the configuration with 3 sources S1S2S2 already used in the two previous parts will be treated. Correlation between the two sources S2 will be uncorrelation (**D**), correlation in Phase (**P**) and correlation in Anti-Phase (**A**); Reverberation will be treated in case it is not present, if it is present with a plate at 45° or at 0°, if both are present with or without obstacles.
Figures 5.47 to 5.53 present a summary of all conventional beamforming preformances criteria respect to the combination of S2 sources correlation and reverberation for the different frequencies.

Conclusions

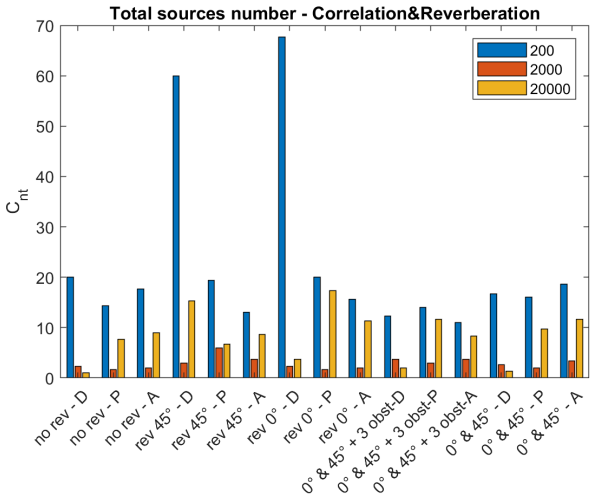

Figure 5.47: C_{nt}

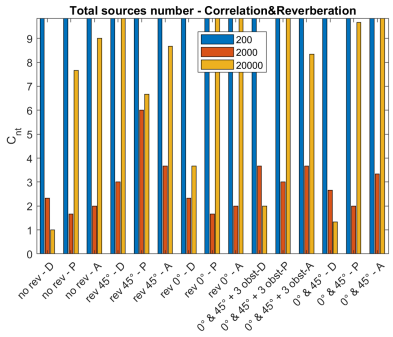

Figure 5.48: C_{nt} zoom

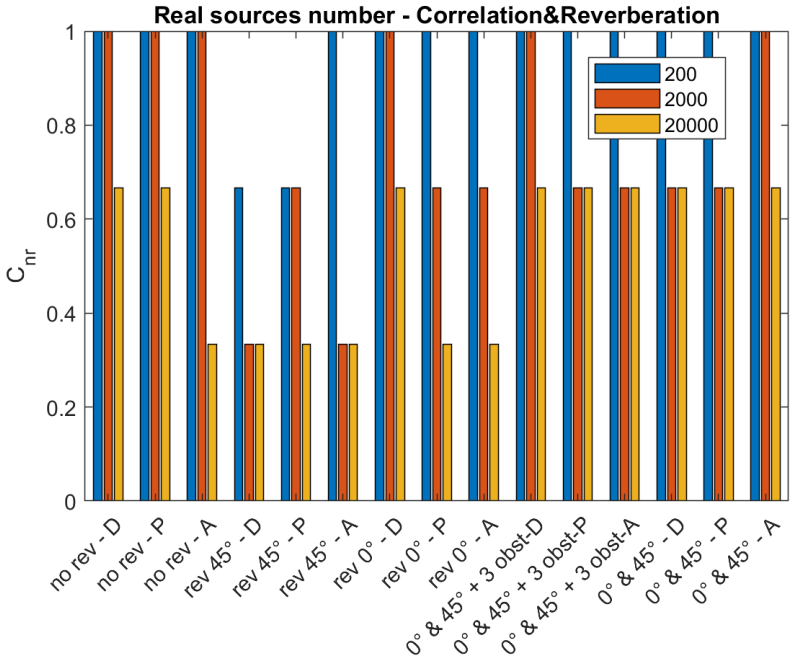

Figure 5.49: C_{nr}

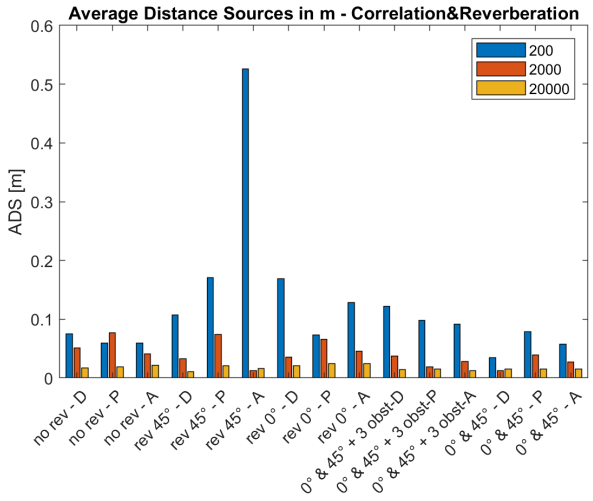

Figure 5.50: ADS in metres

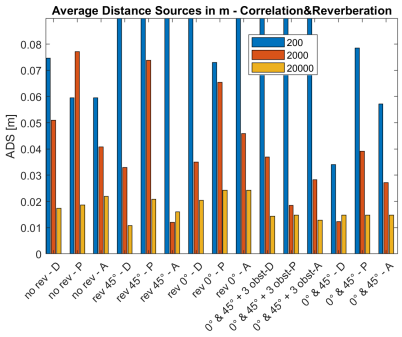

Figure 5.51: ADS - zoom

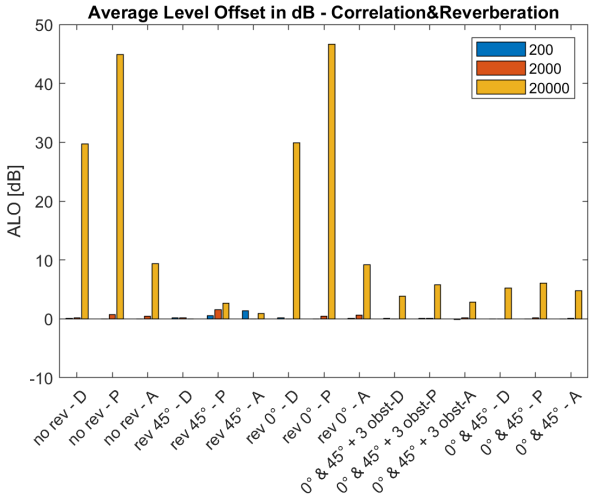

Figure 5.52: ALO in dB

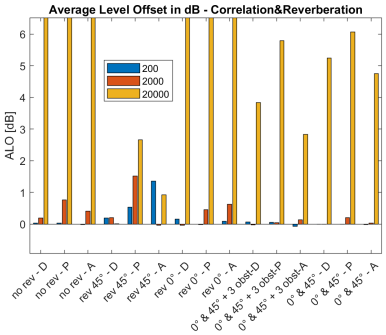

Figure 5.53: ALO - zoom

The purpose was to see how beamforming performances have been degraded if its hypothesis were not respected. Results are a combination of the two parameters together: reverberation at 45° leads to find closer sources and so lower ALO; reverberation at 0° does not affect particularly: it finds even more sources (C_{nt} for all frequencies). Combining the two together without any obstacles C_{nt} remains as for the case without reverberation, so C_{nr}, but ADS and ALO tend to decrease. Combining them with obstacles ADS at low frequency tends to increase, but not for the other frequencies. However using obstacles there is a reduction even bigger in ALO for all the frequencies. Correlation contributes in general to have less sources identified at low frequency. In case of Phase correlation (P) ADS and ALO tend to increase for each frequency, in case of Phase-opposition (A) ADS and ALO tend to increase at low frequency and decrease for other frequencies. Correlation can be also used to point out all sources: looking at criteria is not appreciable because C_{nr} remains almost the same for the same cases of reverberation, but Phase (P) and Phase-opposition (A) find often two different sources, especially at 2000 Hz.

5.1.8 Sound Level

Sources usually emit in our cases at base sound pressure level, which leads to higher levels for sources S2 respect to source S1, especially at high frequencies. In this section we are going to see what is the impact on the conventional beamforming source maps if sources S2 emit at lower sound pressure level. Configurations with two (S1S2) or three (S1S2S2) uncorrelated sources without reverberation are considered. In case of three sources both s2 have sometimes a lower sound pressure level.
Figures 5.54 to 5.60 show examples of the impact of S2 sound pressure levels on beamforming source maps for three sources at different frequencies. In this case the source S1 is in the center of the source plane and the lowering of sources S2 SPL allows to distinguish S1 on maps ($C_{nr} = 1$) for mid and high frequencies, whereas it was not the case with the base SPL ($C_{nr} = 0.66$).

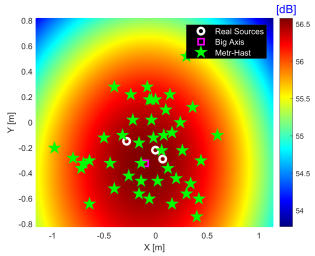

Figure 5.54: 200 Hz

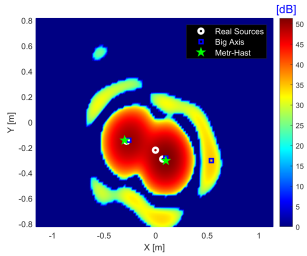

Figure 5.55: 2000 Hz

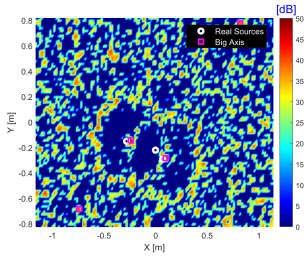

Figure 5.56: 20000 Hz

Figure 5.57: Base sound level.

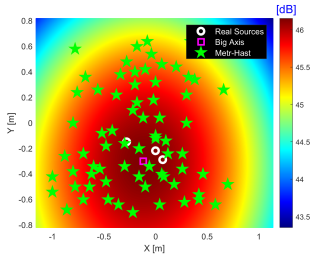

Figure 5.58: 200 Hz

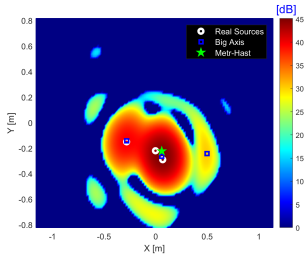

Figure 5.59: 2000 Hz

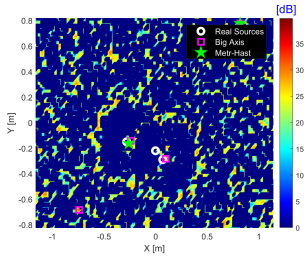

Figure 5.60: 20000 Hz

Figure 5.61: attenuation of -9.5 dB for s2s3.

Conclusions

Figures 5.62 to 5.66 present a summary of all conventional beamforming performances criteria respect to the S2 sources sound pressure level for the different frequencies.

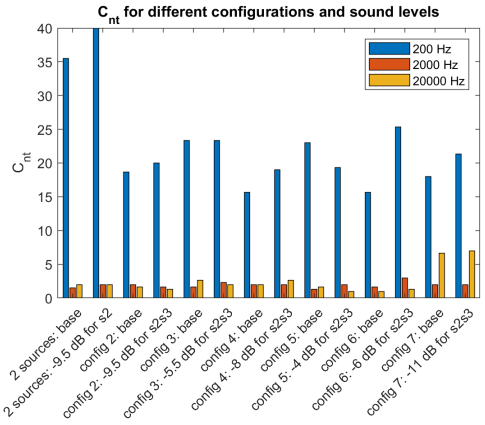

Figure 5.62: C_{nt}

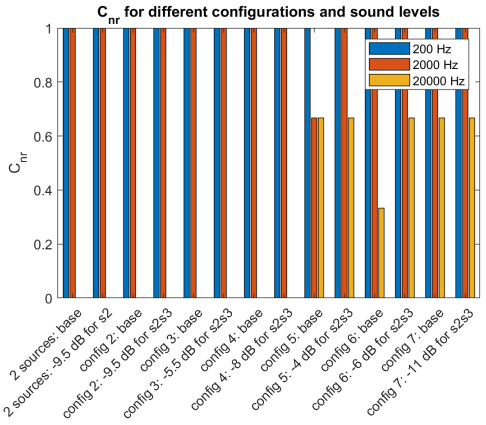

Figure 5.63: C_{nr}

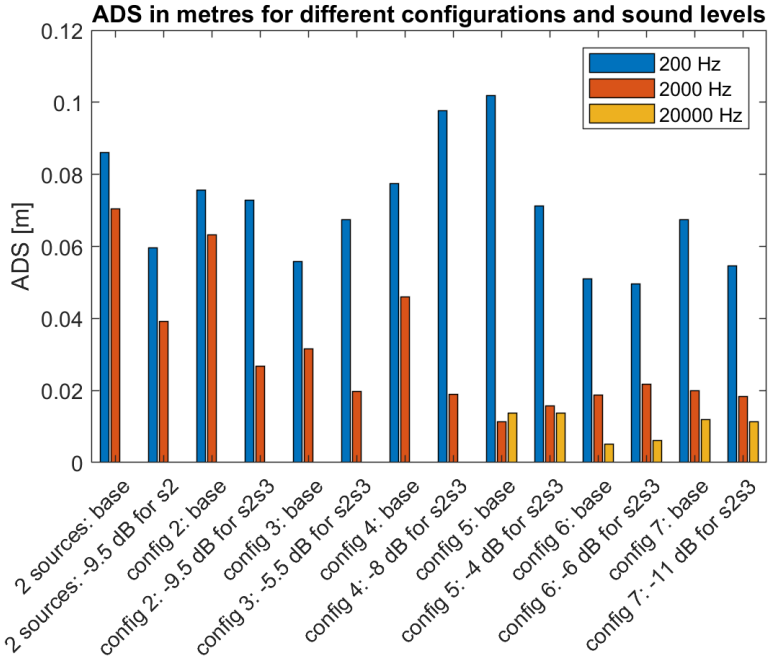

Figure 5.64: Average Distance Sources (ADS) in metres

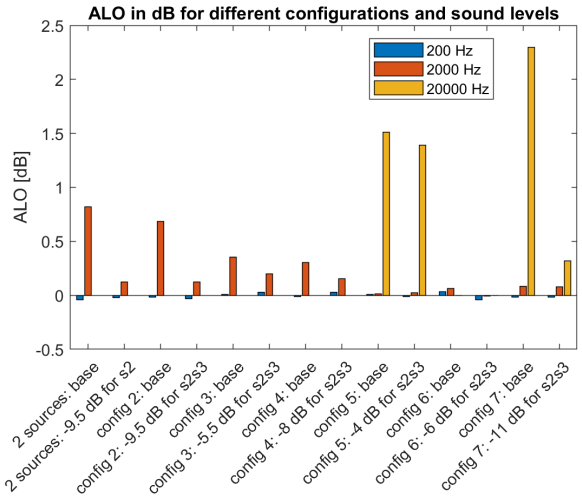

Figure 5.65: ALO in dB

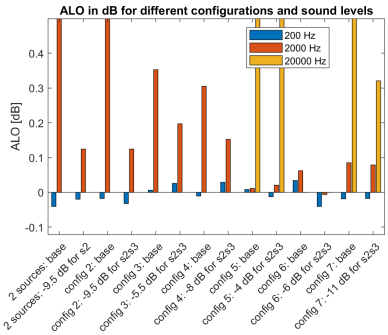

Figure 5.66: ALO - zoom

Looking at Figure 5.62 we can see a general increase of the total number of potential sources identifed with the decrease of S2 sources sound pressure level: this can be determined by the fact that 1 source out of 3 have a bigger intensity, so there is more chance to find sources close to this one and so more sources found within it. From figure 5.63 we can see how sound level does not affect very much the identification of real sources on maps: this is more due to the source configuration selected. Looking at Figures 5.64 and 5.65 an increasing sound pressure level tends to find closer sources and so lower ALO.

5.1.9 Distance between array and source planes

In most of the cases distance between array and source planes has been kept at 3 metres, in this section we are going to see if there are any changes by a smaller or bigger distance. This is studied in the case of two uncorrelated sources S1 and S2 with base sound pressure level.
At low frequency (200 Hz) we can notice that below 3 metres ghost sources number tends to decrease (see Figure 5.67).

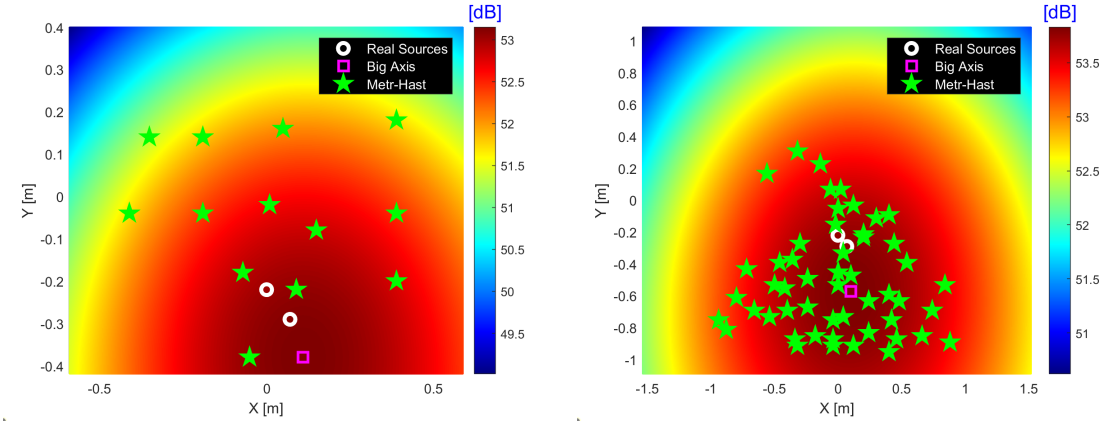

Figure 5.67: Two uncorrelated sources S1 and S2 at 200 Hz for different array and source plane distances: 1.5m (left) and 4m (right).

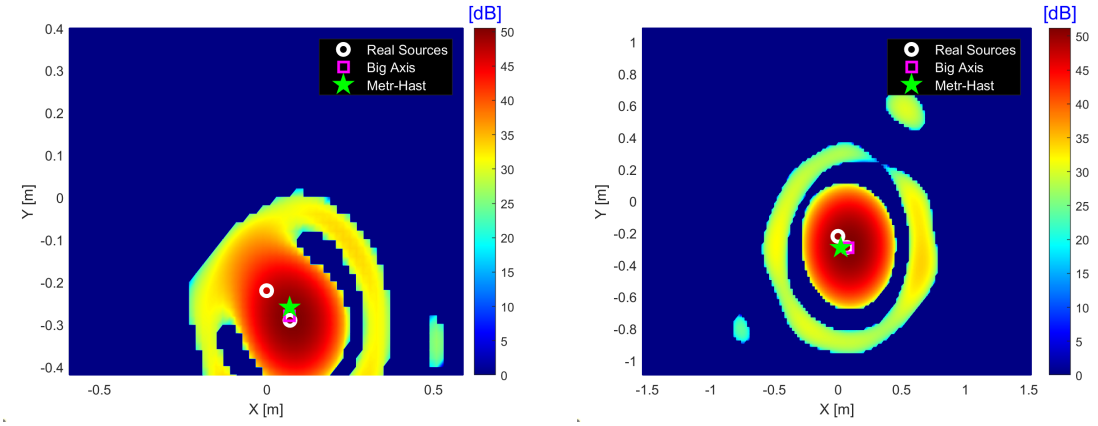

Figure 5.68: Two uncorrelated sources S1 and S2 at 2000 Hz for different array and source plane distances: 1.5m (left) and 4m (right).

It is possible to see that at 2000 Hz there are not any particular changes if not the distance itself (see Figure 5.68).
For high frequency (20000 Hz) it is different: the number of ghost sources identified by the systematic analysis is more important when the distance between the source and array decreases (see Figure 5.69).

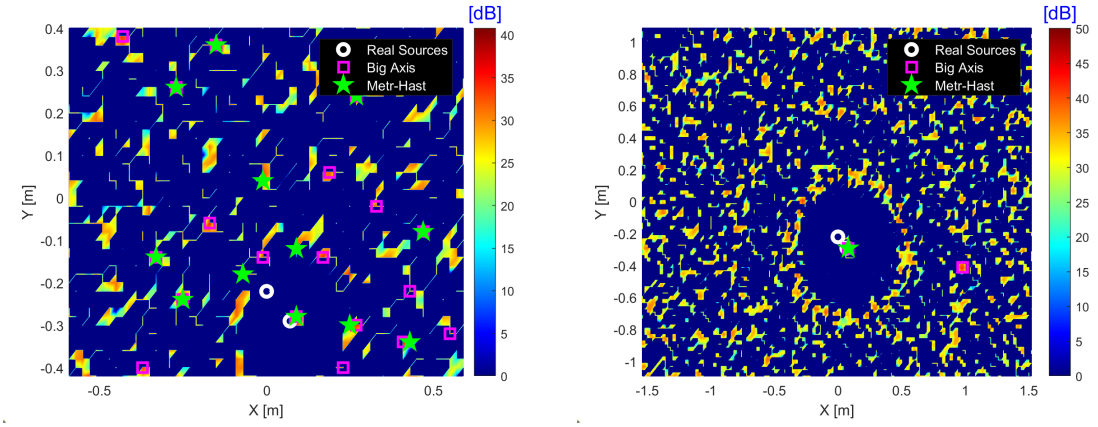

Figure 5.69: Two uncorrelated sources S1 and S2 at 20000 Hz for different array and source plane distances: 1.5m (left) and 4m (right).

Conclusions

Figures 5.70 to 5.74 present a summary of all conventional beamforming performances criteria respect to the distance between array and source planes for the different frequencies.

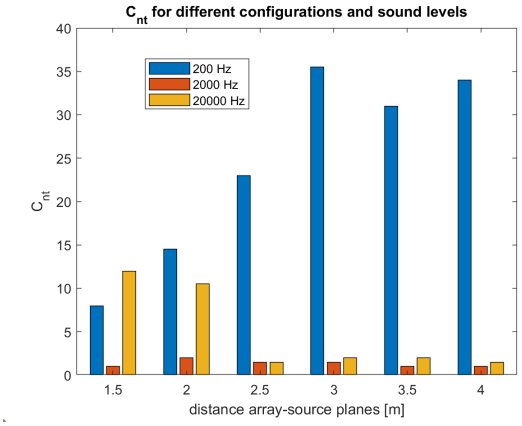

Figure 5.70: C_{nt}

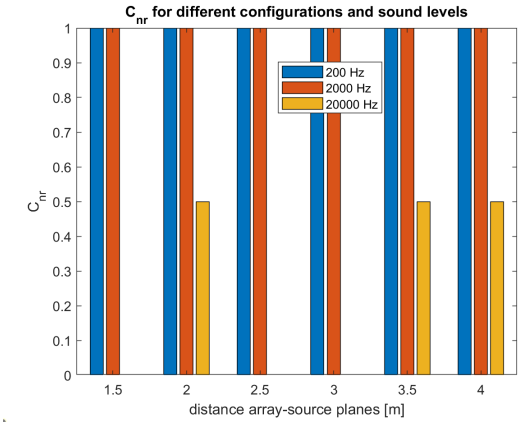

Figure 5.71: C_{nr}

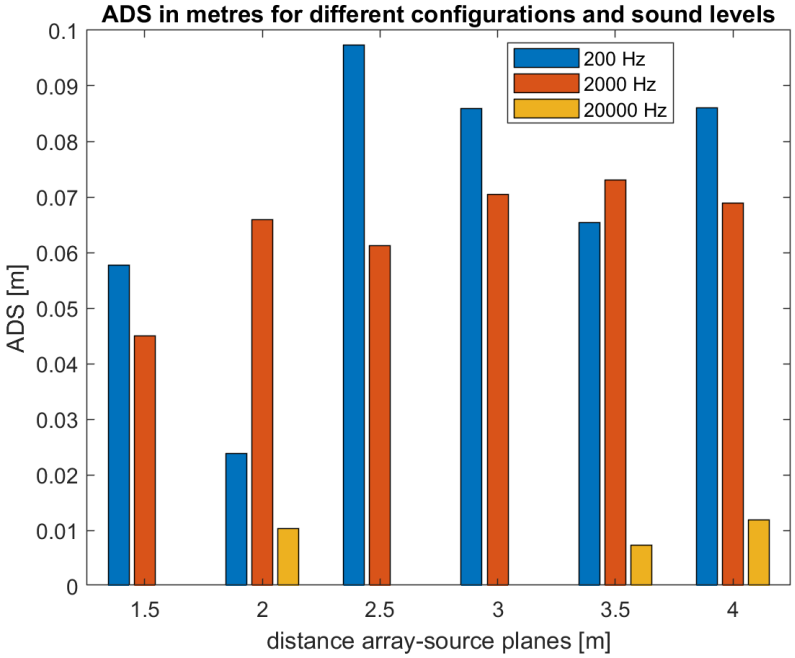

Figure 5.72: Average Distance Sources (ADS) in metres

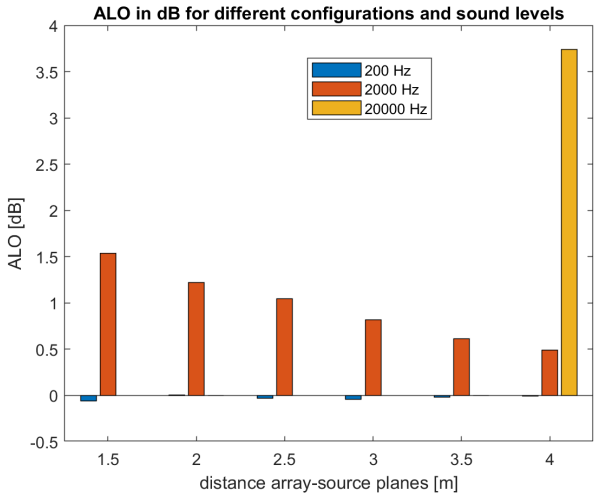

Figure 5.73: ALO in dB

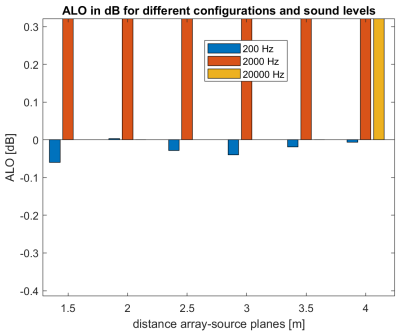

Figure 5.74: ALO - zoom

Looking at Figure 5.70 we can see how the total number of sources identified by the systematic analysis decreases in high frequency when the distance between array and source planes increases. For mid frequency the total number of sources remains constant, so there are not many changes with distance. For low frequency behaviour is the opposite of high frequency: the total source number tends to increase with distance and it is visible also in the first images of the section (figures 5.67). As these potential sources are mainly identified by Metropolis-Hastings algorithm, time spent maps are shown in Figures 5.75 and 5.76 for the frequency 200 Hz and different distances between array and source planes.

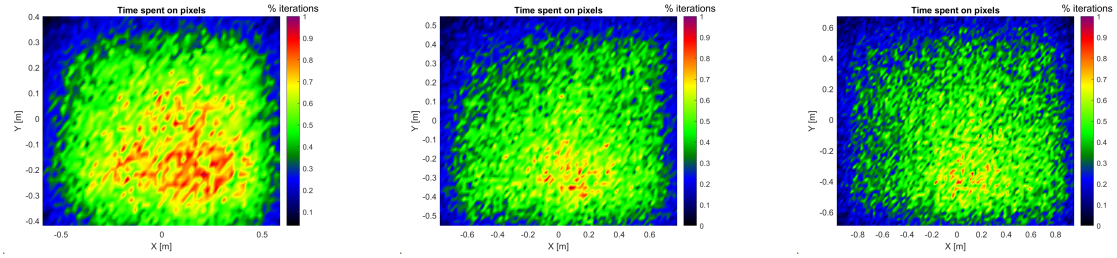

Figure 5.75: Time spent maps for the two uncorrelated sources S1 and S2 at 200 Hz for different array and source plane distances: 1.5 m (left), 2 m (center) and 2.5 m (right).

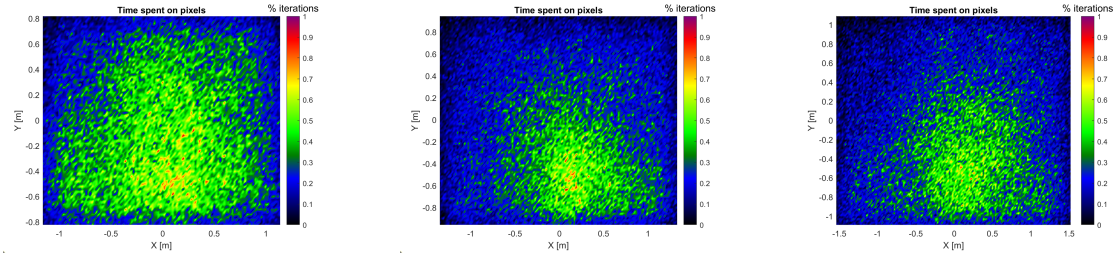

Figure 5.76: Time spent maps for the two uncorrelated sources S1 and S2 at 200 Hz for different array and source plane distances: 3 m (left), 3.5 m (center) and 4 m (right).

Looking at these figures it is clear like at low distance Metropolis-Hastings algorithm spends more time in a few pixel: as a result there will be only a few potential sources found (red region). For high distance as 4 m the algorithm does not spend so much time on the same pixels: as a result there are not any pixels in red, so the whole area is more uniform and tends to a green; so there will be more potential sources identified because the algorithm does not find any "important" pixels.
Looking at Figure 5.71 distance does not affect capability to find more real sources. Also on ADS distance has not many influences. Nevertheless it affects ALO at mid frequency: if the distance increases, systematic analysis can find sources with closer sound pressure level in dB of the real sources.

5.1.10 Tilt angle between source and array planes

It can be interesting to understand the impact on conventional beamforming source maps if there is an angle between array and source planes. Until now these planes have been parallel with no tilt angle involved. This is studied for different frequencies in the same configuration than the distance between source and array planes: two uncorrelated sources S1 and S2 with base sound pressure level, the distance between array and source planes is 3 m (see Figures 5.77 and 5.78).

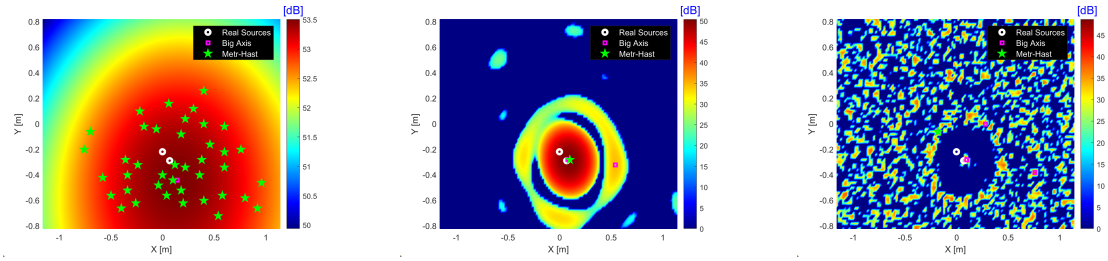

Figure 5.77: Two uncorrelated sources S1 and S2 without angle between array and source planes at 200 Hz (left), 2000 Hz (center) and 20000 Hz (right).

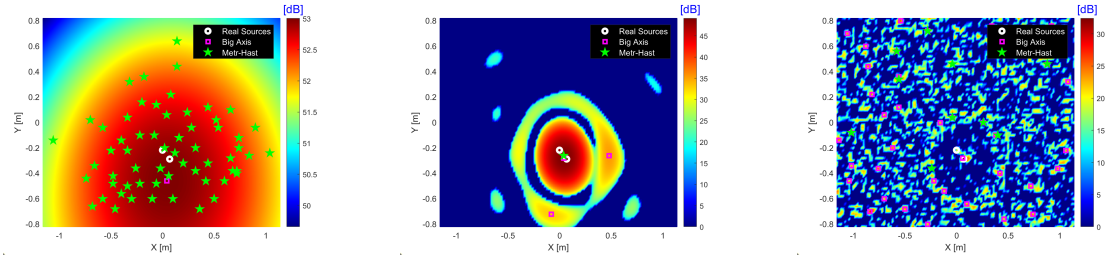

Figure 5.78: Two uncorrelated sources S1 and S2 with an angle of 60° between array and source planes at 200 Hz (left), 2000 Hz (center) and 20000 Hz (right).

Conclusions

Figures 5.79 to 5.84 present a summary of all conventional beamforming performances criteria respect to the angle between array and source planes for the different frequencies.

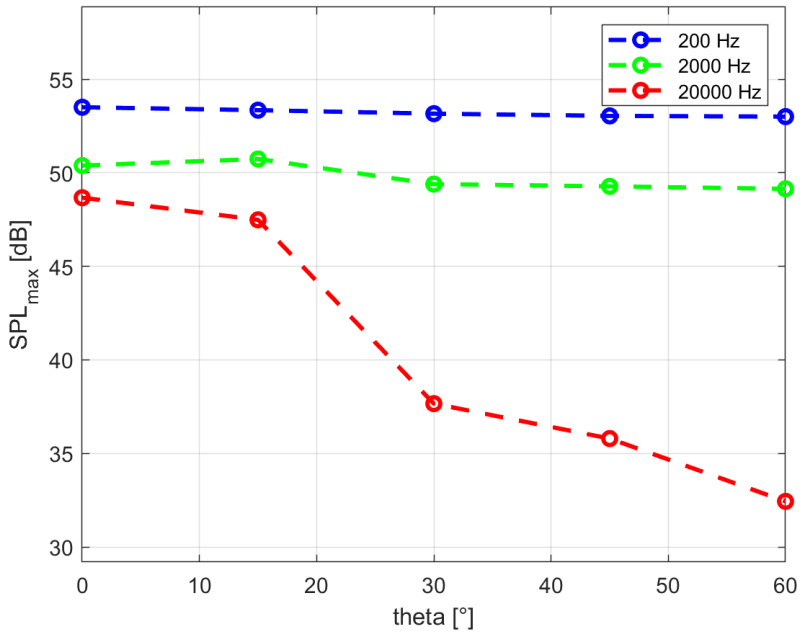

Figure 5.79: Maximum SPL of beamforming source maps respect to the frequency and the angle between the array and source planes.

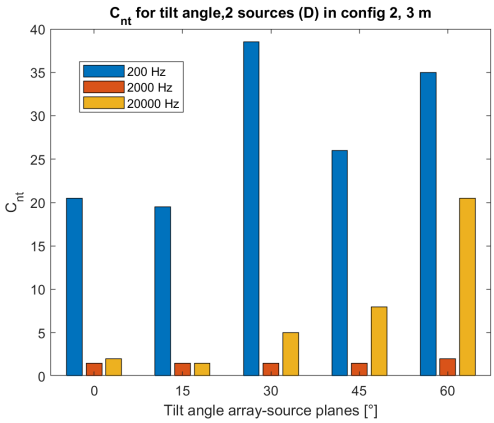

Figure 5.80: C_{nt}

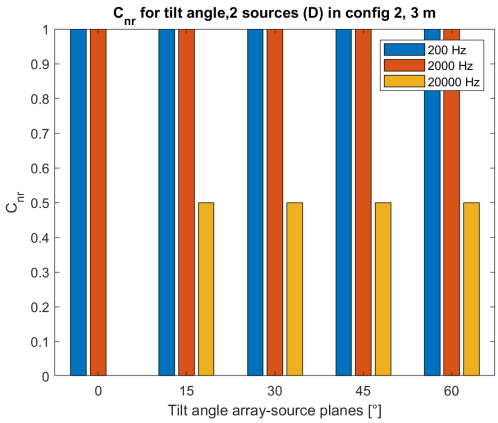

Figure 5.81: C_{nr}

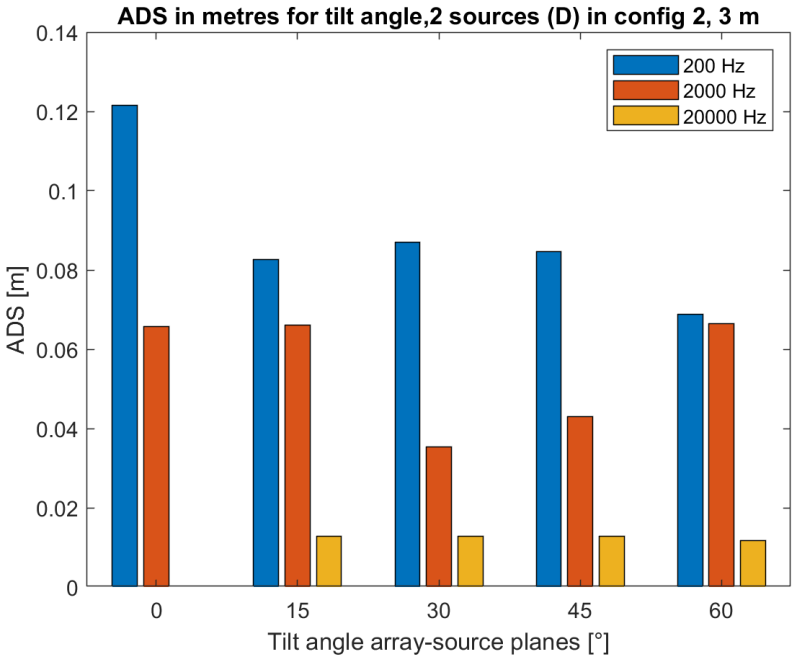

Figure 5.82: Average Distance Sources [m]

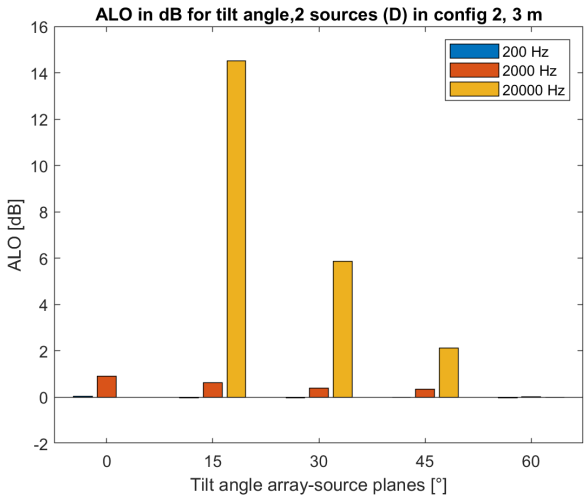

Figure 5.83: ALO in dB

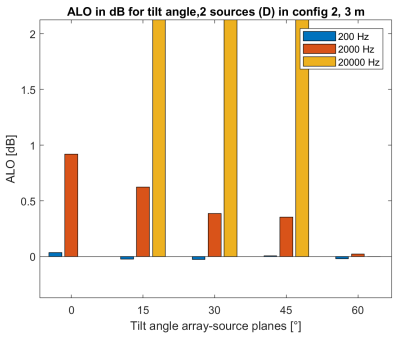

Figure 5.84: ALO - zoom

At high frequency (20000 Hz) sources become directive (especially S2 which is a compression driver) and the maximum sound pressure level obtained on conventional beamforming source maps is thus related to the distance between the array and source planes. Sound pressure level of S2 is lower if the tilt angle increases, as shown in Figure 5.79. For this reason number of ghost sources then increases and some sidelobes will be considered as sources.
For the other frequencies SPL of the source S2 remains constant.
Looking at Figure 5.83 there is confirm of what written before about SPL: ALO tends to increase when there is a tilt angle at high frequency respect to the case where array and source planes are parallel. However it decreases when the tilt angle increases at high and mid frequency due to Metropolis-Hastings algorithm which finds different sources in position and number every time.

5.1.11 Combination of sound pressure level and distance between source and array planes

In this section we take a look on the influence of sound pressure level at which S2 emits and the distance between source and array planes. This is done for the same configuration used in previous parts: two uncorrelated sources S1 and S2. We evaluate it for frequencies 200, 2000 and 20000 Hz.
Figures 5.85 and 5.86 are the two extreme examples in source maps.

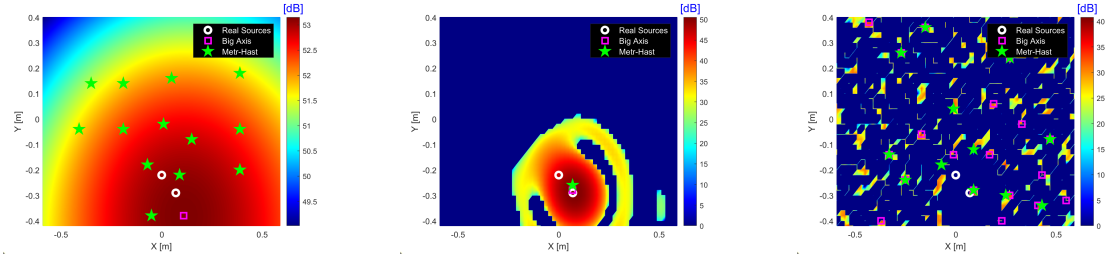

Figure 5.85: Two uncorrelated sources S1 and S2 for a distance of 1.5 m between array and source plane and base sound pressure level at frequencies: 200 Hz (left), 2000 Hz (center) and 20000 Hz (right).

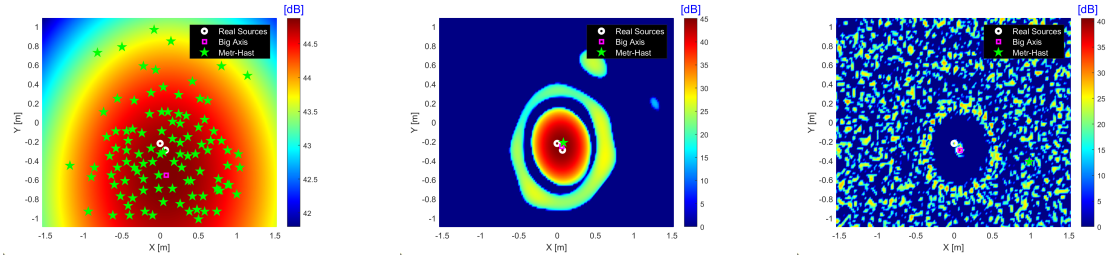

Figure 5.86: Two uncorrelated sources S1 and S2 for a distance of 4 m between array and source plane and sound pressure level of source S2 9.5 dB lower than base sound pressure level at frequencies: 200 Hz (left), 2000 Hz (center) and 20000 Hz (right).

Conclusions

Figures 5.87 to 5.94 present a summary of all conventional beamforming perfromances criteria respect to both the distance between array and source planes and the S2 relative sound pressure level for the different frequencies.

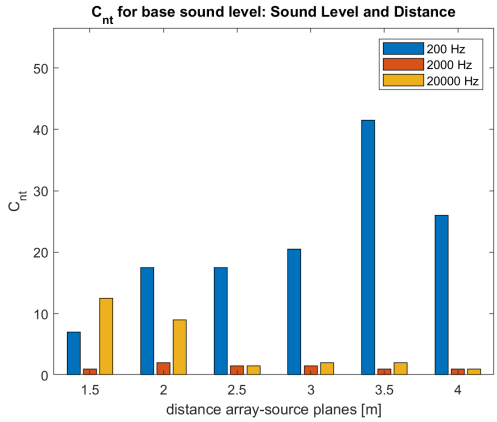

Figure 5.87: C_{nt} for base level

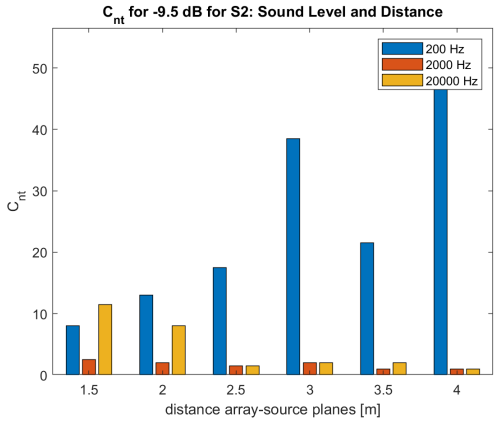

Figure 5.88: C_{nt} for -9.5 dB for S2

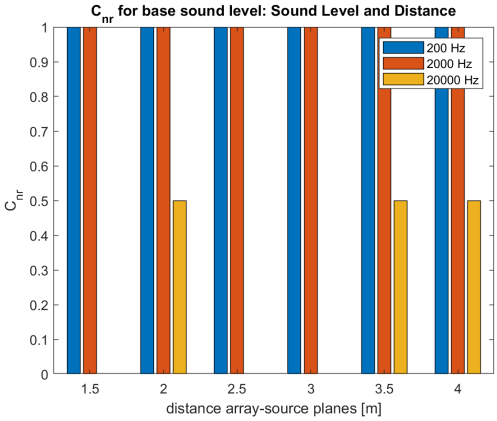

Figure 5.89: C_{nr} for base level

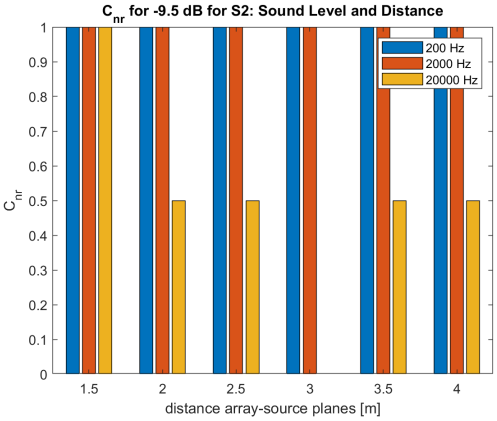

Figure 5.90: C_{nr} for -9.5 dB for S2

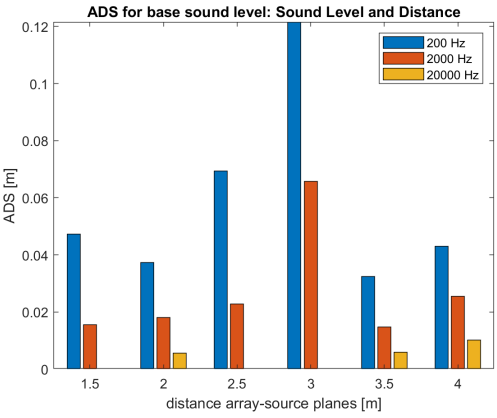

Figure 5.91: ADS for base level

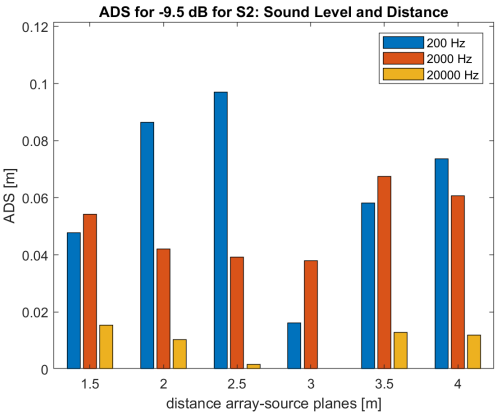

Figure 5.92: ADS for -9.5 dB for S2

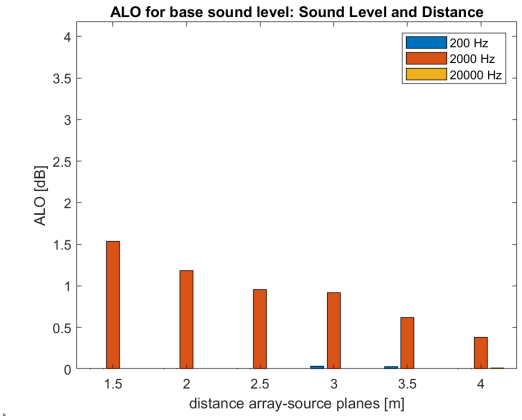

Figure 5.93: ALO for base level

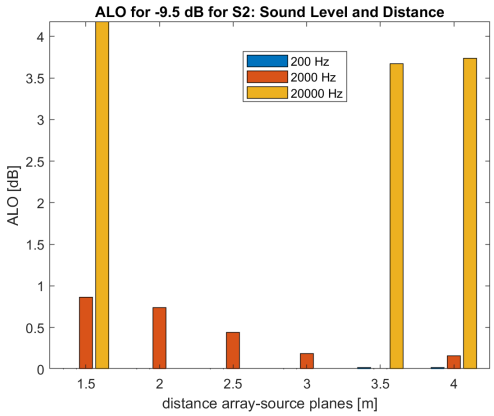

Figure 5.94: ALO for -9.5 dB for S2

These two parameters contribute as a combination of the two: number of total sources tends to increase with distance and sound pressure level for low frequency; it is the opposite for high frequency, while for mid frequency there are not any particular differences (Figures 5.87 & 5.88).
For the identification of real sources it looks like there are not any particular differences with distance, but the decrease of sound pressure level of source S2 can help to find more sources in high frequency (see Figures 5.89 and 5.90). Nevertheless this detection contributes to an increase of ALO in high frequencies, as shown in figure 5.94. For mid frequency the capability to detect real sources does not change with distance and sound pressure level, but increasing both ALO tends to decrease (Figures 5.93 & 5.94).
However ADS is not influenced by distance, but only by sound pressure level, especially at 2000 Hz: sources are further from the real ones but at lower ALO. This means that a change in sound pressure level contributes to a change of SPL map.
For high frequency sound pressure level change contributes to have bigger ALOs, in contrast with mid-frequency.

5.1.12 Combination of sound pressure level and tilt angle

In this section we are going to see the influence of both the sound pressure level of source S2 and the angle between source and array planes on the same configuration than for the previous part: two uncorrelated sources S1 and S2. We evaluate it for frequencies 200, 2000 and 20000 Hz.
Figures 5.95 to 5.96 present extreme examples to show what happens.

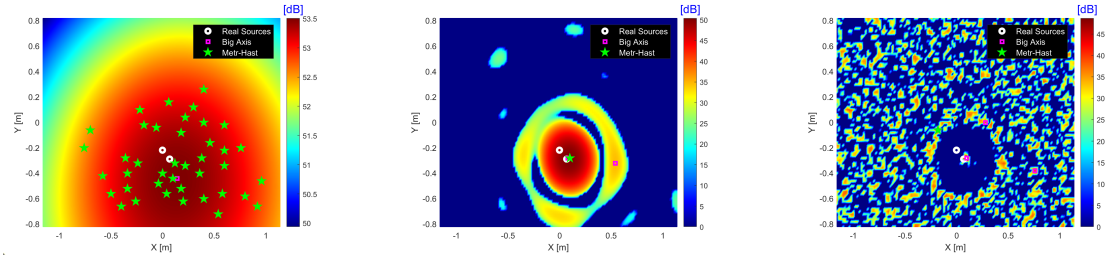

Figure 5.95: Two uncorrelated sources S1 and S2 for an angle of 0° between array and source planes and base sound pressure level for source S2 at frequencies: 200 Hz (left), 2000 Hz (center) and 20000 Hz (right).

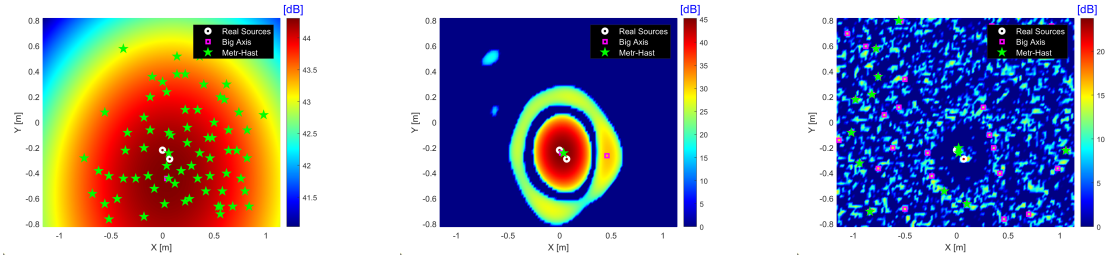

Figure 5.96: Two uncorrelated sources S1 and S2 for an angle of 60° between array and source planes and sound pressure level of source S2 9.5 dB lower than base sound pressure at frequencies: 200 Hz (left), 2000 Hz (center) and 20000 Hz (right).

Conclusions

Figures 5.97 to 5.104 present a summary of all conventional beamforming performances criteria respect to both the angle between array and source planes and the S2 relative sound pressure level for the different frequencies.

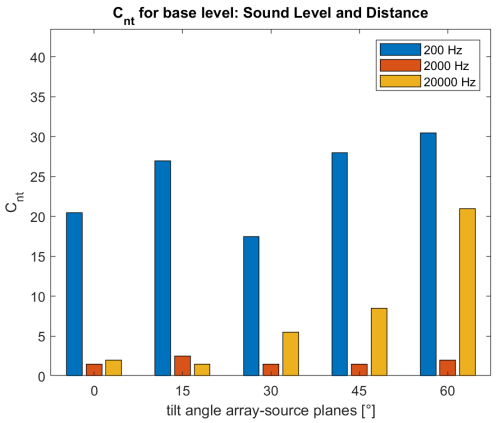

Figure 5.97: C_{nt} for base level

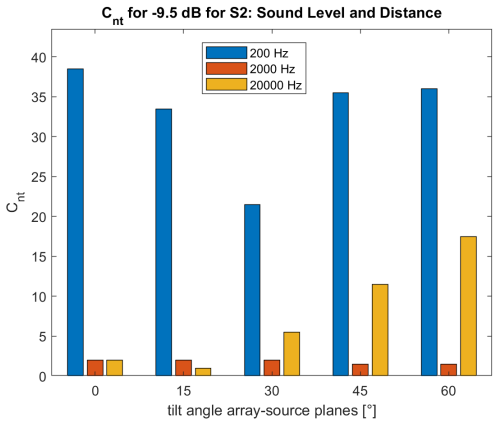

Figure 5.98: C_{nt} for -9.5 dB for S2

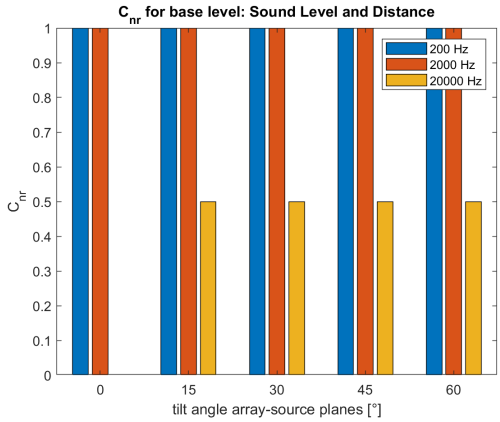

Figure 5.99: C_{nr} for base level

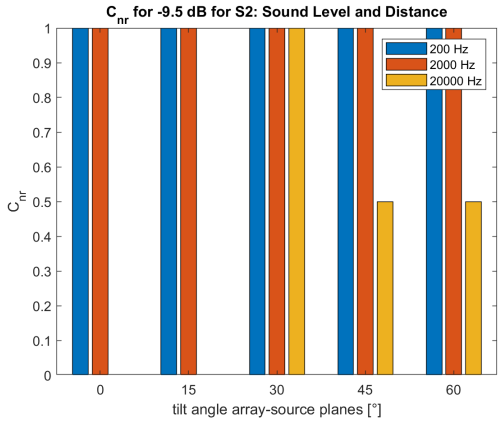

Figure 5.100: C_{nr} for -9.5 dB for S2

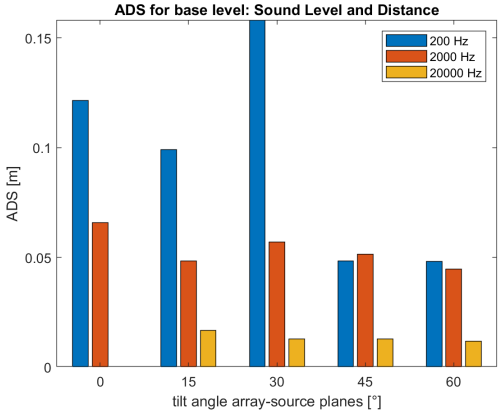

Figure 5.101: ADS for base level

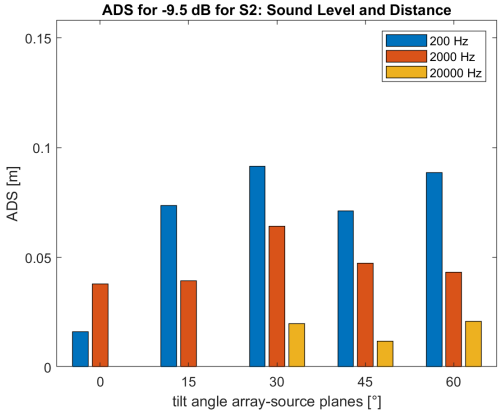

Figure 5.102: ADS for -9.5 dB for S2

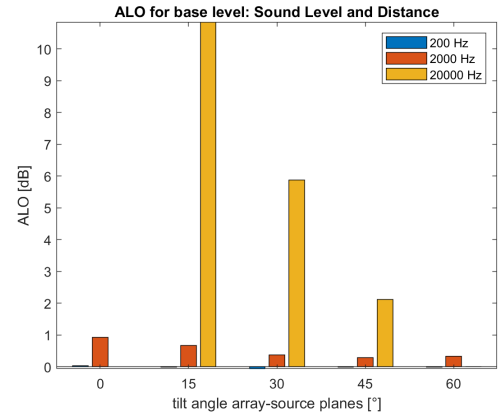

Figure 5.103: ALO for base level

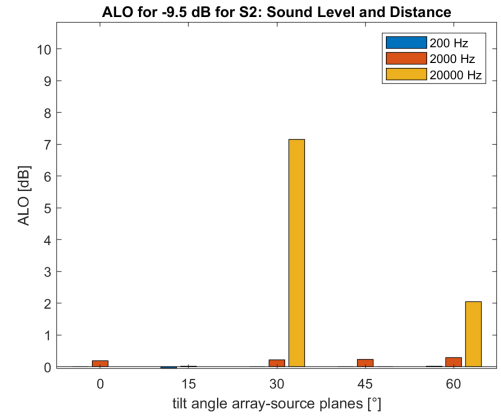

Figure 5.104: ALO for -9.5 dB for S2

Looking at Figures 5.96 and 5.95 we can see how sound pressure level and tilt angle contributes to find at 20000 Hz different sources: in a case S1 and in the other S2. This does not happen in any other cases or in tilt angle or sound pressure level alone suggesting that this type of combination above certain values of angle and sound pressure level can bring different source maps.

Total number of sources increases if tilt angle and sound pressure level increase for low and high frequency. At mid frequency any variations are not particularly visible (figures 5.97 & 5.98).
For a tilt angle of 30° the reduction of S2 sound pressure level of 9.5 dB allows to identify all real sources on conventional beamforming source mpas for all frequencies. They seem not to have a particular affection onto Average Distance Sources at each frequency, but an increasing tilt angle can contribute to decrease ALO; an increase in sound pressure level instead gives an increase in ALO (figures 5.103 & 5.104).

5.2 CLEAN-SC

In this section the performances of the deconvolution algorithm CLEAN-SC will be assessed respect to conventional beamforming one by applying the systematic analysis on the source maps. This is first done on the configuration with three uncorrelated sources S1S2S2 without reverberation at different (see Figures 5.105, 5.106 and 5.107). To remind the reader about CLEAN-SC see section dedicated. At first an example in maps of beamforming and CLEAN-SC will be shown for the case of 3 sources S1S2S2 uncorrelated (**D**) and without reverberation.

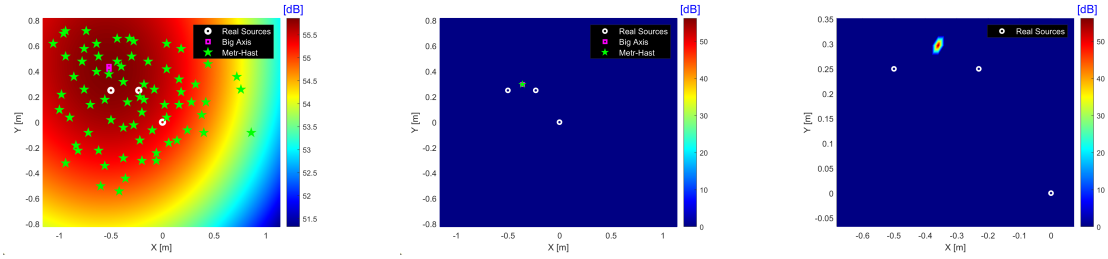

Figure 5.105: Three uncorrelated sources S1S2S2 maps obtained by conventional beamforming (left) and CLEAN-SC (center and right) at 200 Hz.

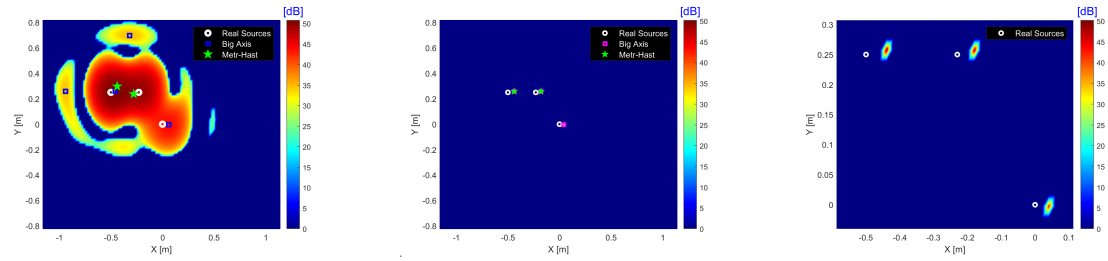

Figure 5.106: Three uncorrelated sources S1S2S2 maps obtained by conventional beamforming (left) and CLEAN-SC (center and right) at 2000 Hz.

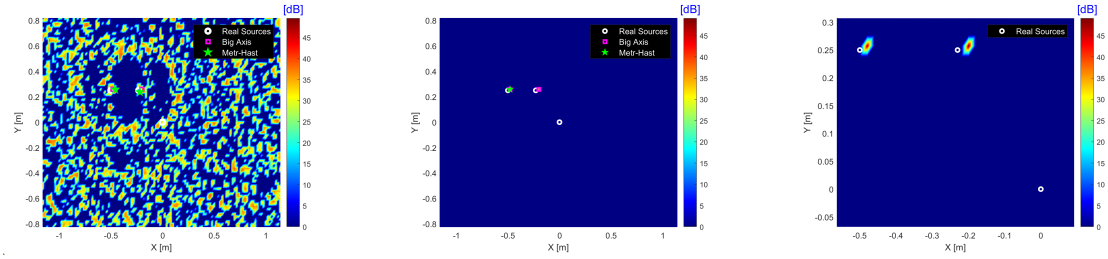

Figure 5.107: Three uncorrelated sources S1S2S2 maps obtained by conventional beamforming (left) and CLEAN-SC (center and right) at 20000 Hz.

Using CLEAN-SC the spatial resolution is improved and Sources will be found in very small areas. As the reader can see, CLEAN-SC has a huge capability of *cleaning* the map. Here we evaluate how precise can be this method by using the systematic analysis.

Conclusions

Figures 5.108 to 5.111 present a summary of the comparison of conventional beamforming and CLEAN-SC performances criteria respect to the source correlation and the reverberation for the different frequencies.

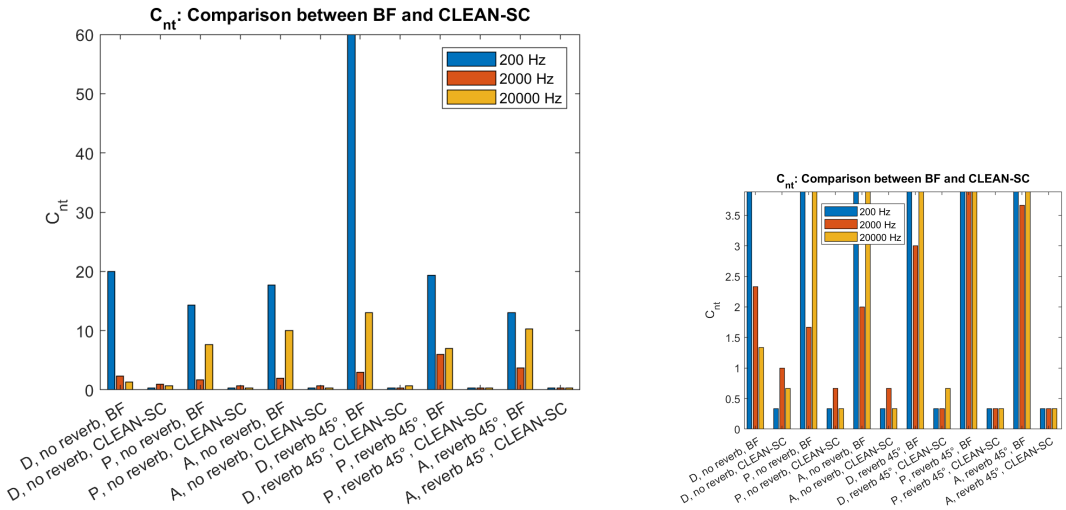

Figure 5.108: Comparison beamforming - CLEAN-SC: Total number of sources; zoom on the right.

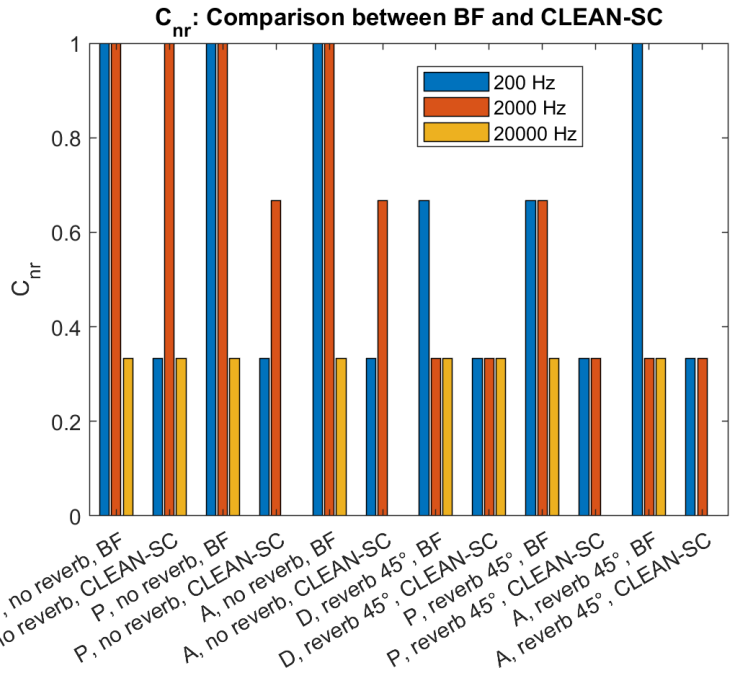

Figure 5.109: Comparison beamforming - CLEAN-SC: C_{nr}, real sources found.

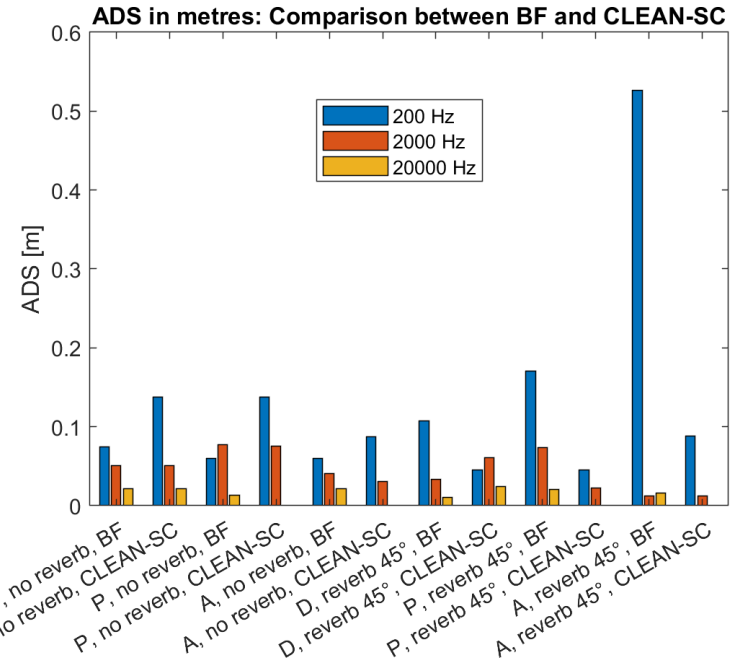

Figure 5.110: Comparison beamforming - CLEAN-SC: ADS in metres.

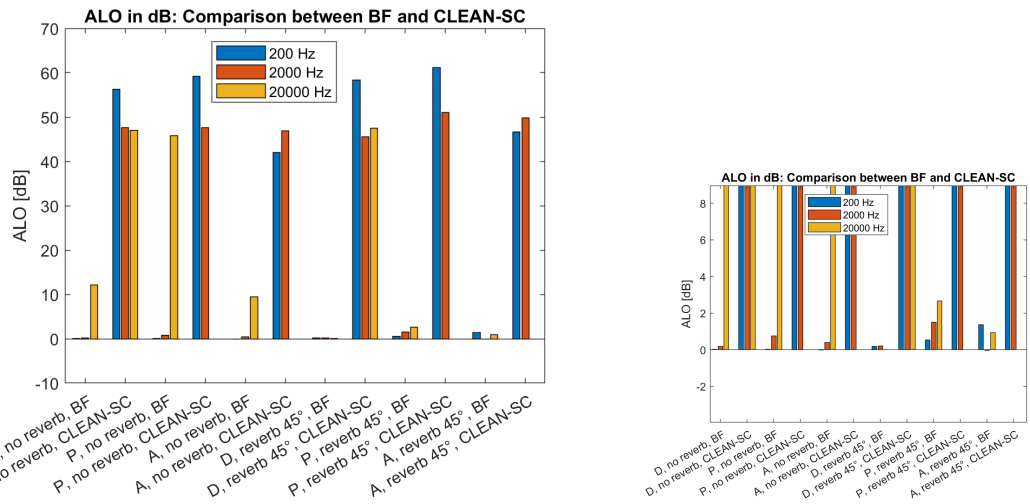

Figure 5.111: Comparison beamforming - CLEAN-SC: ALO in dB; zoom on the right.

Looking at Figure 5.108 first to point out is the low number of total sources found by CLEAN-SC with respect to beamforming: they are usually below the number of real sources; this is due to the excellent cleaning of beamfoming-maps: only a few small colored areas are saved from this *cleaning*, reducing the probability to find many sources. Additionally the cleaning process being based on the source uncorrelation assumption, the number of real sources idientified on CLEAN-SC source maps is lower when S2 sources are in phase or in phase opposition (see Figure 5.109).
Another fact is that CLEAN-SC when finds something has a great probability to find sources really closed to the real ones: at high frequency this is also true if we take into account some resolution problems. Reverberation does not affect very much CLEAN-SC maps if not in decreasing distance between sources (ADS), figure 5.110. ALO for CLEAN-SC on the opposite increases very much wrt to beamforming: maps have more region at SPL null, so it is easier to have bigger ALO.

5.3 Coherence - Anticoherence

In this section we are going to apply the systematic analysis on coherence and anti-coherence source maps and compare them with conventional beamforming without correlation with a reference transducer. The reference transducer used here is a volume acceleration sensor integrated on source S1 outlet. The same three sources S1S2S2 configuration than the previous part will be studied in case of correlation (P or A) or uncorrelation (D) for the two sources S2S2 and of the presence or not of reverberation. Sound pressure level is kept at base level, as distance between array and source plane at 3 m and tilt angle equal to 0°.

5.3.1 Conclusions

Figures 5.112 to 5.125 present a summary of the comparison of conventional beamforming performances criteria respect to the source correlation and the reverberation for the different frequencies.

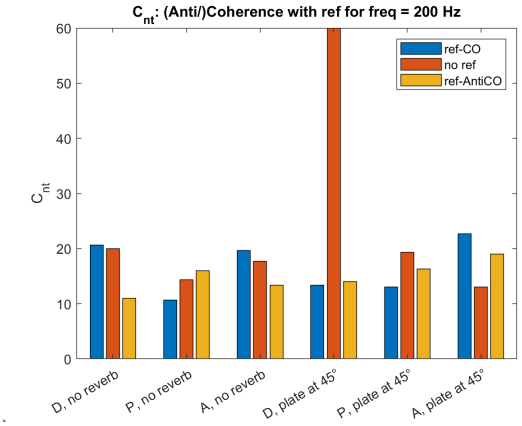

Figure 5.112: C_{nt}

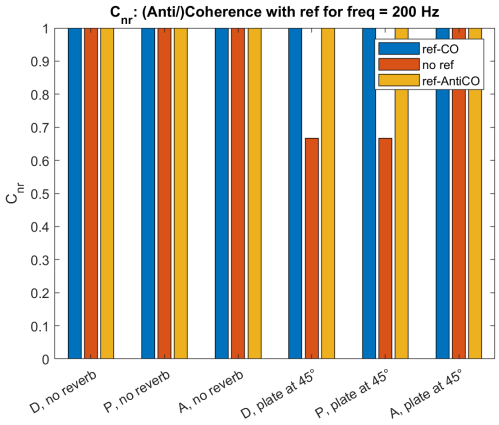

Figure 5.113: C_{nr}

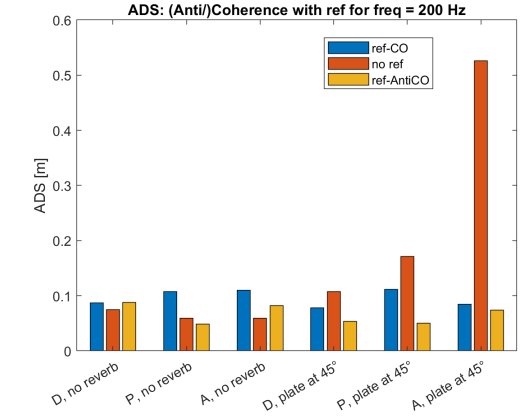

Figure 5.114: ADS [m]

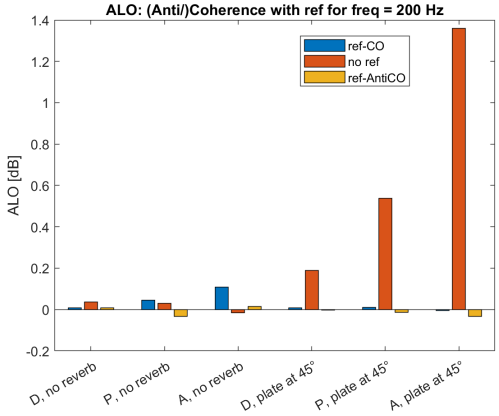

Figure 5.115: ALO [dB]

Figure 5.116: Criteria for frequency = 200 Hz.

At low frequency the correlation with S1 reference transducer does not affect the number of total and real sources found, but let to find closer sources in distance to the real ones (ADS is lower for both Coherence and Anti-coherence) and in ALO: especially in case of reverberation ALO tends to increase; using a reference transducer it remains very low.

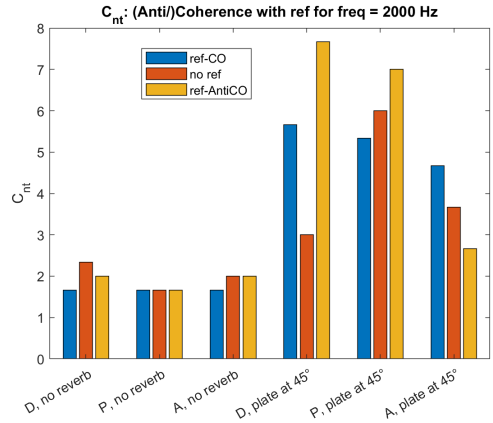

Figure 5.117: C_{nt}

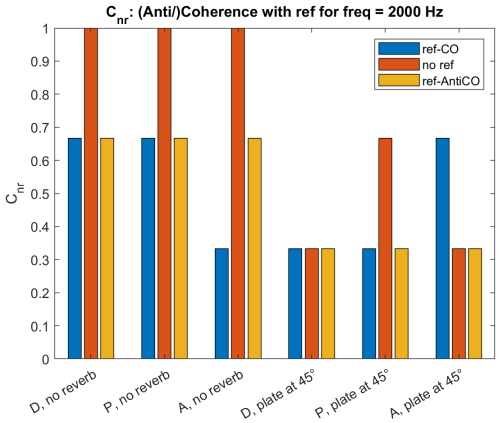

Figure 5.118: C_{nr}

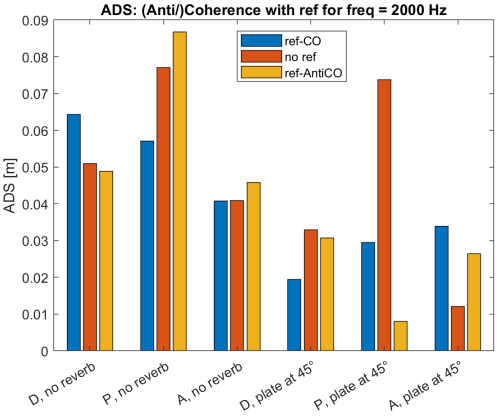

Figure 5.119: ADS [m]

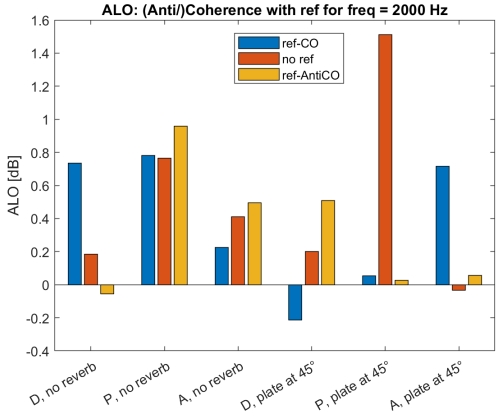

Figure 5.120: ALO [dB]

Figure 5.121: Criteria for frequency = 2000 Hz.

Looking at the case of mid frequency, 2000 Hz, there is not a clear tendancy in using a reference transducer. However a Coherence or Anti-coherence correlation with a reference can be used to point out only S1 source or S2 sources respectively, as it is possible to see in figure 2.21.

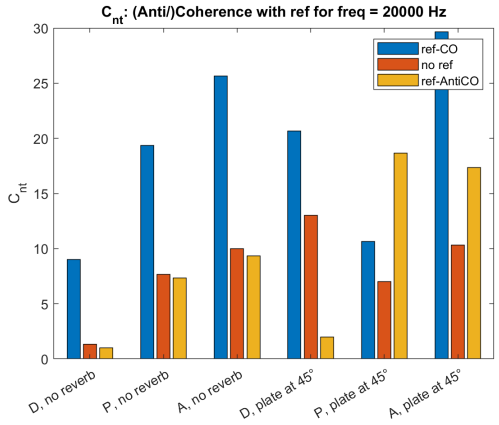

Figure 5.122: C_{nt}

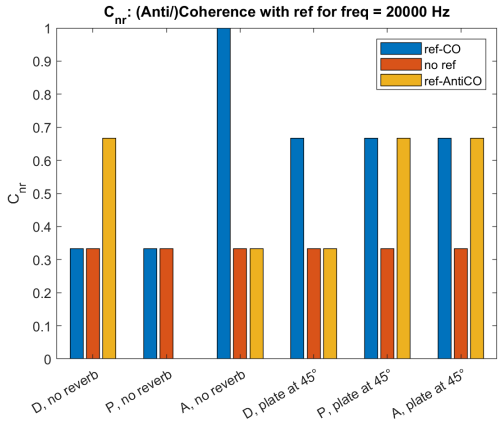

Figure 5.123: C_{nr}

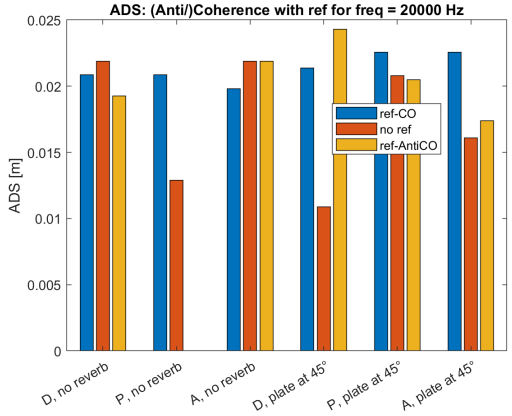

Figure 5.124: ADS [m]

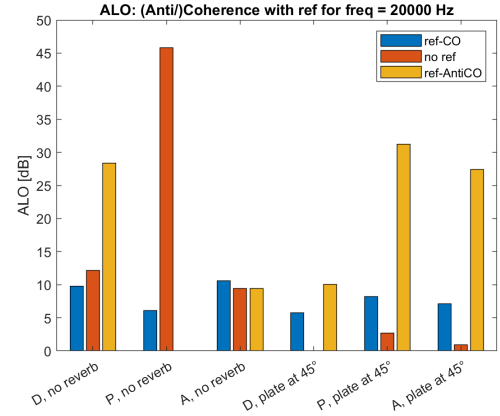

Figure 5.125: ALO [dB]

Figure 5.126: Criteria for frequency = 20000 Hz.

Using the correlation with S1 reference transducer we obtain usually more potential sources than before: this is probably due to the fact that in case of this correlation there is a tendancy to decrease the SPL of the map (see figure 2.25). This happens in truth also for the other frequencies. In case of high frequency however all small areas at lower SPL are closer to the rest of the map suggesting many more peaks. At high frequency the correlation with a reference transducer allows to improve the maps by finding the real sources in the case of reverberation.

5.4 Applied example: small scale low Reynolds number UAV rotor

In this section a real case example of aeroacoustic is shown: a small scale low Reynolds number rotor comparable to drone rotors. The rotor is located at the center of the ISAE-SUPAERO anechoic room at the top of a rotor test stand, as can be seen in figure 5.128 [13]. This facility is acoustically treated in the frequency range 80–16000Hz, see chapter 3 for anechoic room dimensions. A beam can be positioned below the rotor at several distances from the rotor disk plane. The rotor is driven by means of a Faulhaber electric brushless motor, which presents low noise emissions [13]. Rotor profile is NACA0012 with a chord of 2.5 cm, tilt angle is 10°,

diameter is 20 cm and it has two blades rotating at 8000 rpm.
A directivity antenna with 13 1/4 in. GRAS 40PH microphones is used to measure the farfield noise radiated 1.62 m away from the rotor center, for latitude angles (also defined as polar angles) ϑ every 10° from -60° to 60° , where 0° corresponds to the rotor disk plane [13].
The beam is 40 cm long, has a diameter of 2 cm and it is set 2 cm under the rotor disk plane as you can see in figure 5.128.

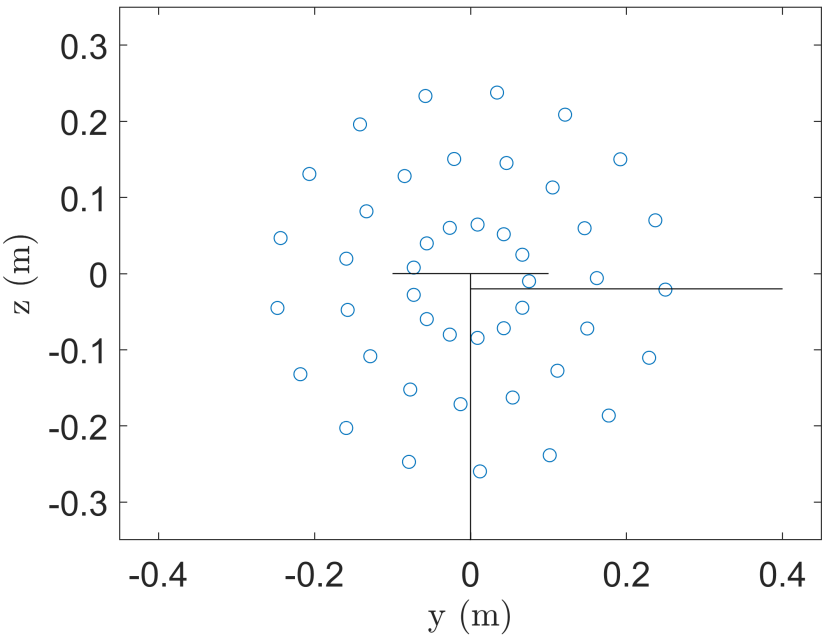

Figure 5.127: Array localisation.

Here noise produced by the rotor in interaction with the beam is searched by using different source localisation algorithm presented previously (see Figure 5.127): in particular we take a look at fifth harmonic of the blade passing frequency (1300-1400 Hz) which is increased in the presence of the beam [13]. As the interaction noise is studied here the rotation is not taken into account in the source localisation post processing. The microphone array A_{45} presented in Part 4.1 is used and positionned parallel to the plane defined by the rotor and the beam axis (see Figure 5.127) [12].
For source localisation algorithm using a reference transducer, this additional transducer is placed on the top of the beam at 80% of the rotor blade length.
Acoustic data are acquired at a sampling frequency of 51.2 kHz, during 16 s [13].

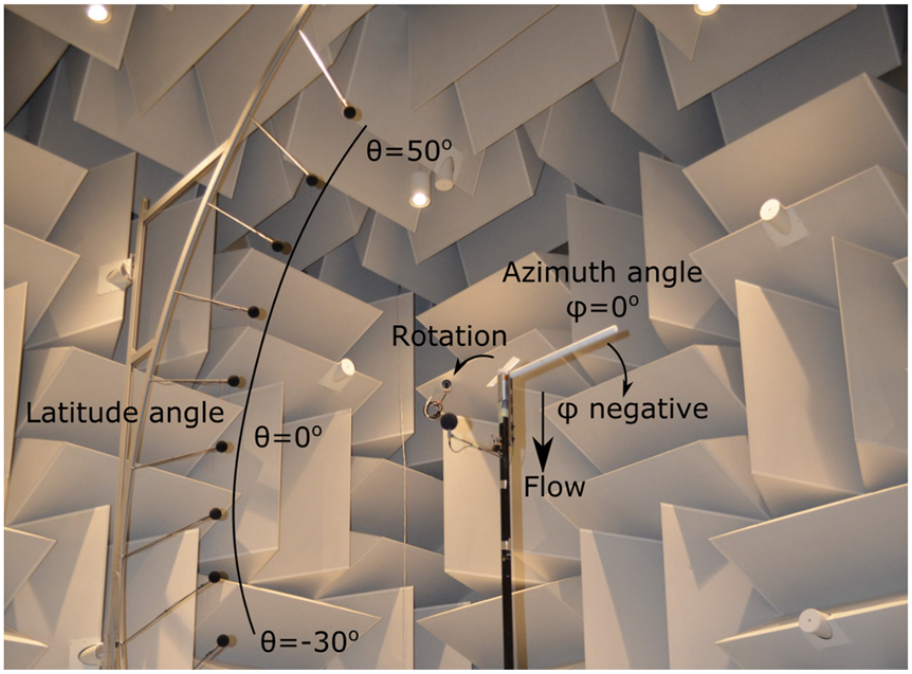

Figure 5.128: Experimental setup [13].

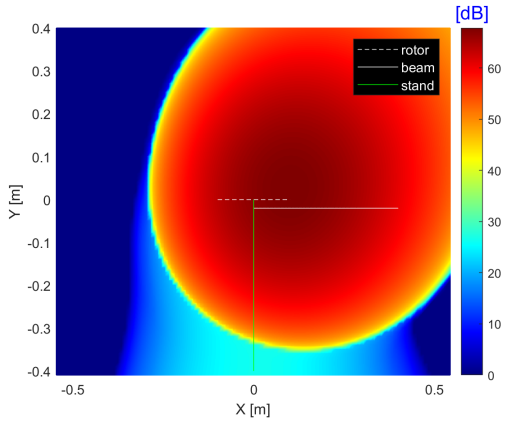

Figure 5.129: Conventional beamforming

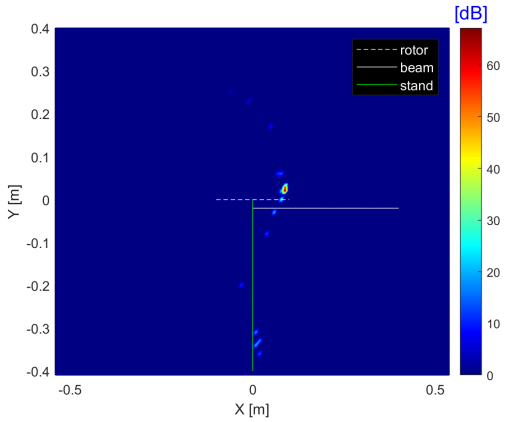

Figure 5.130: CLEAN-SC

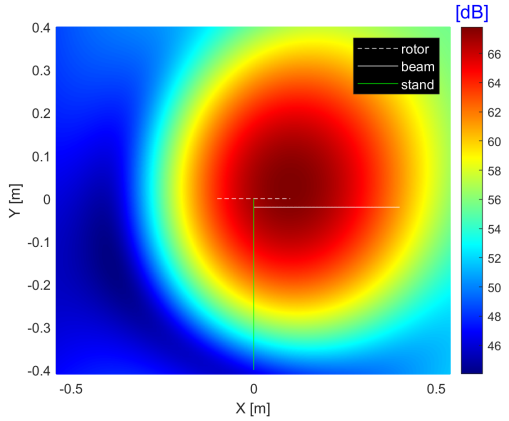

Figure 5.131: Coherence

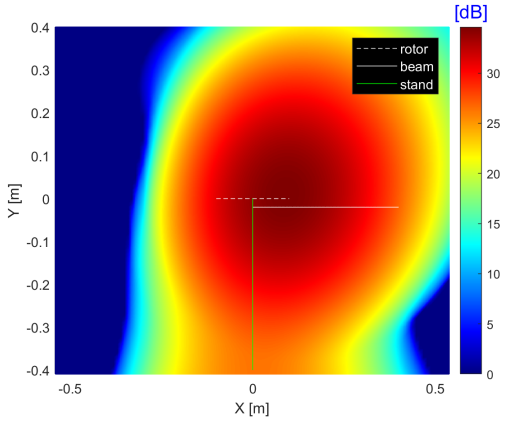

Figure 5.132: Anti-Coherence

Figure 5.133: Rotor-beam source maps obtained by different sound source localisation algorithms for the fifth blade passing frequency harmonic.

As you can see from images conventional beamforming brings a map where red occupies the whole helix if not more: spatial resolution is low. In case of coherency with a reference tranducer we can see how the region responsable for noise creation becomes smaller while keeping same maximum SPL than conventional beamforming map: the spatial resolution is improved and the result indicated that the noise emitted at the fifth harmonic of the blade passing frequency is associated to pressure fluctuation on the beam. In case of anti-coherence with a reference transducer the spatial resolution is improved as before but SPL are much smaller, which confirms that the interaction noise at this frequency is correlated with the pressure fluctuation on the beam. Then it is possible to see how a deconvolution (CLEAN-SC) method works: it cleans a lot the map and indicates that the area responsible for the noise generation is a point located near the blade tip on the beam side: in this point there is a change of the pressure field due to the passage of the blade over the beam. Numerical solutions already showed that this was due to beam unsteady loading [13].

Chapter 6

Conclusions

This Master Thesis has the purpose of proposing a systematic analysis of the performances of sound source localisation algorithms by assessing the quality of resulting source maps.
The core of the systematic analysis is using a combination of *Local Maxima with big axis* and *Metropolis-Hastings* algorithms: the first one simply searches peaks on the map of strongest Sound Pressure Levels; here it is optimised to start the research on the big axis of each contour. The second algorithm is a statistical approach which uses a Markov Monte Carlo chain to iteratively explore the SPL source map through a random walk [14]. This gives a new map corresponding to time spent on each map point. Peaks are searched on the time-spent map. At the end the result of these two algorithms are combined to give a list of potential sources on the map. A combination can be powerful because they are complementary.
This fusion method is used to calculate performances criteria from the list of potential sources in order to assess the quality of source maps. Those criteria are then used to study the influence of some parameters (source correlation, reverberation, source localisation algorithms,...) on the source maps quality.
This approach has confirmed some limitations of the conventional beamforming: at low frequency the spatial resolution is so low that it is difficult to find the exact position of a real source (many potentials are found); in case of Phase-correlation between two sources conventional beamforming does not work properly creating a region at strong SPL in the middle of the two; reverberation, which is a real-case scenario in world life where there are always physical disturbing objects, can make sound localisation sources tougher to apply and to trust in: reflective walls are seen as new sound sources added in the plane. Distance between array and source planes is important to optimise to be in far field for the biggest frequency range possible and to have the best spatial resolution possible; angle between planes can be difficult to manage: in real life it is difficult to be perfectly oriented towards sound sources, but this brings some uncertainties on the localisation of sound sources like the addition of several potential ones and the underestimation of SPL.
Additionally to conventional beamforming, a deconvolution method, CLEAN-SC, and a method based on a reference transducer has been presented and their performance has been evaluated through the systematic analysis. Both CLEAN-SC and the algorithm using a reference transducer give source maps with a spatial resolution better than the conventional beamforming and seem globally more robusts to other parameters (source correlation, reverberation). The maximum SPLs of the

maps obtained by correlation or anti-correlation with a reference transducer, which gives an additional information. The aeroacoustic test case illustrated the different performances of the tested source algorithm on more realistic configuration.

6.1 In future

In future the aim is to use this systematic analysis of sound source localisation algorithm performances to assess other deconvolution algorithms and compare them with new algorithms. As written in introduction it is important to constantly develop and study new methods that help to better understand the noise generation mechanisms to reach the goal of reducing noise pollution. Acoustic field is one of main subjects for the future aviation and social life, so a continous developping of sound source localisation methods is requested.

Appendix

Appendix A

Configurations and source positions

A.1 Configurations

Config Source	Source 1 - S1	Source 2 - S2	Source 3 - S2
1	(0;0)	(-0.5;0.25)	(-0.23;0.25)
2	(0;-0.22)	(0.07;-0.29)	(-0.28;-0.15)
3	(-0.55;0.255)	(0.07;-0.17)	(-0.29;0.03)
4	(0;0.21)	(0.18;-0.31)	(-0.18;-0.31)
5	(0.12;-0.265)	(0.265;0.11)	(-0.265;0.11)
6	(0.415;0.19)	(0.165;-0.3)	(-0.36;-0.07)
7	(-0.42;-0.015)	(0.35;0.25)	(0.09;-0.32)

Table A.1: Different configurations of sources position.

A.2 Study cases

Config is for configuration, see tableA.1 for details; if it is not present sources positions will be specified in a lower section. However, if one or two sources are present for a configuration you need to see the right line, see what type of source is present and choose the correct position. *dist-z* is the distance in metres between source-plane and array-plane. *Sound level* is in dB. *rev* is for reverberation. *D* is for Decorrelated, *P* in Phase (so correlated) and *A* in Anti-phase (correlated as well).

Run	Config	type S	D, P, A	dist-z	°	Sound level	rev
6	1	S1	D	3	0	-13.9	NO
7	/	S1	D	3	0	-13.9	NO
8	/	S1	D	3	0	-13.9	NO
9	/	S1	D	3	0	-13.9	NO
10	/	S1	D	3	0	-13.9	NO
17	1	S2	D	3	0	-13.9	NO
18	/	S2	D	3	0	-13.9	NO
20	/	S2	D	3	0	-13.9	NO
22	/	S2	D	3	0	-13.9	NO
24	/	S2	D	3	0	-13.9	NO

26	/	S1S2	D	3	0	-13.9	NO
28	1	S1S2S2	D	3	0	-13.9	NO
30	1	S1S2S2	D	3	0	-13.9	NO
31	/	S1S2	D	3	0	-13.9	NO
33	/	S1S2	D	3	0	-13.9	NO
35	/	S1S2	D	3	0	-13.9	NO
37	/	S1S2	D	3	0	-13.9	NO
39	/	S1S2	D	3	0	-13.9	NO
41	/	S1S2	D	3	0	-13.9	NO
43	/	S1S2	D	3	0	-13.9	NO
44	2	S1S2	D	3	0	-23.4 for S2	NO
49	1	S1S2	D	3	0	-13.9	NO
50	1	S1S2	D	3	0	-15.9 for S2	NO
51	1	S1S2S2	D	3	0	-13.9	NO
52	1	S1S2S2	P	3	0	-13.9	NO
53	1	S1S2S2	A	3	0	-13.9	NO
56	2	S1S2S2	D	3	0	-13.9	NO
57	2	S1S2S2	D	3	0	-23.4 for s2s3	NO
58	2	S1S2S2	P	3	0	-13.9	NO
59	2	S2S2S2	P	3	0	-23.4 for s2s3	NO
60	2	S1S2S2	A	3	0	-13.9	NO
61	2	S1S2S2	A	3	0	-23.4 for s2s3	NO
68	3	S1S2S2	D	3	0	-13.9	NO
69	3	S1S2S2	D	3	0	-19.4 for s2s3	NO
70	3	S1S2S2	P	3	0	-13.9	NO
71	3	S1S2S2	P	3	0	-19.4 for s2s3	NO
72	3	S1S2S2	A	3	0	-13.9	NO
73	3	S1S2S2	A	3	0	-19.4 for s2s3	NO
74	4	S1S2S2	D	3	0	-13.9	NO
75	4	S1S2S2	D	3	0	-21.9 for s2s3	NO
76	4	S1S2S2	P	3	0	-13.9	NO
77	4	S1S2S2	P	3	0	-21.9 for s2s3	NO
78	4	S1S2S2	A	3	0	-13.9	NO
79	4	S1S2S2	A	3	0	-21.9 for s2s3	NO
80	4	S1S2	D	3	0	-13.9	NO
82	4	S1S2	P	3	0	-13.9	NO
84	4	S1S2	A	3	0	-13.9	NO
86	5	S1S2S2	D	3	0	-13.9	NO
87	5	S1S2S2	D	3	0	-17.9 for s2s3	NO
88	5	S1S2S2	P	3	0	-13.9	NO
89	5	S1S2S2	P	3	0	-17.9 for s2s3	NO
90	5	S1S2S2	A	3	0	-13.9	NO
91	5	S1S2S2	A	3	0	-21.9 for s2s3	NO
92	6	S1S2S2	D	3	0	-13.9	NO
93	6	S1S2S2	D	3	0	-19.9 for s2s3	NO
94	6	S1S2S2	P	3	0	-13.9	NO
95	6	S1S2S2	P	3	0	-19.9 for s2s3	NO
96	6	S1S2S2	A	3	0	-13.9	NO

97	6	S1S2S2	A	3	0	-19.9 for s2s3	NO
98	7	S1S2S2	D	3	0	-13.9	NO
99	7	S1S2S2	D	3	0	-24.9 for s2s3	NO
100	7	S1S2S2	P	3	0	-13.9	NO
101	7	S1S2S2	P	3	0	-24.9	NO
102	7	S1S2S2	A	3	0	-13.9	NO
103	7	S1S2S2	A	3	0	-24.9 for s2s3	NO
107	7	S1S2S2	D	3	0	-13.9	NO
108	7	S1S2S2	D	3	0	-24.9 for s2s3	NO
109	7	S1S2S2	P	3	0	-13.9	NO
110	7	S1S2S2	P	3	0	-24.9 for S2s3	NO
111	7	S1S2S2	A	3	0	-13.9	NO
112	7	S1S2S2	A	3	0	-24.9 for s2s3	NO
113	2	S1S2	D	3.5	0	-13.9	NO
114	2	S1S2	D	3.5	0	-23.4 for s2	NO
115	2	S1S2	D	4	0	-13.9	NO
116	2	S1S2	D	4	0	-23.4 for s2	NO
117	2	S1S2	D	2.5	0	-13.9	NO
118	2	S1S2	D	2.5	0	-23.4 for s2	NO
119	2	S1S2	D	2	0	-13.9	NO
120	2	S1S2	D	2	0	-23.4 for s2	NO
121	2	S1S2	D	1.5	0	-13.9	NO
122	2	S1S2	D	1.5	0	-23.4 for s2	NO
123	2	S1S2	D	3	15	-13.9	NO
124	2	S1S2	D	3	15	-23.4 for s2	NO
125	2	S1S2	D	3	30	-13.9	NO
128	2	S1S2	D	3	45	-13.9	NO
129	2	S1S2	D	3	45	-23.4 for s2	NO
130	2	S1S2	D	3	60	-13.9	NO
131	2	S1S2	D	3	60	-23.4 for s2	NO
132	2	S1S2	D	3	30	-13.9	NO
133	2	S1S2	D	3	30	-23.4 for s2	NO
141	1	S1S2S2	D	3	0	-13.9	45°
147	1	S1S2S2	D	3	0	-13.9	0°
206	1	S1S2S2	D	3	0	-13.9	*
230	1	S1S2S2	D	3	0	-13.9	**

Table A.2: Study cases

$*$ is for *2 plates at* 0° *and* 45° *+ 3 obstacles*
$**$ is for *2 plates at* 0° *and* 45°

A.2.1 Configurations "/"

Here it is possible to see the positions of the sources in case the configuration is not specified (/)

Runs	**Source 1**	**Source 2**	**Source 3**
7	(0.41;-0.13)	/	/
8	(-0.2;0.33)	/	/
9	(-0.17;0.28)	/	/
10	(-0.38;-0.39)	/	/
18	/	(0.33;0.14)	/
20	/	(0.56;0.06)	/
22	/	(0.19;-0.09)	/
24	/	(-0.03;-0.32)	/
26	(0;0)	(-0.5;0.25)	/
31	(0;0.095)	(-0.34;0.25)	/
33	(0.09;0.035)	(-0.19;0.21)	/
35	(0.09;0.31)	(-0.09;0.12)	/
37	(0.32;0.23)	(0.18;0.06)	/
39	(0.15;-0.095)	(0.315;-0.02)	/
41	(0.06;-0.185)	(0.17;-0.11)	/
43	(0;-0.22)	(0.07;-0.29)	/

Table A.3: Sources' position of configurations not present.

Bibliography

[1] Renzo Arina. *0.Presentazione*. Note relative al Corso di Aerodinamica per la Laurea Magistrale in Ingegneria Aerospaziale, tenute nell'anno accademico 2023-2024. Dipartimento di Ingegneria Meccanica e Aerospaziale Politecnico di Torino.

[2] Renzo Arina. *1.Introduzione*. Note relative al Corso di Aerodinamica per la Laurea Magistrale in Ingegneria Aerospaziale, tenute nell'anno accademico 2023-2024. Dipartimento di Ingegneria Meccanica e Aerospaziale Politecnico di Torino.

[3] Renzo Arina. *3.Propagazione in campo acustico libero*. 2024.

[4] Renzo Arina. *7. Sorgenti acustiche*. 2024.

[5] Thomas Brooks and William Humphreys. "A Deconvolution Approach for the Mapping of Acoustic Sources (DAMAS) Determined from Phased Microphone Arrays". en. In: *10th AIAA/CEAS Aeroacoustics Conference*. Manchester, GREAT BRITAIN: American Institute of Aeronautics and Astronautics, May 2004. ISBN: 978-1-62410-071-0. DOI: 10.2514/6.2004-2954. URL: https://arc.aiaa.org/doi/10.2514/6.2004-2954 (visited on 02/17/2025).

[6] Paolo Chiariotti, Milena Martarelli, and Paolo Castellini. "Acoustic beamforming for noise source localization – Reviews, methodology and applications". en. In: *Mechanical Systems and Signal Processing* 120 (Apr. 2019), pp. 422–448. ISSN: 08883270. DOI: 10.1016/j.ymssp.2018.09.019. URL: https://linkinghub.elsevier.com/retrieve/pii/S088832701830637X (visited on 01/30/2025).

[7] European Commission. Directorate General for Research and Innovation. and European Commission. Directorate General for Mobility and Transport. *Flightpath 2050 :Europe's vision for aviation : maintaining global leadership and serving society's needs*. eng. LU: Publications Office, 2011. URL: https://data.europa.eu/doi/10.2777/50266 (visited on 12/05/2024).

[8] D. Habault et al. "Active Control in an Anechoic Room: Theory and First Simulations". en. In: *Acta Acustica united with Acustica* 103.3 (May 2017), pp. 369–378. ISSN: 1610-1928. DOI: 10.3813/AAA.919066. URL: http://www.ingentaconnect.com/content/10.3813/AAA.919066 (visited on 02/14/2025).

[9] *https://theproaudiofiles.com/sound-pressure-levels-part-1-of-2/*.

[10] Jeremy Jomain. *Methode d'analyse systematique des cartes de localisation de sources acoustiques pour l'evaluation des performances*. French. Stage de Recherche - C esure 2024. Toulouse: ISAE-SUPAERO et ONERA, Feb. 2024, p. 56.

[11] Bruel & Kjaer. "Technical Review Beamforming". In: No.1 2004 (2004), p. 55.

[12] Hélène Parisot-Dupuis. "https://hal.science/hal-04887552v1/file/17750-Parisot-Dupuis_17481.pdf". In: ().

[13] Hélène Parisot-Dupuis et al. "Aeroacoustic radiation of low Reynolds number rotors in interaction with beams". English. In: (Aug. 2023), p. 14. DOI: http://dx.doi.org/10.1121/10.0020672.

[14] Hélène Parisot-Dupuis et al. "Systematic analysis of acoustic source localization maps for performance assessment". English. In: Nantes , France, Aug. 2024, p. 12.

[15] Siemens. *https://community.sw.siemens.com/s/article/window-types-hanning-flattop-uniform-tukey-and-exponential*.

[16] Pieter Sijtsma. "CLEAN Based on Spatial Source Coherence". en. In: *International Journal of Aeroacoustics* 6.4 (Dec. 2007), pp. 357–374. ISSN: 1475-472X, 2048-4003. DOI: 10.1260/147547207783359459. URL: https://journals.sagepub.com/doi/10.1260/147547207783359459 (visited on 02/17/2025).